SYNTHESIS, CHARACTERISATION AND HYDROXY CARBONATED APATITE (HCA) FORMATION STUDIES ON SOL-GEL DERIVED SiO_2-CaO-P_2O_5, SiO_2-CaO-Na_2O-P_2O_5, SiO_2-CaO-BaO-Na_2O-P_2O_5 GLASS SYSTEMS

Thesis

Submitted in partial fulfillment of the requirements for the degree of
DOCTOR OF PHILOSOPHY

by

KIRAN PEDANABOYINA
(Registration No: 110694PH11F02)

DEPARTMENT OF PHYSICS

NATIONAL INSTITUTE OF TECHNOLOGY KARNATAKA,

SURATHKAL, MANGALORE – 575025,

FEBRUARY, 2019

D E C L A R A T I O N

by the Ph.D. Research Scholar

I hereby declare that the Research Synopsis Entitled **"synthesis, characterisation and hydroxy carbonated apatite (HCA) formation studies on sol-gel derived SiO_2-CaO-P_2O_5, SiO_2-CaO-Na_2O-P_2O_5, SiO_2-CaO-BaO-Na_2O-P_2O_5 glass systems"** which is being submitted to the National Institute of Technology Karnataka, Surathkal in partial fulfilment of the requirements for the award of the Degree of Doctor of Philosophy in Physics is a bonafide report of the research work carried out by me. The material contained in this Research Thesis has not been submitted to any University or Institution for the award of any degree.

110694PH11F02, KIRAN PEDANABOYINA
(Register Number, Name & Signature of the Research Scholar)
Department of Physics

Place: NITK-Surathkal
Date:

C E R T I F I C A T E

This is to certify that the Research Thesis entitled **"synthesis, characterisation and hydroxy carbonated apatite (HCA) formation studies on sol-gel derived SiO_2-CaO-P_2O_5, SiO_2-CaO-Na_2O-P_2O_5, SiO_2-CaO-BaO-Na_2O-P_2O_5 glass systems"** (Register Number: 110694PH11F02) as the record of the research work carried out by him, is accepted as the Research Thesis submission in partial fulfilment of the requirements for the award of degree of Doctor of Philosophy.

Prof. N.K. Udayashankar	Prof. H.D. Shashikala
Research Guide	Research Guide
(Name and Signature with Date and Seal)	(Name and Signature with Date and Seal)

Chairman – DRPC
(Name and Signature with Date and Seal)

To my sister Srujana, Parents, Family members and my beloved God Lord Shiva

Acknowledgments

Foremost, it is my immense pleasure to thank my research supervisors, Prof. N.K. Udayashankar and Prof. H.D. Shashikala for their excellent and eminent guidance throughout my research work and introducing me to the exciting areas of research in "synthesis, characterisation and hydroxy carbonated apatite (HCA) formation studies on sol-gel derived SiO_2-CaO-P_2O_5, SiO_2-CaO-Na_2O-P_2O_5, SiO_2-CaO-BaO-Na_2O-P_2O_5 glass systems." I am grateful for their constant encouragement, support and freedom to work. I was inspired greatly from their discipline and guiding students constantly in spite of their busy schedules.

I thank National Institute of Technology Karnataka for giving me the opportunity for doing research and Ministry of Human Resource Department (MHRD)-Government of India for awarding research scholarship. I thank the members of my Research Progress Assessment Committee (RPAC) Dr. Ravishankar K.S., Department of Metallurgical and Materials engg, Dr. Darshak R Trivedi, Department of chemistry, for their suggestions during every stage of my dissertation work.

I am grateful to all the faculty members Dr. M.N. Satyanarayana (HOD in department of Physics), Dr. H.S. Nagaraja, Dr. Ajith for their cooperation and support.
I express my sincere thanks to V. Ramakrishna and Dr. M. Trebbin Hamburg Center for Ultrafast Imaging (CUI), University of Hamburg, Luruper Chaussee 149, 22761 Hamburg, Germany for allowing me to use facilities for characterization of Raman, FESEM/EDX, XRD. I also thank Chemical Engineering and Chemistry department in the Institute for providing various characterization facilities.

I would like to acknowledge the help and cooperation of the Physics staff including Mrs. Veena, Mrs. Ashalatha, Mr. Dhanraj, Mrs. Saritha, Ms. Usha, Mr. S. Nayak and Mr. Chandranna in carrying out my research and daily activities in the department.

I thank my beloved mother and father and my brother-in-law for their endless love and bestowing me all that because of which I stand today as what I am. I express my

sincere thanks to all my sisters and all my family members for their unending love and affection.

I would like to express my gratitude to my well wisher BK D. Sudhakar for giving support morally and financially. I would like to express my gratitude to my well wishers and my beloved friend P.B.V.P.K. Kishore and his parents and family members. Finally, I would like to express my gratitude to my friends, B. Naveen Kumar Reddy, M.R. Kiran, Subhashini, Dr. Venkat, Dr. Santhosh, Vijaya A.R., Raman Reddy, Mahendra K, Brian Jeevan Fernandes, Suchithra, Akhila, Bhattacharya, Subhashini, Ramesh M, Ramesh K and others at NITK. I would like to express my gratitude to John (MIT) for providing facilities for my research work and others for their encouragements, the motivation and direct or indirect help they gave me to finish this work. For sure I would not have been able to come to complete my work without them and the energy I got from all the activities I could undertake with them.

KIRAN PEDANABOYINA

ABSTRACT

$58SiO_2$-(19-x)P_2O_5-(23+x)CaO (where x=0, 5, 10 and 15 mol %), $58SiO_2$-(38-x)CaO-xNa_2O-4P_2O_5 (where x=5, 10, 15 and 20 mol %) and $58SiO_2$-(32-x)BaO-xCao-6Na_2O-4P_2O_5 (where x=15, 20, 25 and 30 mol %) samples were synthesized using conventional sol-gel method at 700 °C sintering temperature. Thermal and structural properties were studied using thermo gravimetric analysis (TGA) and differential thermal analysis (DTA), X-ray diffraction (XRD), scanning electron microscopy (SEM), Fourier transform infrared (FTIR) and Raman spectroscopy. TGA/DTA and XRD analysis confirmed that the variations in crystalline or amorphous nature of synthesized glass samples depended on both onset crystalline temperatures as well as chemical composition. Using Raman spectra non-bridging oxygen concentrations were estimated. The hydroxy carbonated apatite [HCA] layer formation on samples soaked for 7 days in simulated body fluid (SBF) was analyzed. The growth of HCA self assembled layers on the sample surface was discussed as a function of NBO/BO ratio. Results indicated that the number of Ca^{2+} ions released into SBF solution in the dissolution process and weight loss of SBF treated samples vary with NBO/BO ratio. Transmission electron microscopy (TEM) with selected area electron diffraction (SAED) analysis also confirmed that HCA crystals were formed during SBF treatment. Raman and Infrared spectroscopic analyses have given strong evidence for HCA crystal layer formation through the identification of CO_3^{2-} and PO_4^{3-} groups. The changes in NBO/BO ratios were observed to be proportional to HCA forming ability. Among all glass samples, the glass with high CaO concentration (ternary system) shows more HCA forming ability. Calcium phosphosilicate glasses with less concentrations of BaO and Na_2O in comparision with CaO favour the HCA formation in tertiary glass system.

Key words: Sol-gel; Calcium oxide; SBF; HCA layer.

CONTENTS

List of figures

List of tables

Nomenclature

Symbol	Definition	Unit
3D	3 dimensional	
Na_2O	Sodium oxide	
CaO	Calcium oxide	
P_2O_5	Phosphorous pent oxide	
SiO_2	Silicon di oxide	
B_2O_3	Di boron tri oxide	
GeO_2	Germanium di oxide	
Ag_2O	Silver oxide	
Al_2O_3	Alumina	
BO	Bridging oxygen	
V- P_2O_5	Vitreous Phosphorous pent oxide	

T_g	Glass transition temperature	°C
As	Arsenic	
Sb	Stibium	
Si	Silicon	
Nd	Neodymium	
Er	Erbium	
pH	potential hydrogen	
TEOS	Tetra ethyl ortho silicate	
MTES	Methyl tri ethoxy silane	
MTMS	Methyl tri methoxy silane	
VTMS	Vinyl trimethoxy silane	
APS	Aminopropyl trimethoxysilane	
MAPTS	Metacryloxypropyl trimethoxysilane	
HNO_3	Nitric acid	
CH_3	Methyl	
C_2H_5	Ethyl	
C_3H_7	Propyl	
C_4H_9	Butyl	
HR TEM	Hi resolution transmission electron microscopy	
FTIR	Fourier transforms infrared spectroscopy	
MAS-NMR	Nuclear magnetic resonance spectroscopy	
NBO	Non bridging oxygen	

Ag_2O	Silver oxide
XRD	X-ray diffraction
TCP	Tri calcium phosphate
TEM	Transmission electron microscopy
NH_4HF_2	Ammonium hydrogen di fluoride
CaF_2	Calcium fluoride
HA	Hydroxy apatite
Li_2O	Lithium oxide
Fe_3O_4	Ferric **oxide**
HAP	Hydroxy apatite
HCA	Hydroxy carbonated apatite
SBF	Simulated body fluid
BaO	Barium oxide
TGA	Thermo gravimetric analysis
DTA	Differential thermal analysis
SEM	Scanning electron microscopy
FESEM	Field emission scanning electron microscopy
EDX	Energy dispersive X-ray analysis
UV	Ultraviolet
Vis	Visible
KH_2PO_4	Potassium di hydrogen phosphate
$CaCl_2$	Calcium chloride

$NaHCO_3$	**Sodium hydrogen carbonate**	
$MgCl_2.6H_2O$	Magnesium chloride hexa hydrate	
KCl	Potassium chloride	
NaCl	Sodium chloride	
DSC	Differential scanning calorimetry	
T_x	Onset crystalline temperature	°C
T_m	Melting temperature	°C
ΔC_v	Heat capacity	
ΔT	Thermal stability	°C
$CaCO_3$	Calcite	
$Na_2Ca_2Si_3O_9$	Combeite	
SE	Secondary electrons	
BSE	Back scattered electrons	
CTEM	Conventional transmission electron microscopy	
eV	Electron volts	
SAED	Selected area electron diffraction	Nm
$D_{(hkl)}$	Interplanar distance	
λ	X-ray wavelength	Nm
KBr	Potassium bromide	
P	Capillary force	
Γ	Liquid surface tension	
WL	Weight loss	

Si-OH	Silanol
IR	Infrared radiation
JCPDS	Joint committee on powder diffraction studies

Chapter 1

INTRODUCTION

Glass is a unique material which has been quoted as an ‘‘indispensable and brilliant material for a better and future existence”. The word “glass” evolves from the Latin word ‘glacies’ meaning “ice” and by far most utilized property of glass is its transparency, which comes as a result of its inherent isotropic nature. Today’s glass can be reasonably custom-made to fit into any environmental conditions and offer particular developments and performance. Archaeological study tells that glass was first made in the Middle East, around the 3000 B.C (Rao 2002).

In modern glass industry, one of the challenges for engineers and scientists is to develop highly transparent glass materials with low glass transition temperature (T_g). X-ray diffraction and electron diffraction data show that there are no long-range regular, periodic atomic arrangements in the structure. However, glasses exhibit similar short-range ordered structural entities of their crystalline counterparts in a 3D random-network configuration. Therefore glasses are called non-crystalline solids or amorphous materials. They exhibit uniform glass formation behavior. The glass macroscopic properties such as optical transmission, absorption, refraction of light etc, are observed to be always equal in all directions. It means that glass is an isotropic material and crystals are generally anisotropic materials (Shelby 2005).

A glass is a network of atoms (most commonly silicon) bonded to each other through covalent bonds with oxygen atoms. A silica based glass is formed of silicate tetrahedra bonded together in a random arrangement. Window glass is usually based on the soda-lime-silica (Na_2O-CaO-P_2O_5) system. Bio active glasses also often contain these components, but in different proportions.

1.1 structural theories of glass formation

Goldschmidt introduced a theory for glass formation based on the glass structure. The general formula of glass is R_nO_m, where R is cation and O is oxygen anion. The ionic radius ratio of cation to oxygen anion is in the range 0.2 - 0.4. In this range one cation is surrounded by four oxygen ions and forms tetrahedral structure.

Zachariasen discussed the glass formation based on the atomic arrangement. The atomic arrangement in glass structure is characterized by an extended three-dimensional network which lacks periodicity and symmetry. Zachariasen's well-known conditions for glass formation are listed below.

For an oxide A_mO_n to form a glass

(a) an oxygen atom must not be linked to more than two A atoms

(b) the number of oxygen atoms surrounding A must be small

(c) the oxygen polyhedra must share corners only but not faces or edges

(d) At least three corners in each oxygen polyhedron should be shared in three-dimensional network.

1.2 Classification of glass systems

The structure of the glass is based on the network formers, network modifiers, and intermediate units. The network formers can form glasses by themselves readily. The main network formers are SiO_2, P_2O_5, B_2O_3 and GeO_2. The network modifiers are helpful for the formation of glasses through mixing with the network formers, but they cannot form a glass by themselves. Examples of network modifiers are alkali and alkaline earth oxides. The characteristic nature of the intermediate units is in between that of network formers and network modifiers, they cannot form the glass by themselves (Yamane and Asahara 2000). Required glasses can be prepared by adding one or more additional compounds such as Ag_2O, Al_2O_3 etc., to network formers. Among all glasses (compared to phosphate and borate), much interest has been shown in silicate glasses in terms of improvement of the structural, optical, thermal and electrical properties by changing the

concentration of alkali, alkaline oxides without losing their amorphous nature (Saravanapavan et al. 2003).

1.2.1 Structure of silicate glasses

The vitreous silica has the tetrahedron structure with three-dimensional network. The basic building block, the silicon-oxygen tetrahedra has the co-ordination number of 4 with 4 bridging oxygens. These tetrahedra are linked at all four corners to form a continuous 3-dimensional network. Each oxygen atom is shared in between two silicon atoms, which occupy the centers of linked tetrahedra. Increasing the composition of alkali or alkaline oxides decreases the number of bridging oxygens and increases the number of non-bridging oxygens by maintaining the total charge neutrality in between alkali or alkaline cation and oxygen anion.

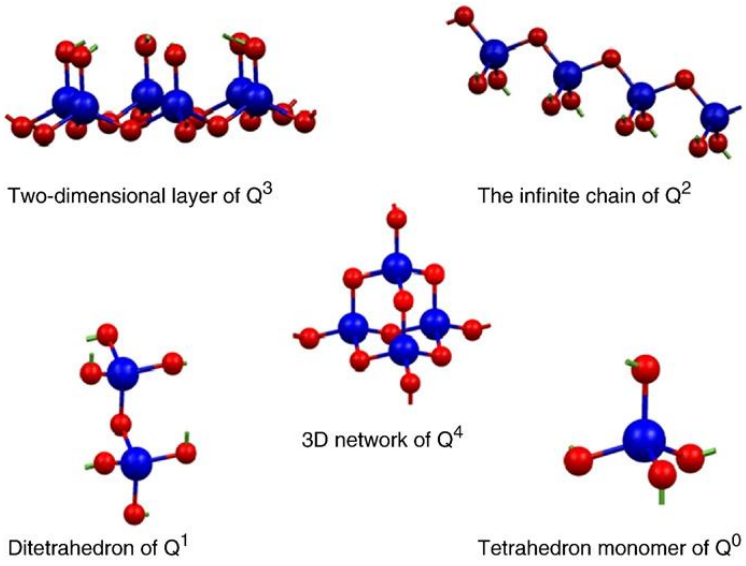

Figure 1.1 The spatial structure of Q^n units. Blue sphere is Si atom and red one is O atom. In the structure, the red rods stand for direct connection between oxygen and other silicon atom, while the green rods stand for the combination between oxygen atoms and network modifiers (Ma et al. 2010).

The number of bridging oxygens can be shown by the notation Q^n where n is the number of bridging oxygens. For v-silicate glass (V-SiO_2) the bridging oxygens starts from (n=4) to Q^0 (n=0). Q^4 shows the SiO_4^{4-} tetrahedra with four bridging oxygens, Q^3 shows the SiO_4^{3-} tetrahedra with three bridging oxygens and one non bridging oxygen, Q^2 shows the SiO_4^{2-} tetrahedra with two bridging oxygens and two non bridging oxygens, Q^1 shows the SiO_4^{1-} tetrahedra with one bridging oxygen, three non bridging oxygens and Q^0 shows the SiO_4 tetrahedra with four non bridging oxygens. While adding alkali or alkaline oxides to SiO_2, the tetrahedra change from Q^4 to Q^3, $Q^3$to Q^2, Q^2 to Q^1 and Q^1 to Q^0 (Ma et al. 2010).

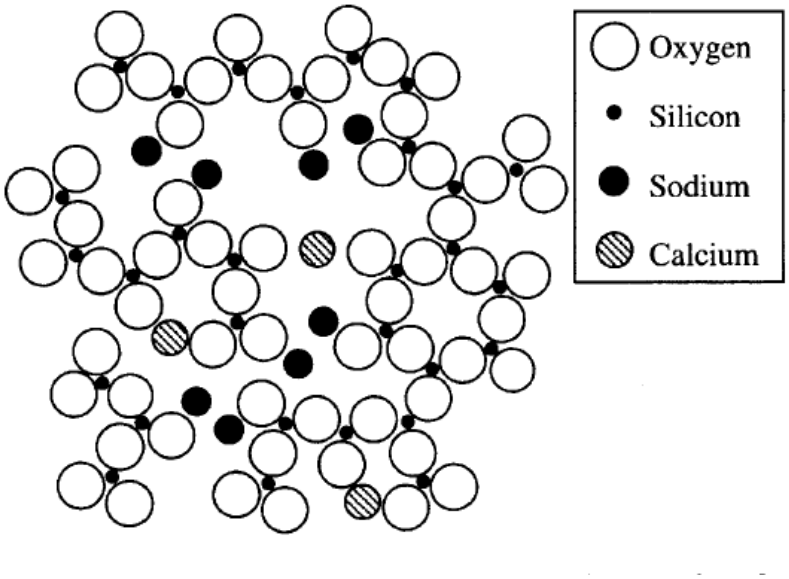

Figure 1.2 Schematic drawing of a 2-dimensional structure for a soda - lime – silicate glass. A fourth oxygen would be located above each silicon in the 3-dimensional structure (Shelby 2005).

1.2.2 Structure of phosphate glasses

Like silicate glasses, phosphate glass structure does not show any long range order or significant symmetry of atomic arrangement, but they do have short range order. The glass forming component in phosphate glasses is P_2O_5, and the basic unit in the

phosphate glass structure is the ortho phosphate (PO_4^{3-}) tetrahedron, which is phosphorous atoms surrounded by four oxygen atoms. As one of the oxygen atoms is connected to the phosphorous atom by a double bond, only three other oxygen atoms can act as "bridges" to other ortho phosphate tetrahedra. By forming such bridges, individual ortho phosphate tetrahedra can be linked to each other by covalent POP bonds. The oxygens in these POP linkages are commonly called bridging oxygens (BOs). Ortho phosphate tetrahedra can thereby be arranged to form chain, rings or branching networks. P_2O_5 is called a network former because it is possible to make a glass using P_2O_5 only. Pure P_2O_5 glass can be produced under certain conditions, but as it is very reactive and hygroscopic, it is of scientific interest only. The durability can be increased, however, by adding other components, called network modifiers such as calcium oxide (CaO).

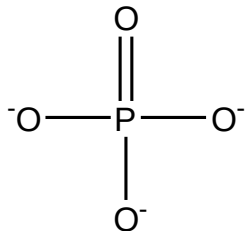

Figure 1.3 Basic phosphate tetrahedron in glass structure

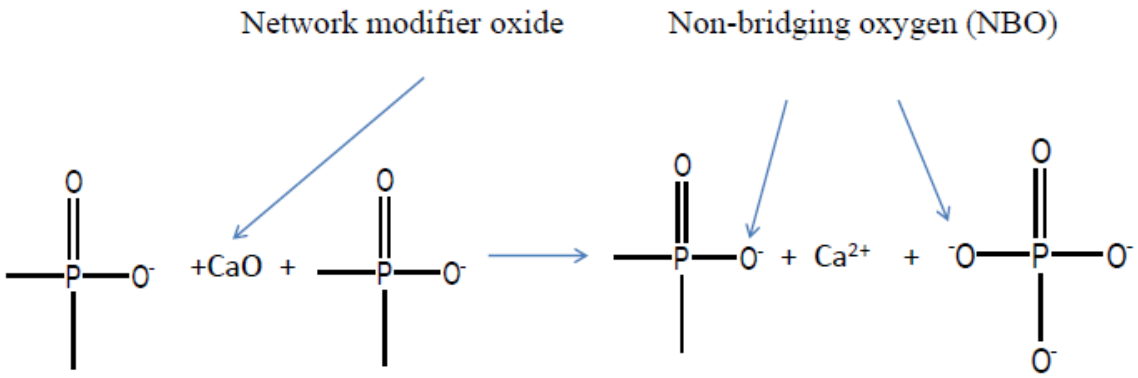

Figure 1.4 Schematic of clearage of P-O-P linkages by network modifier, turning bridging oxygens (BOs) into non-bridging oxygens (Jones and Clare 2012)

Vitreous P_2O_5 (V-P_2O_5) has a 3D network structure analogous to P_2O_5 crystalline structure. In this structure P has coordination bond with four oxygens. Among them three are bridging oxygens and the fourth one is double bonded non bridging oxygen. Phosphate glasses have low glass transition temperature (T_g) and high thermal expansion coefficients than silicate glasses. The phosphate glass properties can change the chemical durability and can be improved glass strength significantly by the addition of alkali and alkaline earth oxides into the glassy network (Brow et al. 2000).

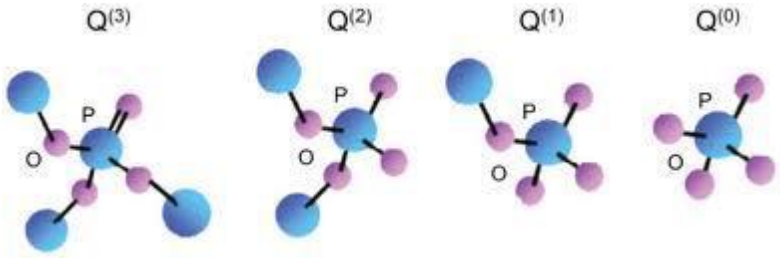

Figure 1.5 Phosphate tetrahedral sites that can exist in phosphate glasses (Brow 2000).

As shown in Figure 1.5 vitreous P_2O_5 structure contains three dimensional network of corner sharing PO_4 tetrahedra. Each PO_4 tetrahedra has a P=O double bond (non bridging oxygen). The alkali oxide addition to V-P_2O_5 de-polymerizes the phosphate network and the bridging oxygens is replaced by non-bridging oxygens. Phosphate tetrahedra (PO_4) with three bridging oxygens are described as Q^3 species. These Q^3 species are generally referred to as 'ultra phosphates', and Q^2 species are indicated as 'meta phosphate' glasses with two bridging oxygens. The structure of Q^2 species generally consists of infinitely long rings and/or chains. Phosphate tetrahedra with just one bridging oxygen are called as Q^1 units, and are called as 'pyrophosphates'. Q^0 species are called as 'Orthophosphate' units, for which there are no bridging oxygens attached to the single phosphate tetrahedron. Glasses that are major in Q^1 and Q^0 species have also been referred to as 'invert glasses'. Alkali oxide addition to P_2O_5 glasses, changes the structure from Q^3 to Q^2 to Q^1 to Q^0.

1.2.3 Phosphosilicate glasses

The silicate network structure in phosphosilicate glasses at low SiO_2 content is dominated by the Si_6 network formation. The optical basicity of SiO_2 is higher than P_2O_5.

Due to this reason the effective negative charge on the oxygen in SiO_2 is also higher compared to P_2O_5. For a small amount of SiO_2 addition to P_2O_5 content, the positive charge on Si^{4+} ion must be balanced by oxygen with relatively low effective negative charge. More than four oxygen ions are required to balance the positive charge on silicon. Due to this reason silicon coordination number is changed as six instead of four.

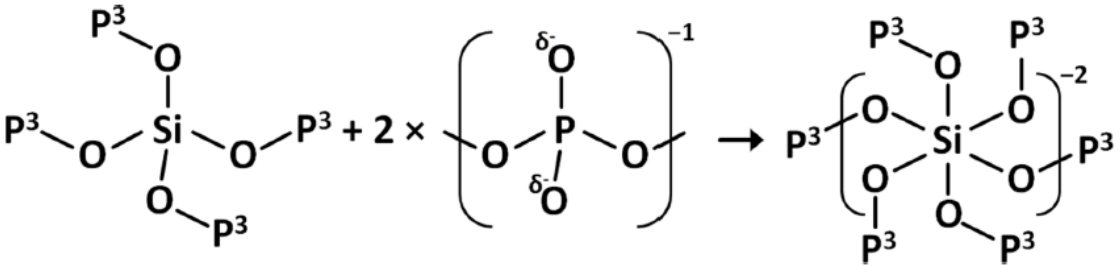

Figure 1.6 Schematic of formation of phosphosilicate glasses (Christian et al. 2015)

1.2.4 Borate glasses

In borate glasses B_2O_3 is the network former. Alkali oxide addition to B_2O_3 causes the change in boron oxide structure from triangular to tetrahedral without non bridging oxygens. Two boron-oxygen tetrahedral formations consume the one additional oxygen provided by the alkali oxide such as R_2O. Each tetrahedron has a -1 unit charge deficiency, due to this reason the two alkali oxides provide sufficient charges for the compensation of the two tetrahedral units. The large $(BO_{4/2})^-$ units act as anions with a loosely associated alkali cation. A continuous increase in the alkali oxide addition causes the boron shift from 3 to 4-fold coordination. Due to high compatibility with rare earth elements, borate glasses have so many applications in the optical and optoelectronic fields.

1.2.5 Germanate glasses

For germanate glasses GeO_2 is the network former. The structure of vitreous Germania is very similar to that of vitreous silica, with germanium-oxygen (Q^4) units. The diameter of the silicon is small compared to germanium. The Ge-O distance is also high with 0.173 nm bond length. The Ge-O-Ge bond angle is smaller compared to Si-O-Si bond angle. Gas diffusion studies suggested that the structure of vitreous germania is

more compact compared to vitreous silica. Therefore the free, or interstitial volume of vitreous germania is slightly less compared to vitreous silica, Due to this structural defects are more common in vitreous germania than vitreous silica.

1.2.6 Halide and oxyhalide glasses

Due to lowest refractive index and a highest Abbe number, BeO_2 glasses are the only halide glasses which are used extensively in all practical applications. These glasses have ionic bonds in the glass structure, and therefore, the glasses show so many advantages such as good transparency in the infrared region, low phonon energies, low glass transition temperature. And also they have potential as hosts for active rare earth ions (Adam 2001). But, these halide glasses having hygroscopic and highly toxic nature and have extreamly limited practical application. In that sense, the combination of halides and oxides, particularly oxyhalide glasses appear to be very interesting and attractive materials for so many practical applications (Nazabal et al. 2012).

1.2.7 Chalcogenide glasses

Chalcogenide glasses are obtained by melting the chalcogenide elements or their compounds with As, Ge, Sb, Si etc. within a silica glass ampoule or in a vacuum to avoid the oxidation effect. Chalcogenide glasses can be doped with rare earth elements such as Nd, Er etc., for numerous applications such as optical devices, nonlinear optics, windows, prisms and also can be used as host materials for infrared lasers.

1.3 GLASS PREPARATION METHODS

Glasses are prepared mainly using three methods, they are

1. Melt-quenching technique

2. Chemical vapor deposition technique

3. Sol-gel technique

1.3.1 Glass by melt-quenching technique

This method is based on the fusion of crystalline raw materials into viscous liquid and quenching into a glass. The high flexibility of geometry of glass and glasses with the composition of alkali, alkaline earth elements can be prepared by using this method. This method is not suitable for preparation of the high refractory materials such as SiO_2, TiO_2 etc (Shelby 2005).

1.3.2 Glass by chemical vapor deposition method

This method is based on the thermally activated homogeneous oxidation or hydrolysis of initial metal halide vapor to form particulate glass material 'soot', it is followed by viscous sintering of the soot into solid inclusion-free glass bodies. By using this method ultra high purity glasses can be prepared. This method is not suitable for the preparation of glasses with the addition of alkali, alkaline earth and rare-earth elements.

1.3.3 Glass by sol-gel technique

Glass preparation using sol-gel method was introduced by H. Dislich for the borosilicate glass preparation in the year 1971(Shelby 2005). The sol-gel process begins with formation of a sol. The sol consists of dispersive colloids in a liquid medium. It turns into porous wet gel by the coagulation of these colloids. Then the wet gel gets converted into dried gel in drying process. In sintering process the dried gel gets converted into a pore-free dense glass or glass film at a temperature slightly above the glass transition temperature of the eventual glass.

The sol-gel process is an inorganic polymerization route for the design of new materials in optical, electrical, bio-medical and solar energy applications. This technique is useful for the preparation of new porous nano-materials. The sol-gel method is influenced by various factors such as precursors, pH/Catalysts, water, TEOS molar ratio, temperature, aging and drying. The most common precursors are salts, oxides, hydroxides, complexes, alkoxides, and amines. Among these precursors, the alkoxides

are the most commonly used precursors (such as metal alkoxides of titanium, zirconium or aluminium).

These metal alkoxides can react with water easily compared to alkoxisilanes, due to their lower electro negativity and higher Lewis acidity. Alkoxysilanes are useful for preparation of good homogeneous solution without phase separation. The most commonly used alkoxysilane precursors are Tetraethyl orthosilicate (TEOS), Tetra methyl orthosilicate (TMOS), Methyl triethoxysilane (MTES), Methyl trimethoxysilane (MTMS), Vinyl trimethoxysilane (VTMS), 3-aminopropyl trimethoxysilane (APS), γ-metacryloxypropyl trimethoxysilane (γ-MAPTS). TEOS increases the sol viscosity. These precursors are available at low cost and are available as non-toxic species. The pH value of the solution controls the microstructure of the metal oxide in sol-gel process in the hydrolysis and condensation reactions. Acid catalyzed conditions are favorable for the completion of hydrolysis. The alkali catalyzed conditions are favorable for increasing the condensation rate.

1.3.3.1 Steps in sol-gel process

1.3.3.1. 1 Hydrolysis

In sol-gel method hydrolysis process is used to prepare polymerized sols. The sol preparation is based on using precursors, catalysts and required water quantities. Metal alkoxides (such as TEOS) are used as precursors in sol-gel technique. These precursors do not dissolve in water. Catalyst (such as HNO_3) addition causes the solubility of precursors in water and the formation of the homogeneous solution. This process is accompanied by stirring. In hydrolysis process metal alkoxides form the metal hydrates as represented below.

$$Me(OR)_n + nH_2O \longrightarrow Me(OH)_n + nROH \quad \text{.....1.1}$$

where, Me is metal ion, R alkyl group.

1.3.3.1.2 Aging

The clear solution is poured into a cylindrical Teflon beaker and left in a hot air oven at a temperature (that is below the boiling point of alkanol) with tightly sealed cover to enhance gel formation through hydrolysis.

Two partly hydrolyzed molecules can link together in a condensation reaction

$(OR)_3$-Si-OH+OH-Si-$(OR)_3$ ⟶ $(OR)_3$-Si-O-Si-$(OR)_3$+H_2O……1.2

$(OR)_3$-Si-OR+OH-Si-$(OR)_3$ ⟶ $(OR)_3$-Si-O-Si-$(OR)_3$+R-OH……1.3

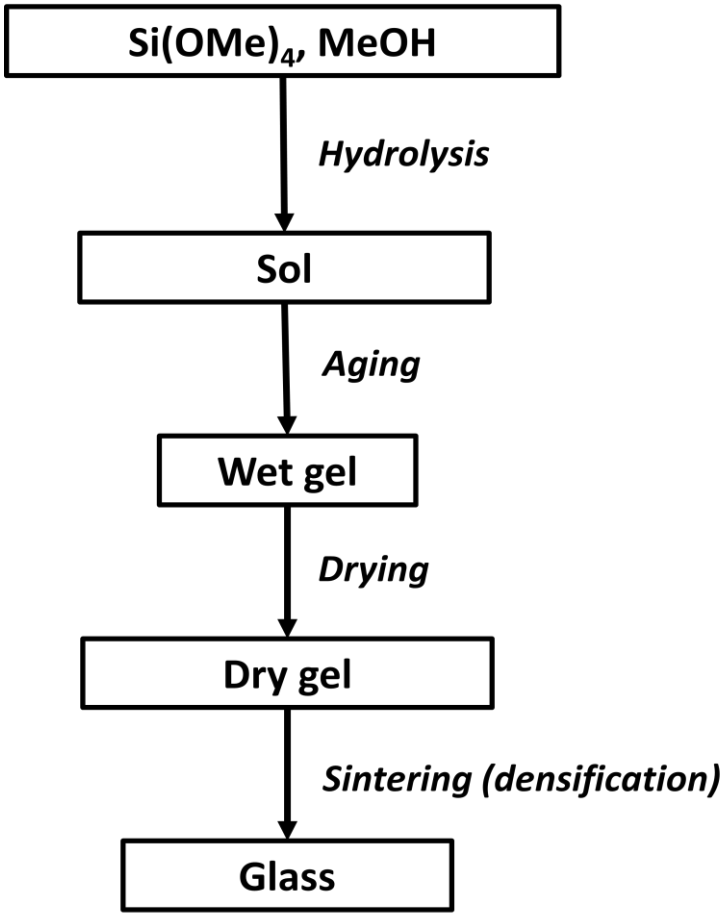

Where Me is CH_3, C_2H_5, C_3H_7 etc

Figure 1.7 Flowchart for the preparation of sol-gel glass (Shelby 2005)

Condensation liberates small molecules such as water or alcohol. After dehydration and condensation process wet-gel will be formed, this process is called as aging. This type of reaction can be continued to build larger and larger silicon containing molecules by polymerization process. The de-hydrolysis and condensation reaction followed by aging at the same temperature until it separates from the container wall by syneresis of a small amount of liquid and wet-gel will be formed. The excess of water and alcohol can be removed using drying process.

1.3.3.1.3 Drying

The wet-gel needs to dry slowly to evaporate the liquid. For that purpose pin holes should be formed on the cover. In this process no more shrinkage occurs. Slow drying is necessary to avoid fracture of the gel, due to capillary force induced by the evaporation of the liquid.

1.3.3.1.4 Heating

The dried silica gel is subjected to heat treatment at a temperature about 1000 °C for densification into a pore free glass. For silicate glass preparation the highest required temperatures in sol-gel method is 1000 °C, which is less than silicate melting point (i.e. 2000 °C). Using sol-gel method glasses with alkali and alkaline earth oxide elements can be prepared easily. But using other techniques like the chemical-vapor-deposition it is difficult to prepare these glasses with alkali and alkaline earth oxide elements. In fact sol-gel process is a low temperature process. Most alkoxides precursors are in a liquid state, so it is relatively easy to purify them by repeated distillation. Since this process is a crucible less process, there is no possibility of contamination from the container. It is also possible to obtain glass of very high purity such as those used for fabrication of optical fiber. Some special glasses with alkali and alkaline earth oxides, which cannot be prepared by melt-quenching technique and chemical vapor deposition technique, can be easily prepared by sol-gel method (Yamane and Asahara 2000).

The hydrolysis and condensation reactions of metal alkoxides are schematically expressed by the equations.

$Me(OR)_n + nH_2O = Me(OH)_n + nROH$……...1.4

$m\ Me(OH) = mMeO_{n/2} + (mn/2)H_2O$……1.5

Where Me=Si, Al, Ti etc, R=CH_3, C_2H_5, C_3H_7 etc.

The following table shows alkoxide precursors.

The main drawback of this process is the large amount of shrinkage of a wet gel upon drying which leads to a fracture. This problem may overcome by optimizing the process parameters. In sol-gel process sol preparation mainly depends on process parameters such as precursors and pH value etc. Due to the less electropositive charge of silicon tetra ethyl ortho silicate (TEOS), it is less sensitive in hydrolysis process compared to the transition metal alkoxides. The pH value can stabilize the sols without agglomeration through the reduction of the surface charges by the evaporation of the solvent depending upon the particle to particle distance. In this case, the surface charges are decreased and the gelation takes place. It was observed that the pH value influences the porosity, density and volume of shrinkage on drying process (Milea et al. 2011).

Table 1.1 List of alkoxides precursors (Shelby 2005)

Alkoxide	**Formula**	**Boiling point (°C)**	**Ambient pressure (mm Hg)**
Boron n-butoxide	$B(OBu^n)_3$	128	760
Aluminium n-propoxide	$Al(OPr^n)_3$	205	1.0
Aluminium n-butoxide	$Al(OBu^n)_3$	242	0.7
Aluminium tert- butoxide	$Al(OBu^t)_3$	151	1.3
Tetra ethyl ortho silicate	$Si(OEt)_4$	168	760
Tetra methyl ortho silicate	$Si(OMe^*)_4$	153	760

Me*: CH_3, Et:C_2H_5, Pr:C_3H_7, n-Bu:C_4H_9.

Rajendran et al. (2002) prepared calcium silica phosphate glass with Na_2O addition by melt quenching technique. They studied the mechanical properties like the elastic module, attenuation, Vickers hardness, fracture toughness and fracture surface energy at room temperature. They observed that the strength of the glass network continued up to 45wt%of SiO_2 content through the acoustical parameters such as velocities, attenuation, module, Debye temperature and Poisson's ratio. At above 45wt% of SiO_2, the synthesized glass showed the softness behavior and they observed that Si-O-Si bands were broken with the non bridging oxygen formation in the silica glass network.

Saravanapavan et al. (2003) synthesized the mesoporous calcium silica phosphate glasses by sol-gel method. They observed that due to the slower stabilization in sol-gel process for smaller specimen size, low Ca gels showed clear and transparent nature, where as the high Ca gels showed transparent to translucent nature and gels with still higher Ca content were opaque. They also observed that with increase in the sintering temperature the glass structure changed into crystalline structure.

Sooraj Hussain et al. (2004) prepared calcium phosphosilicate gels by sol-gel method. Increase in SiO_2 concentration lead to increase in the crystalline nature, decrease in the amorphous nature.

Rafiqul Ahsan et al. (2005) prepared a ternary silicate glass system with CaO and P_2O_5 combination. Through IR spectra they observed that the P_2O_5 structure changed from orthophosphate to metaphosphate state and from metaphosphate to pyrophosphate state with increase in P_2O_5 content. Due to this reason the silicon position changed from tetrahedra to octahedral state with increase in P^{+5} ions.

Carta et al. (2007) synthesized the P_2O_5-CaO-Na_2O ternary glass by sol-gel method. They observed that with increase in CaO/Na_2O ratio, Q^2 (metaphosphoric) groups have increased. This result showed that the increase in CaO leads the increases the amorphous nature.

Ma et al. (2010) synthesized the calcium silica phosphate glass by sol-gel method. They observed that with increase in sintering temperature from 890 °C to 929 °C the amount of pseudo wollastonite structure decreased and the wollastonite structure increased. It indicated that the amorphous nature of the glass changed into crystalline nature with increase in the temperature.

Mozafari et al. (2010) synthesized the mesoporous calcium silica phosphate glasses by sol-gel method. They observed that the size and shape of the pore was not only associated with the calcium content but also depended upon the textural parameters of the glass. It was also observed that the high specific area lead to the high release of calcium which allowed the formation of the pore with large size.

Aguiar et al. (2010) prepared the SiO_2–P_2O_5–CaO glass system by using sol-gel method and on the basis of bonding configuration they studied the structural and textural properties at different stabilization temperature conditions. Raman and infrared spectroscopic studies demonstrated the heat treatment, causes a repolymerisation of the glass structure. They induced the configurational transitions from reactive chains to the more stable condensed rings through incorporation of calcium cations into the glass network. High-resolution transmission electron microscopy analysis revealed that H and/or Ca-rich orthophosphate groups were present with nano crystalline areas in the amorphous glass materials based on stabilization temperature.

Aguiar et al. (2011) prepared bioactive SiO_2–P_2O_5–CaO glass by sol-gel method and also studied the short range organization of the glass by using high-resolution transmission electron microscopy (HRTEM), Fourier transform infrared (FTIR) and magic angle spinning-nuclear-magnetic resonance spectroscopy (MAS-NMR) characterization techniques. By using these combined techniques they clarified the role of phosphorus and calcium during the heat-treatment stage. They observed that the formation of the P–O–NBO groups promoted by the incorporation of calcium into the glass structure which induced the formation of Ca-rich orthophosphate units. It showed, the decrease of the inter planner distance with the rearrangement of the glass

nanostructure. It indicated that the Si–O bond reaction role was more effective in the polymerization than P–O bond.

Sava et al. (2012) synthesized the silica phosphate glasses by the sol - gel method. They observed that, the gel formation time increased with the increase in the water quantity in the hydrolysis process independent of temperature conditions. Also, they observed that the increase in pH value decreased the gel formation time. They have also observed that the increase in the phosphorous oxide amount increased the gel formation time in selective pH values. On heating, they observed that there will be evaporation of organic material and water content which caused the formation of the Si-O-P bond. The characterizations carried out revealed that even at small amounts of phosphorous oxide, it was possible to form mixed network between phosphorous oxide and silicon oxide.

Vulpoi et al. (2012) prepared SiO_2-CaO-P_2O_5 ternary glass system with Ag_2O nano particles. They have carried out the structural, morphological and textural investigations. In their results XRD pattern showed that the samples had tricalcium phosphate (TCP) nanostructure phase. Using TEM images it was observed that spherical shaped silver nano particles with various sizes existed inside the glasses which were dependent on the percentage of Ag_2O content.

Daguano et al. (2012) prepared calcium silica phosphate glass with MgO. They observed mechanical properties like hardness and fracture toughness by Vickers micro-hardness measurements under the influences of various loads. It was observed that by applying the indentation under higher loads, the hardness decreased with increasing loads. It was due to higher plastic deformation in the material and increase in the penetration depth.

1.4 Applications of Sol-gel derived bio glasses

Sol-gel derived glasses can be used in many biomedical applications such as Tissue engineering, dental, cancer therapy etc.

Prabhu et al. (2013) synthesized MgO doped calcium phosphosilicate glasses. They observed that increase of MgO caused the increase in pore diameter. It was also

observed that the increase in MgO caused the improvement of biological properties without toxic effect.

Li et al. (2014) synthesized the NH_4HF_2, CaF_2 doped Na_2O-CaO-P_2O_5-SiO_2 glass ceramics by sol-gel technique and studied mechanical properties. They observed that NH_4HF_2 doped glasses had less hardness than CaF_2 doped glasses. NH_4HF_2 doped glass ceramics showed good bioactivity than CaF_2 doped glass ceramics in environment of simulated body fluid solution. So, glass ceramics with lower hardness were good for biomedical application. Zarifah et al (2016) studied the effect of hydroxyapatite reinforced with 45S5 glass on physical, structural and mechanical properties at different sintering temperature conditions. It was observed that density and hardness of glass were decreased with increase in HA reinforcement. Since HA layer decomposed and formed tricalcium phosphate, sodium calcium phosphate and calcium phosphate silicate, it leads to the pores formation in glass structure.

Amirhossein et al (2017) synthesized sol-gel derived 58S bio-glass with lithium addition and studied in vitro bioactive properties. Si and Ca ions dissolution was more for 5 mol% doped 58S glass than that of 10 mo% Li_2O doped glass, due to this reason 5 mol% Li_2O doped 58S glass got more HCA on its surface than 10 mol% Li_2O doped glass. Finally, it has been concluded that 5 mol% Li_2O addition showed good bioactivity whereas 10 mol% Li_2O addition suppressed the bioactivity. It indicated that lesser Li_2O content favors the bio-activity of sol-gel derived 58S glass.

Silicate-based bioglass nano particles are gaining increasing attention in various bio applications due to their distinctive properties. Bioactive nano particle characteristics, such as composition and morphology, determining the bio glass nano particle properties depend on synthesis process. Controlled synthesis of sol-gel derived bioglass nano particle, is critical to their effective use in biomedical applications. In the last decade, many investigations focused on bioglass nano particle synthesis which had been already reported. Mainly bioglass nano particles can be produced through the sol-gel or melt-quench approach. Boccaccini and Zheng, (2017) reviewed the strategies of sol-gel

processing of bioglass nano particles, including different catalysts effect for initiating the hydrolysis and condensation of silicate precursors and also combining sol-gel chemistry with other preparation techniques. Bioactive nano particles are particularly interesting biomaterials in bone rerelated applications, they have potential for other biomedical applications such as soft tissue repair/regeneration.

Anjaneyulu and Vijayalakshmi, (2017) studied the effect of sol-gel derived hydroxyapatite/Fe_3O_4 composites coatings on Ti-6Al-4V in biomedical applications. For this study they used Fe_3O_4 concentrations as 1, 3 and 5 wt% respectively. *In vitro* bioactivity study confirmed that the composite coated Ti-6Al-4V was highly bioactive and induced bone like apatite formation in Fe_3O_4 nano particles presence, it involves the nucleus formation by developing Fe-OH groups on the coated surface. The corrosion resistance study proved that 1 wt% of Fe_3O_4 with hydroxy apatite composite coatings showed good anticorrosion behavior than the 3 and 5 weight% of Fe_3O_4 coated composite due to lower Fe-OH groups. From all these observations it can be concluded that HAP/Fe_3O_4 composites coated implants favor the biomedical properties.

Compared to cortial bone, bioactive glasses have poor mechanical strength and higher modules. Due to this reason they cannot implant into load-bearing bone defects alone. So, they cannot be used alone to regenerate a full thickness bone defect-metallic fixation, which is required in those applications to take the cyclic load. Therefore bioactive glass and glass-ceramics are often used to repair bone defects, these defects are surrounded by host bone. However, bio glasses can incorporate in composite structures and form into fibers or scaffolds to improve mechanical properties and biomimetic apatite bone formation speed. Sol-gel derived calcium phosphosilicate glasses created historical wonder in the biomedical field because of their life saving applications. These glasses can form bone and regenerate tissues in physiological environment like simulated body fluid (SBF) solution. The bio active nature of these glasses are mainly depends on both strength of implanted materials like silica glass matrix, and hydroxy carbonated apatite (HCA) layer formation in SBF solution (Jones and Clare 2012).

1.5 Steps in the formation of HCA layer in SBF solution

HCA layer is formed on the glasses in 5 stages when they are immersed in SBF solution.

Step 1 Migration of calcium ions into SBF solution from calcium phosphosilicate glasses: In this process calcium ions migrate into SBF solution and leave oxygen anions in the glass structure.

Step 2 Formation of silanol groups by incorporation of H^+ ions from SBF solution into glass matrix: In this stage, H^+ cations from SBF solution move towards oxygen anions and form silanol groups.

Step 3 Formation of silica gel layer on glass surface by poly condensation process: In polymerization and condensation processes silica gel layer forms on glass surface. This silica gel layer acts as an implanted material for further process.

Step 4 Calcium, phosphate ions leaching on silica gel layer surface causes the amorphous calcium phosphate (apatite) layer formation: After silica gel layer formation, calcium and phosphate ions travel from glass matrix into SBF solution through silica gel layer and form calcium phosphate layer. This calcium phosphate layer is called as apatite layer. Apatite layer has amorphous nature.

Step 5 HCA crystallization takes place due to incorporation of hydroxyl, carbonate ions into apatite layer: Hydroxyl, carbonate ions are present in SBF solution. These ions get incorporated into apatite layer. Due to chemical reaction among hydroxyl, carbonates and apatite layer, apatite layer gets converted into hydroxy carbonated apatite (HCA) layer. HCA layer has similar properties as that of natural bone.

1.5.1 *IN VITRO* STUDIES

Bio active glasses were widely used *in vitro* studies. These glasses showed bioactivity in the SBF test with HCA bio mimetic nano crystalline formation within a few hours. The osteogenic and cytotoxic behavior also assessed *in vitro* using various cell lines. In the presence of bioglass, osteogenic cells show increase in metabolic activity in dissolution process. Cell appearance follows the chemistry of the HCA layer and nano

topography. And they respond to critical concentrations of soluble calcium and silica ions released by the glasses.

1.5.2 *IN VIVO* STUDIES

Animal studies are required before implanting bioglass devices in human body. To reduce the number of animals and to obtain consistent results, effective models are required. The perfect animal model to investigate the efficiency of bio-ceramics in bone regeneration process was developed by Oonishi et al. (2000) using the rabbit leg bone.

The first bioglass product was found by Larry Hench to middle ear prosthesis (Merwin 1986). It was available only in two sizes of cone-shaped implants. Every clinical case was somewhat different, requiring a device it could be shaped by the surgeon. This limited the commercial success of the device and it is also a problem for all bio ceramic implants for injecting the device. Fujibayashi et al (2003) studied comparison of the *in vivo* and *in vitro* behavior for soda lime silicate bio-glasses (phosphate-free glasses). In this case, the *in vitro* bioactivity decreased with increase in silica content. Due to this reason it can be said that optimization of composition concentration is also important factor in bioactive studies.

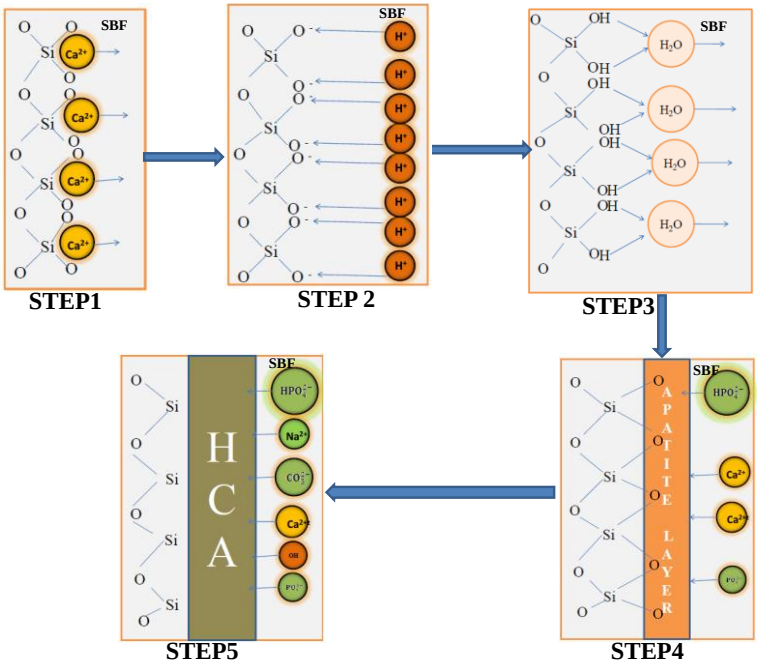

Figure 1.8 Schematic diagram for HCA formation process of silicate bio- active glass

SiO_2-CaO-P_2O_5 based glasses constitute a promising material for bioactive applications such as bone repair, tissue regeneration in the human body, etc (Kokubo and Takadama 2006). Implantation of these materials in the human body induces a specific biological response at the material interface and can be promoted new bone formation without forming fibrous tissues. This new bone can form a bond to living bone which is inside the human body (Bellucci et al. 2014).

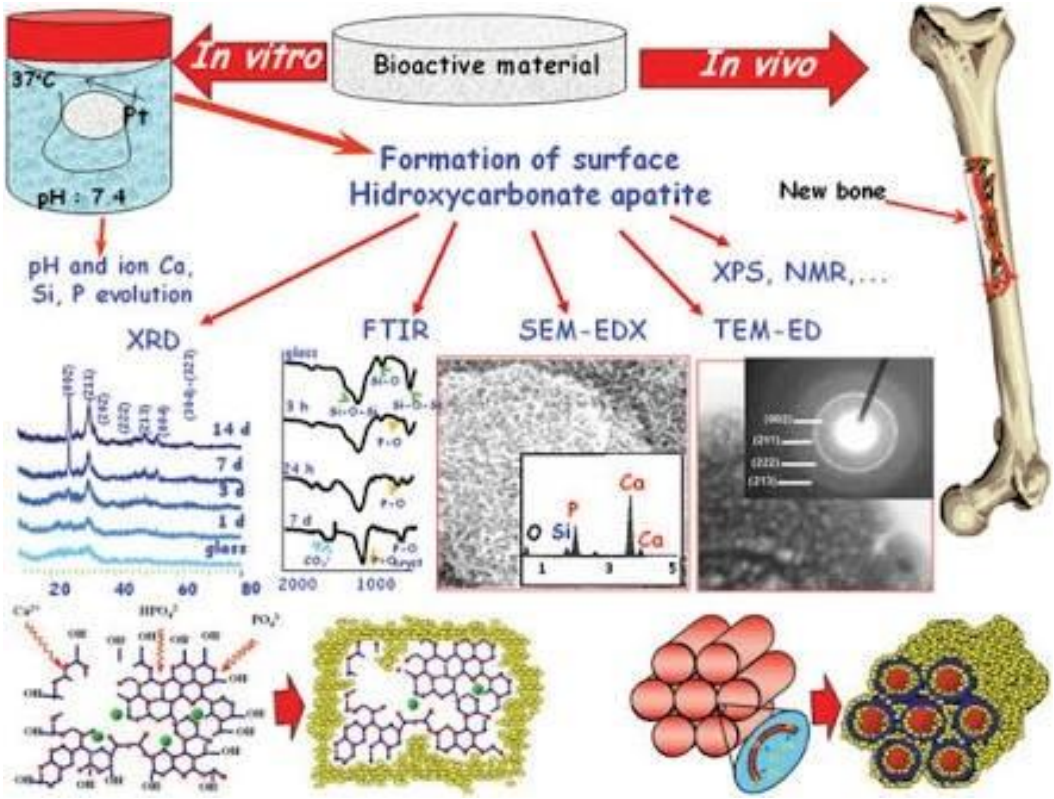

Figure 1.9 Characterization techniques employed to evaluate the bioactive response of bio ceramics after soaking in SBF. Bottom of the figure shows schematic representation (Antonio and Vallet-Regı 2013)

1.6. Scope and objectives of the Thesis

1.6.1 Scope of the Thesis

The bone bonding ability of these materials has been attributed to the deposition and growth of a hydroxyapatite (HA) layer, which is close to bone mineral composition (Bellucci et al. 2014). In crystallization process, HA layer can be converted as hydroxy carbonated apatite (HCA) layer in the presence of SBF solution (Yousefi et al. 2014). Sol-gel technique is an alternative route to synthesize the bioactive glasses with higher purity and homogeneity compare with melts quenching technique (Shelby 2005, Jones and Clare 2012, Carta et al. 2007, Catauro et al. 2014). Compared to the melt quenching method, sol-gel method enables obtaining the glasses with higher porosity and surface area. This feature helps to improve bone bonding rates and favours excellent resorption and degradation in physiological environments (Bellucci et al. 2014, Goller et al. 2004, Arcos et al. 2010).

The limitation of SiO_2 content to get HA layer for SBF soaked calcium phosphosilicate glasses is 60 mol % in melt quenching method and 90 mol% in sol-gel method. Due to this reason, the sol-gel method is the best feasible technique to get a HA layer formation (Wu et al. 2012, Siquira et al. 2013, Radev et al. 2014, Catauro et al. 2014). HCA layer formation in the presence of SBF solution depends on different process parameters such as glass composition (Catauro et al. 2014), porosity (Wu et al. 2012), preparation method (Liu et al. 2012), precursors (Jones and Clare, 2012) and sintering temperature (Hashmi et al. 2013) etc. In bio-medical applications, HCA formation in SBF solution mainly depends on the dissolution behavior of the glass matrix (Peitl et al. 2001).

Laczka et al. (1999) reported that gel polymerization and crystallization process at different temperature conditions, depended on the selection criteria of using precursors for CaO and P_2O_5 contents. Sopcak et al. (2015) reported the precipitation mechanism for $CaO\text{-}SiO_2\text{-}P_2O_5$ system depends on different Ca/P ratios at different pH values, and also revealed that increase in calcium content increases amorphous nature. For SiO_2-CaO glasses HCA forming ability in SBF solution depends on the ratio of sample weight to volume of SBF solution volume in incubation conditions (Shelby 2005).

For SiO_2-CaO-P_2O_5 glasses, the studies related to the improvement in the HCA growth rate in SBF solution are available based on the precursors used in the synthesis process and heat-treatment conditions (Bellucci et al. 2014).

HCA formation of bio glass in bio fluids strongly depends on the dissolution of network modifiers such as CaO, BaO and Na_2O. Change in network modifier concentration changes the glass strength. Change in strength leads to dissolution behavior of glass, it influences the HCA formation. Due to this reason, using *in vivo* studies, calcium phosphosilicate glasses can be studied for biomedical applications such as cancer therapy and tissue engineering, etc.

Bio-activity of glass depends on the dissolution of the glass material in bio-fluids such as simulated body fluid solution. Network formers and network modifiers play major role in the dissolution process. Information on *in-vitro* bio activity studies is available based on network former and modifier compositions. Very less information is available with same kind of network former and different kinds of network modifier compositions.

In SBF treatment HCA forms on SiO_2 layer. P_2O_5 helps to apatite (calcium phosphate) layer formation on silica gel layer after which HCA forms in chemical reaction process with SBF. In dissolution process Ca^{2+}, PO_4^{3-} ions dissolve in SBF solution. The dissolution depends on internal network connectivity strength between network formers and network modifiers. Calcium ionic radius is less than barium. Due to this, calcium ion can increase glass strength where as barium contained glass has less strength.

HCA formation studies are available for barium soda lime phosphosilicate glasses prepared by melt quenching technique, but not for glasses prepared by sol-gel technique. In the present thesis HCA formation studies have been done for ternary calcium phosphosilicate glass system. Based on ternary glass system the quaternary and tertiary glass systems were developed. In the present thesis HCA layer formation for SBF soaked ternary, quaternary and tertiary phospho silicate glasses were studied and NBO/BO ratios are compared.

1.6.2 Objectives of the Thesis

The following are the objectives of the thesis:

1. The synthesis of ternary calcium phosphosilicate dried gels, with various compositions $58SiO_2$-$(19-x)P_2O_5$-$(23+x)CaO$ by varying x from 0 to 15 mol %.

2. The synthesis of ternary calcium phosphosilicate glasses, with various compositions $58SiO_2$-$(19-x)P_2O_5$-$(23+x)CaO$ by varying x from 0 to 15 mol %.

3. The synthesis of quaternary calcium phosphosilicate glasses, with various compositions $58SiO_2$-$(38-x)CaO$-xNa_2O-$4P_2O_5$ by varying x from 5 to 20mol %.

4. The synthesis of tertiary calcium phosphosilicate glasses, with various compositions $58SiO_2$-$4P_2O_5$-$(32-x)$ BaO- $xCaO$-$6Na_2O$ by varying from 15 to 30 mol %.

5. To study the structural and morphological properties of ternary calcium phosphosilicate dried gels.

5. To study the thermal, structural and morphological properties of ternary, quaternary and tertiary calcium phosphosilicate glasses.

6. To study the structural and morphological properties of calcium phosphosilicate glasses during *in vitro* studies.

1.7 Organization of the Thesis

The thesis is organized as follows:

Chapter 1 presents an introduction to glass, an overview of structural theories, and types of glasses, preparation methods. This chapter includes the bio-medical application of glasses. This chapter also gives the information on the literature survey of glasses, their importance in biomedical application and scope and objectives and organization of the thesis.

Chapter 2 deals the synthesis and characterization of calcium phosphosilicate dried gels, glasses. This chapter also discusses the hydroxy carbonated apatite (HCA) layer formation in calcium phosphosilicate glasses with CaO and P_2O_5 variation.

Chapter 3 deals the synthesis and characterization of soda lime phosphosilicate glasses. This chapter also gives an account of hydroxy carbonated apatite (HCA) layer formation in soda lime phosphosilicate glasses with CaO and Na_2O variation.

Chapter 4 deals the synthesis and characterization of barium soda lime phosphosilicate glasses. In this chapter formation of hydroxy carbonated apatite (HCA) layer formation in barium soda lime phosphosilicate glasses with BaO and CaO variation

Chapter 5 gives the overall summary of the results described in the previous chapters. Further, the scope for future research work in this area is also discussed.

CHAPTER 2

SYNTHESIS AND CHARACTERISATION OF CALCIUM PHOSPHOSILICATE GLASSES

Present chapter deals with the synthesis of calcium phosphosilicate dried gels, glasses and also includes the thermal properties of calcium phosphosilicate dried gels. Morphological properties for dried gels, such as surface morphology and porosity were studied using FESEM and EDX analysis. Structural and surface morphological properties of dried gels, synthesized and SBF treated calcium phosphosilicate glasses were studied through XRD, FTIR, Raman spectroscopic characterization techniques. HCA formation in SBF treated samples was confirmed by TEM/SAED analysis. Surface morphological properties were studied using SEM and EDX analysis. Based on composition variation, HCA forming ability studies have been carried out by studying dissolution of phosphate and calcium ions in SBF solution.

2. 1 INTRODUCTION

The oxide glasses like SiO_2, GeO_2, B_2O_3 and P_2O_5 can form three dimensional random networks by themselves (Shelby 2005). Among them only silicate glass can be used as a single component glass. The addition of alkali or alkaline oxides (network modifies) to SiO_2 (network former) leads the formation of non-bridging oxygens and changes the densities of glasses. Change in glass density depends on glass synthesis methods (such as sol-gel and melt quenching method) also. The sol - gel process is a low temperature process (Danial et al. 2010) where as melt quenching is high temperature process. Sol-gel derived glasses have low density (with high porosity) compared to melt quenched glasses. In sol-gel method increase in drying temperature increases the pore densities in the dried gel (Ma et al. 2010). Hench also revealed that drying and stabilization conditions change porosity of sol-gel derived glasses (Hench 2009), which leads to the dissolution of these glasses in SBF solution (Peitl et al. 2001, Lei et al. 2009, Gerhardt and Boccaccini 2010).

In bio-medical applications, HCA formation in SBF solution is mainly due to the dissolution behavior of the glass matrix (Peitl et al. 2001). In dissolution process, glass network connectivity is one of the interesting factors (Jones and Clare 2012). In the case of calcium phosphosilicate glasses, SiO_2 and P_2O_5 are network formers. The commonly used network modifiers such as CaO and Na_2O release cations of Ca^{2+}, Na^+ which migrate into SBF solution. This process eventually leads to the disconnectivity of the glass network and results in the formation of silanol groups. Later, it can affect the formation of silica gel layer through the polycondensation process, on silica gel layer HCA formation takes place (Lukito et al. 2005).

Due to difference in bond strength, SiO_4^{4-} and PO_4^{3-} cannot form complete solution in the glass. But for low P_2O_5 contents SiO_4^{4-} and PO_4^{3-} groups may have co-polymerization capability, because P^{5+} may substitute for Si^{4+}. Higher P_2O_5 content causes the Si-O-P bond formation. The Si-O-P bond causes the bending vibration of SiO_6 octahedral rather than silicon tetrahedra (Ahsan and Mortuza 2005, Ahamd Mooghari et al. 2012).

As reported by the earlier workers, in the case of CaO-P_2O_5-SiO_2 gels, increase in SiO_2 content increases the crystalline intensities of β and γ-($Ca(PO_3)_2$) phases [Sooraj Hussain et al. (2004). Laczka et al. (2000) reported that gel polymerization and crystallization process at different temperature conditions depend on the selection of precursors for CaO and P_2O_5 contents. Sopcak et al. (Sopcak et al. 2015) reported that the precipitation mechanism for CaO-SiO_2-P_2O_5 system depended on different Ca/P ratios at different pH values, and also revealed that increase in calcium content increases amorphous nature.

HCA layer formation in SBF solution also depends on different process parameters such as glass composition (Zhang and Gou 2012), precursors (Jones and Clare 2012) and sintering temperature (Hashmi et al. 2013). For SiO_2-CaO glasses HCA forming ability in SBF solution depends on the ratio of sample weight to volume of SBF solution in incubation conditions (Shelby 2005). For SiO_2-CaO-P_2O_5 glasses, the studies related to the improvement in the HCA growth rate in SBF solution are available based

on precursors used in the synthesis process and heat-treatment conditions (Bellucci et al. 2014). According to Ahsan and Mortuza (2005), the addition of P_2O_5 up to 5 mol % can depolymerize the glass system. In calcium phosphosilicate glasses, orthophosphate units de-polymerize the glass system and can also play the same role as Na_2O, i.e., network modifier. Laczka et al. (1999), Sun et al. (2015) reported that the increase in P_2O_5 composition (P_2O_5>9%) can enhance the degree of polymerization by acting as a network former (Simon and Mocuta 2004)..

In the present chapter, synthesis of $58SiO_2$-(19-x)P_2O_5-(23+x)CaO [x = 0, 5, 10 and 15 mol %] dried gels and gel derived glasses using the sol-gel method has been presented. The effective role of P_2O_5 on structural and surface morphological properties of prepared dried gels and gel derived glasses have been discussed. These glasses were soaked in the SBF solution for 7 days to get HCA formation on the glass surface. Thermal, structural and morphological properties were studied using X-Ray Diffraction (XRD) technique, Thermo Gravimetric Analysis with Differential Thermal Analysis was used to study the thermal properties of these glasses. It may be noted that the studies on NBO/BO ratio effect on HCA forming ability of SiO_2-CaO-P_2O_5 bioactive glass system in SBF solution, are not adequate. In the present study, NBO/BO ratio was found using Raman spectroscopic analysis. The impact of CaO/P_2O_5 content on NBO/BO ratio and the effect of NBO/BO ratio on HCA forming ability of SBF soaked glass samples were studied in detail.

2.2. Materials and methods

2.2.1 Synthesis of calcium phosphosilicate dried gels and glasses

$58SiO_2$-(19-x)P_2O_5-(23+x) CaO (x= 0, 5, 10 and 15 mole %) samples were synthesized by the conventional sol-gel process and named as CPS1, CPS2, CPS3 and CPS4, respectively. The selected precursors for preparation were tetraethylorthosilicate [$Si(OC_2H_5)_4$] (≥99%), triethylphosphate (TEP) [$(C_2H_5O)_3PO$] (≥99%), calcium nitrate tetra hydrate [$Ca(NO_3)_24H_2O$] (98%) Required chemicals for synthesis were purchased from Merck company (Mumbai, India). H_2O and HNO_3 (69%) were taken as [(mol of H_2O)/(mol of TEOS+ mol of TEP) = 10] and [(mol of HNO_3)/(mol of TEOS+ mol of

TEP) = 0.05], respectively. In order to synthesise the glass sample, TEOS was mixed with H_2O and HNO_3 and stirred for one hour. At an interval of one hour, TEP and calcium nitrate, were added subsequently and stirred well. The prepared sols were poured into teflon beakers, sealed and kept inside hot air oven at 60°C temperature for three days for aging purpose. Subsequently the aged gels were dried at 130 °C for 4 hours. These dried gels were ground, made into powders and heated at the rate of 5°C/min up to 700°C and stabilized at that temperature for 4 hours to obtain glass samples in the powder form. After getting powder samples, pellets were prepared using hydraulic press by applying 5 tons of pressure for 5 minutes.

Prepared pellet samples kept in plastic centrifugal tube and filled with SBF solution and kept in incubator at 37 °C for 7days in static (unshakable) condition. The SBF solution selected on the basis of sample weight/SBF solution volume ratio as 10 mg/ml.

The structural properties of calcium phosphosilicate dried gels have been studied by X-ray diffraction technique, using Powder X-ray Diffractometer (PXRD) (JOEL, JDX-8P). The chemical characterization was performed by FTIR method (SHIMADZU spectrometer). For IR analysis, the first 1 mg of calcium phosphosilicate gels were carefully mixed with 300 mg of KBr (infrared grade) and palletized. Then the prepared pellets were analyzed in the range between 400 to 3000 cm^{-1} at a scan rate of 25 scan/min with the resolution of 4 cm^{-1}. Room temperature Raman spectroscopy was performed using a LABRAM-HR800 Laser Raman Spectrometer with 514 nm laser radiation. To avoid laser heating of the samples, the incident power was kept at a low value of 1.99 mW. Field emission scanning electron microscopy (FESEM, Carl Zeiss Ultra 55 model) of the centrifuged samples was used for the morphological analysis of the prepared powder samples. Sigma Scan Pro software was used to determine the average pore size of powder samples of CPS dried gels.

The glass transition temperature (Tg) and onset crystalline temperature (Tx) were identified by the TGA and DTA analysis (SII EXTRAR 6000, Japan) with a flow rate of

10 °C/min in the temperature range 27–1000 °C. Weight loss of samples, before and after SBF treatment was measured using an electronic weighing balance with an accuracy of 0.1mg [Sartorius, BT224s, India]. The structural properties of all samples have been investigated using the Powder X-ray Diffractometer (Rigaku, Miniplux 600, Japan) with a scan rate of 2°/min. Spherical shaped HCA particles of CPS samples were observed by TEM/SAED (JEOL JEM 2100, Japan), SEM (JEOL_JSM-6380LA, Japan) and elements present in the samples were identified by the EDX analyzer (JEOL, Japan). The types of vibration bands were identified by the FTIR spectrometer (SHIMADZU-8400s, North America). For FTIR analysis, the pellets were prepared using 300 mg of KBr mixed with 1 mg quantity of stabilized and SBF treated SCP glasses. The pellets were analyzed in the wave number range between 400 and 1800 cm^{-1}at a rate of 25 scans/min with the resolution of 4 cm^{-1}. Room temperature Raman spectroscopy was performed using a LABRAM-HR800 (Japan). To avoid laser heating of the samples, the incident power was kept at a low value of 2 mW. The pH value of SBF solution was measured using pH meter (Eutech, pH510, India) before and after soaking SCP samples. Ca^{2+} and PO_4^{3-} ion concentrations were measured using Flame Photometer (ELICO CL378, Germany) and UV/Vis absorption spectrometer (HITACHI PM & E 101, Canada). Table 2.1 shows the comparison and sample codes of synthesized glasses.

Table 2.1 Batch composition of $58SiO_2$-$(19-x)P_2O_5$-$(23+x)CaO$ dried gels, glasses.

Glass sample	SiO_2 (mol%)	P_2O_5 (mol%)	CaO (mol%)
CPS1	58	19	23
CPS2	58	14	28
CPS3	58	9	33
CPS4	58	4	38

2.2.2 Preparation of simulated body fluid (SBF) solution

To study the HCA growth properties of the synthesized samples, SBF solution has been selected as physiological environment which has similar properties as those of

human blood plasma. The SBF solution was prepared by dissolving reagent grade KH_2PO_4 (≥98%), $CaCl_2$ (≥98%), $NaHCO_3$ (99%), $MgCl_2.6H_2O$ (98%), KCl (99%) and NaCl (99%) in the de-ionised water at pH=7.4 with tris-buffer (99.8%) while maintaining temperature at 37 °C.

2.3. RESULTS AND DISCUSSION

2.3.1 XRD analysis of dried gel samples

The XRD analysis of CPS gel samples is shown in Figure 2.1(a). All samples have amorphous nature which indicates that CPS gel samples have internal disorder (Sun et al. 2015).

2.3.2 FTIR analysis of dried gel samples

Figure 2.1(b) shows the FTIR spectra of CPS dried gels. Different intensity signal occurs at around at the wave number region 462-478 cm^{-1} related to Si-O-Si bending modes (Table 2.2). The adsorption peaks at 941-972 cm^{-1} are very strong, assigned to the Si-O-Si asymmetric stretching vibrations. Si-O-Si symmetric stretching modes were observed at 825 cm^{-1}. Si-O-NBO bands were assigned at 915-933 cm^{-1}. PO_4^{3-} stretching modes of vibrations were also observed at 1195-1342 cm^{-1}. CPS1 gel has more pronounced stretching modes of PO_4^{3-} tetrahedra and CPS4 glass has the least. Increase in P_2O_5 content leads to shift of PO_4^{3-} stretching vibrations to higher wave number side. Si-O-P (as s), CO_3^{2-} (bend) modes were observed at 1033-1056 cm^{-1}, 1438-1442 cm^{-1} respectively. Water molecules (H-O-H), OH-groups were also observed at 1620-1697 cm^{-1}, 2345-2360 cm^{-1} respectively (Yang et al. 2012).

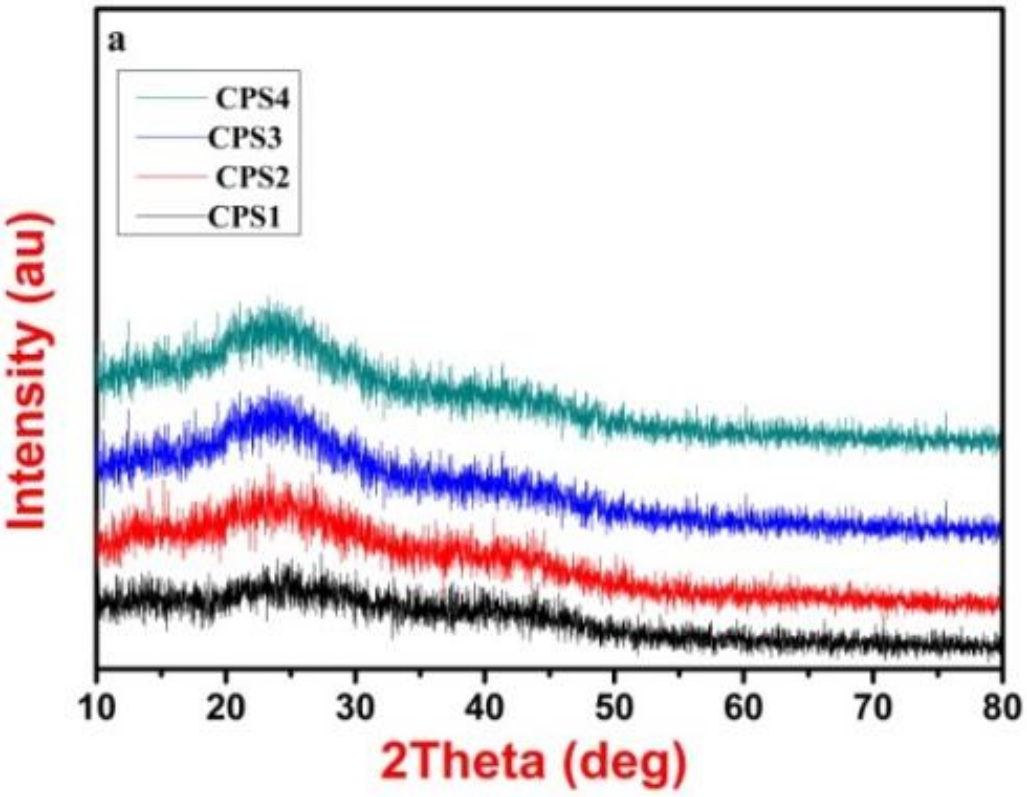

Figure 2.1(a) XRD pattern of CPS dried gels.

2.3.3 Raman spectroscopic analysis of dried gel samples

Raman spectra show that (Figure 2.1 (c)) PO_4^{3-} orthophosphate stretching modes (Q^0(P) as s) are assigned at 1050-1051 cm^{-1} (Sun et al. 2015). Q^0(P) intensities were increased from CPS1 to CPS4 dried gel. It indicates that increase in P_2O_5 addition decreases the $Q^0(P)^-$ intensities (Sun et al. 2015). Because increasing P_2O_5 content increases 3-dimensional network connectivity in polymerization process. In FTIR spectra also intensities of PO_4^{3-} stretching modes were increased from CPS1 to CPS4 dried gel.

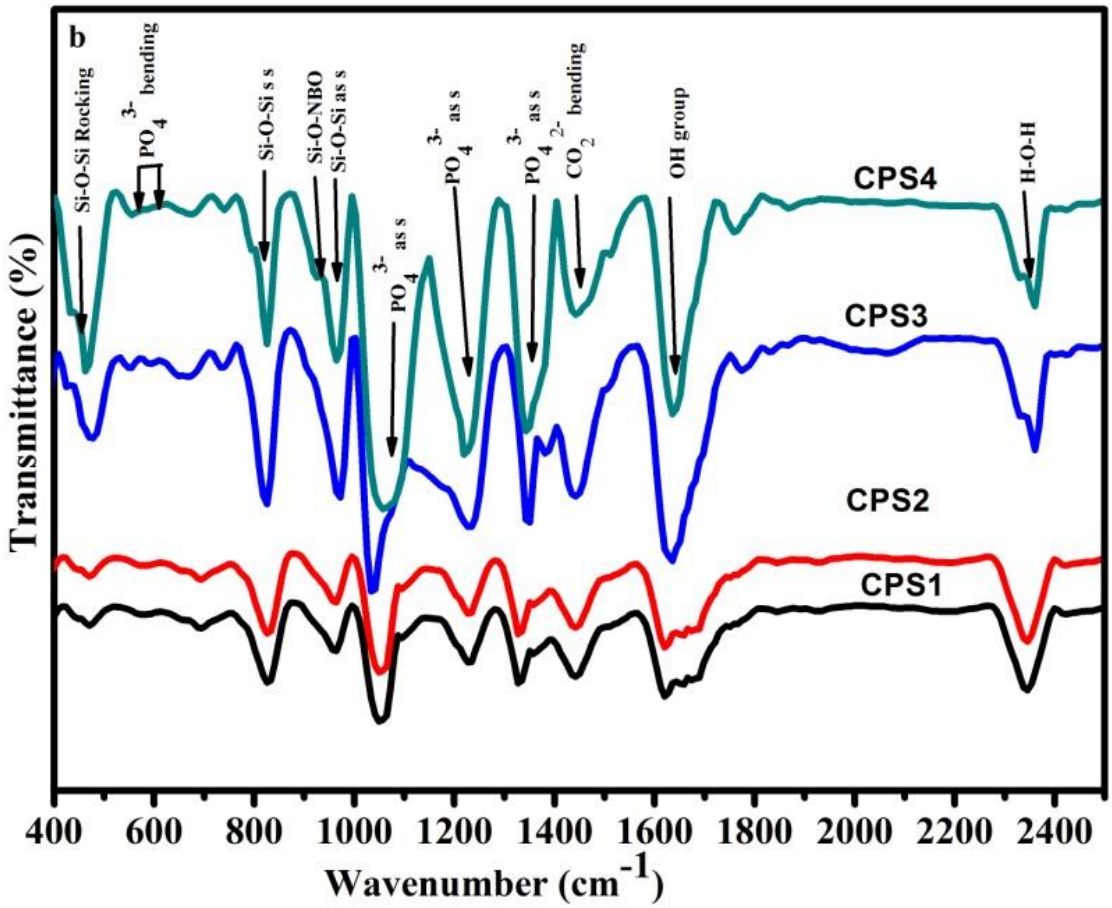

Figure 2.1 (b) FTIR spectra of CPS dried gels.

2.3.4 FESEM/EDX analysis of dried gel samples

Using FESEM images average pore sizes were measured as 143.51, 149.54, 173.25, 182.81 μm for CPS1, CPS2, CPS3, and CPS4 dried gels [as shown in Figure 2.2 and 2.3]. It indicates that increase in P_2O_5 content increases average pore size [Figure 2.4]. EDX analysis confirmed elements present in CPS gels are Si, Ca, P and O (Yang et al. 2012). Porosity influence internal structure as well as sample surface also. Porosity represents the capacity to accommodate water molecules in gel sample. In drying process, large amount of shrinkage leads to fracture on sample surface. The excessive shrinkage is due to a capillary forces, induced by liquid evaporation with micro pores formation. Increase in P_2O_5 with decrease in CaO increases local structural defects. These defects act

as hosts for water molecules. So, increasing P_2O_5 content increases the defect volumes. Increase in volume leads to increase in water molecule accommodations. In drying process water molecules evaporate through sample surface with capillary forces, this leads to pores formation with different sizes on sample surface. The pore size depends on size of evaporated water molecules through gel surface. The evaporated water molecule size may increase with increasing P_2O_5 content in CPS dried gels. It leads to increase in average pore size on sample surface. The capillary force formula is $P=2\gamma\cos\theta/D$, Where P, γ, θ, D are capillary force, liquid surface tension, liquid contact angle and micro pore diameters respectively (Shelby 2005). Due to this reason it can be concluded that increase in P_2O_5 content decreases the surface pore size. The observed average pore sizes were in the order of micrometer.

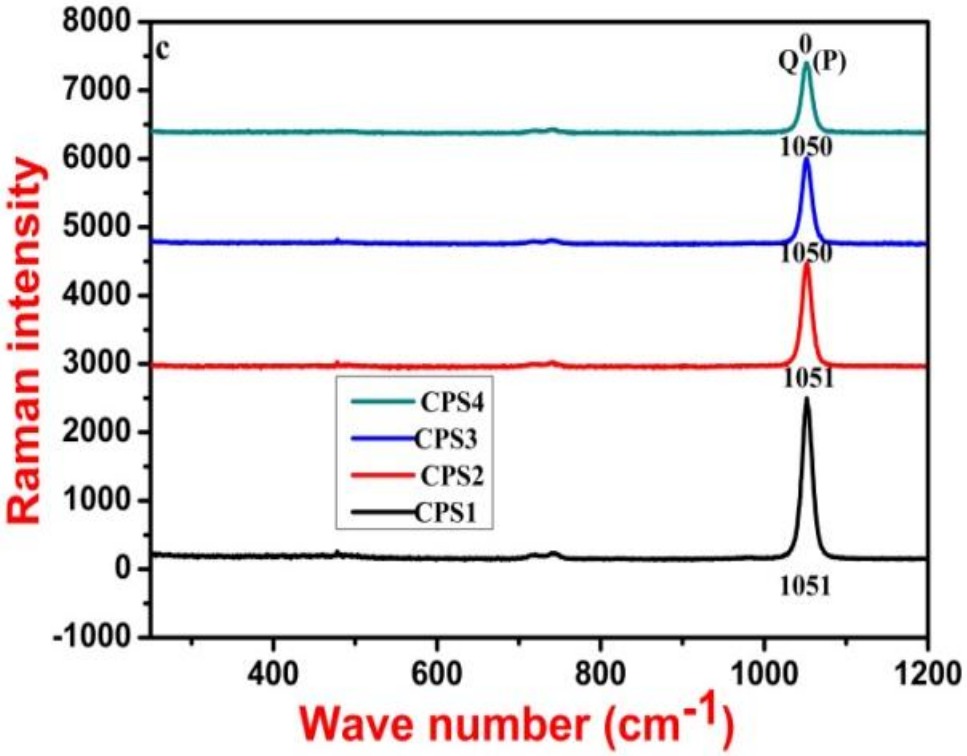

Figure 2.1(c) Raman spectra of CPS dried gels

Table 2.2 FTIR band assignments CPS gels (Infrared transition band in cm^{-1}).

CPS1	CPS2	CPS3	CPS4	Assigned bands	References
478	478	478	462	Si-O-Si rocking	[Li et al. 2014]
625-685	569-650	556-659	565-680	PO_4^{3-} bending	[Peitl et al. 2001]
898	915	918	933	Si-O-NBO (as s)	[Aguiar et al. 2008]
941	964	972	964	Si-O-Si (as s)	[Sun et al. 2014]
1041	1049	1033	1056	PO_4^{3-} (as s)	[Sun et al. 2014]
-	1438	1442	1442	CO_3^{2-} bending	[Li et al. 2014]
1697	1620	1615	1635	OH group	[Bellucci et al. 2011]

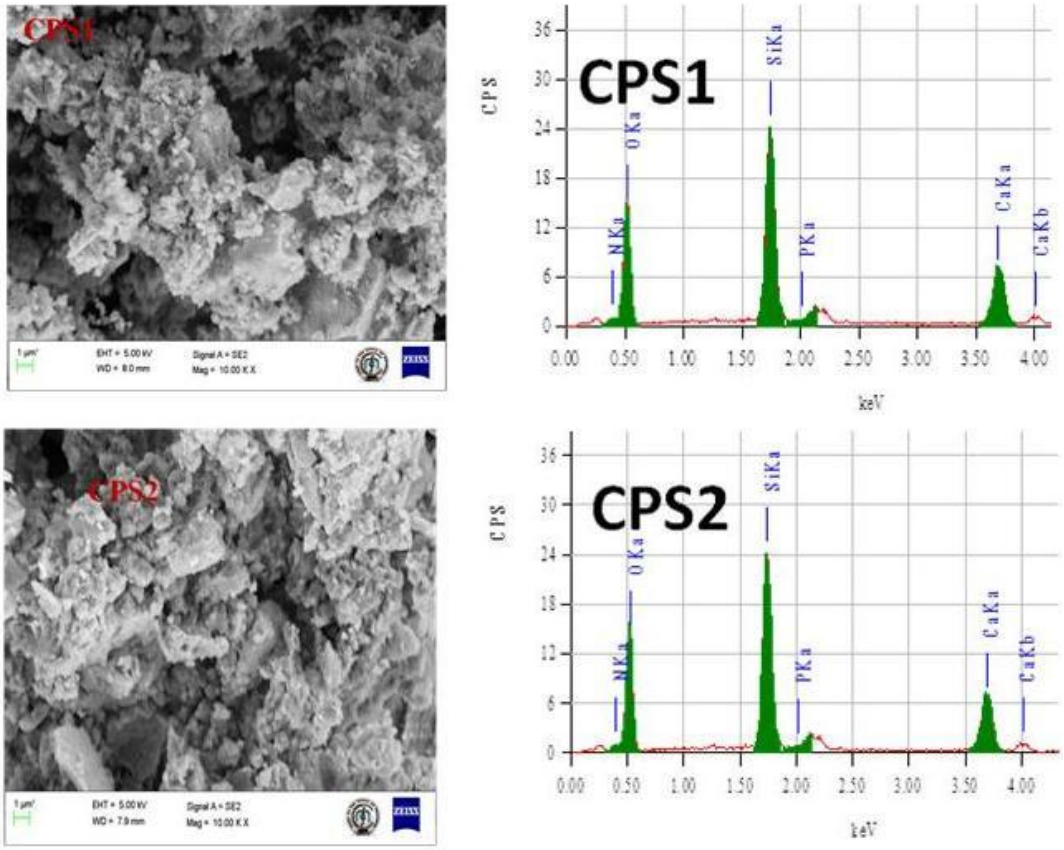

Figure 2.2 FESEM/EDX images of CPS1, CPS2 dried gels

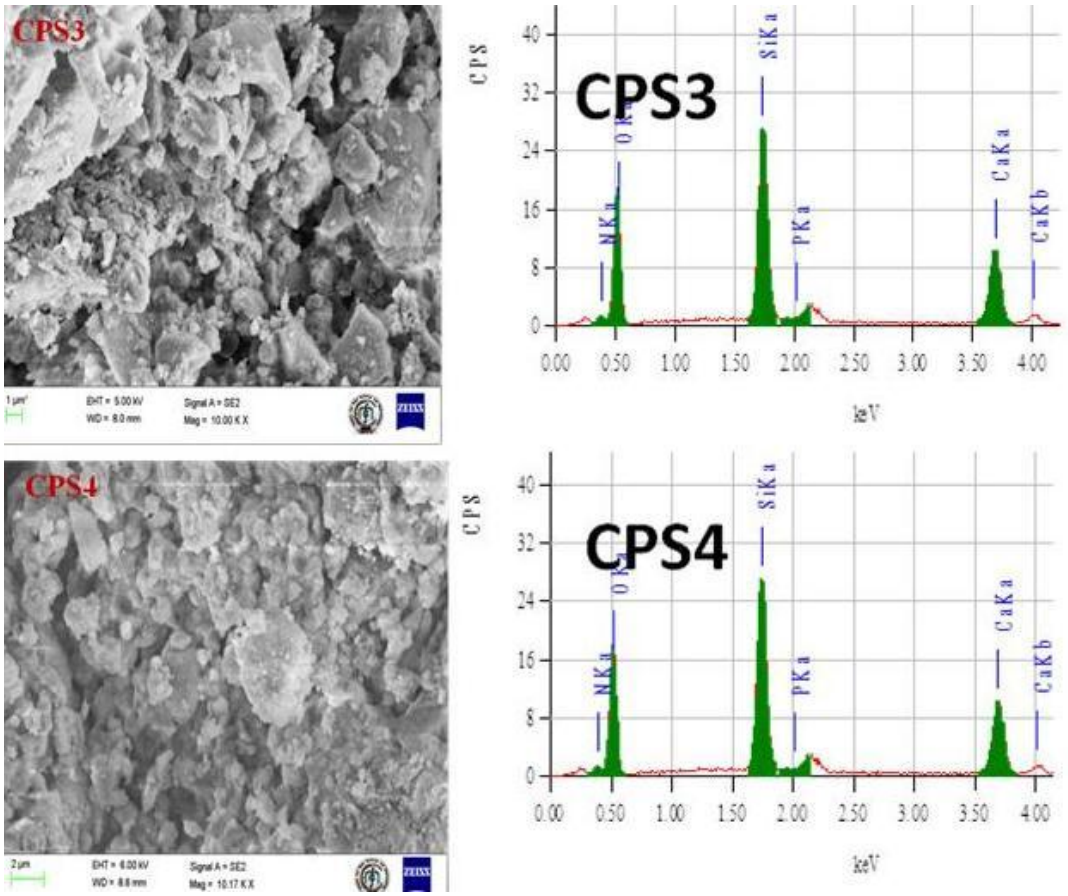

Figure 2.3 FESEM/EDX images of CPS3, CPS4 dried gels

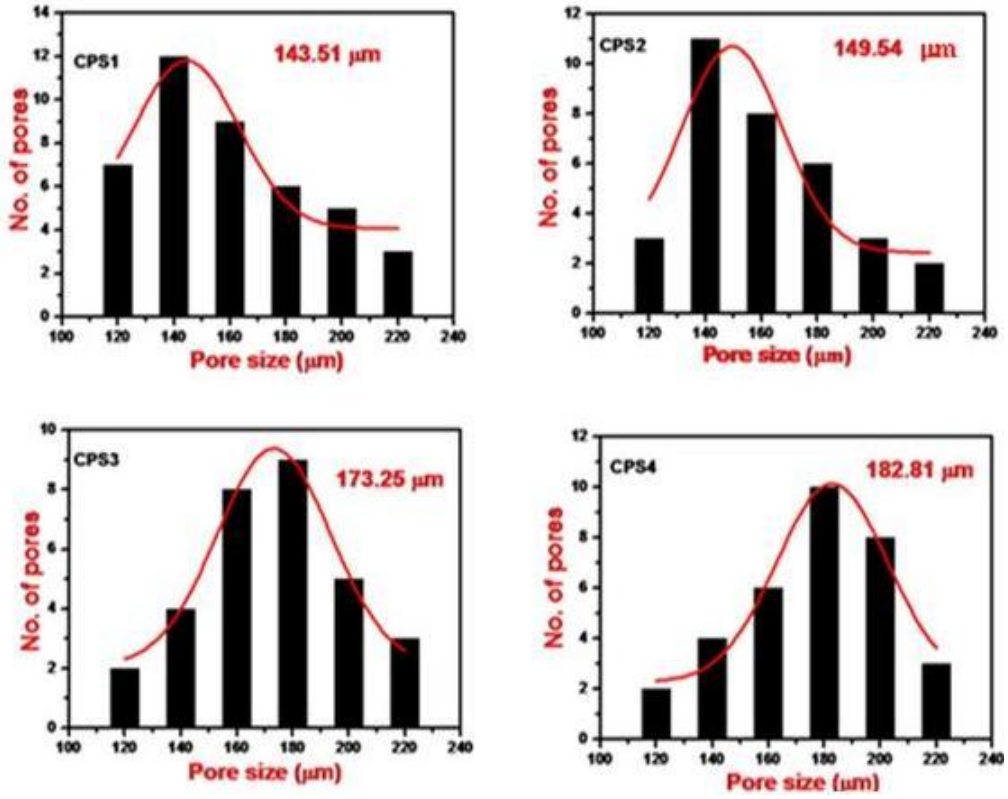

Figure 2.4 pore size distribution of CPS dried gels

2.3.5 TGA/DTA analysis

Thermal behavior CPS samples were studied using TGA/DTA analysis and the results are shown in Figure 2.5 (a-d). Two weight losses (T_{WL1} and T_{WL2}) were observed for CPS samples at different temperature conditions using TGA curves. The first weight loss (WL1) was observed at 452 ˚C – 494 ˚C related to the evaporation of organics (alkoxy groups) (Ma et al. 2011, Masoud et al. 2010). The second weight loss (WL2) related to the thermal evaporation of residual nitrates has been observed at 545 ˚C-563 ˚C (Ma et al. 2011, Yang et al. 2012). Glass transition (T_g) temperature and crystalline onset temperature (T_x) values were measured using the DTA curves for CPS dried gels as shown in Table 2.3 The glass forming ability is related to the variations in T_g and T_x values.

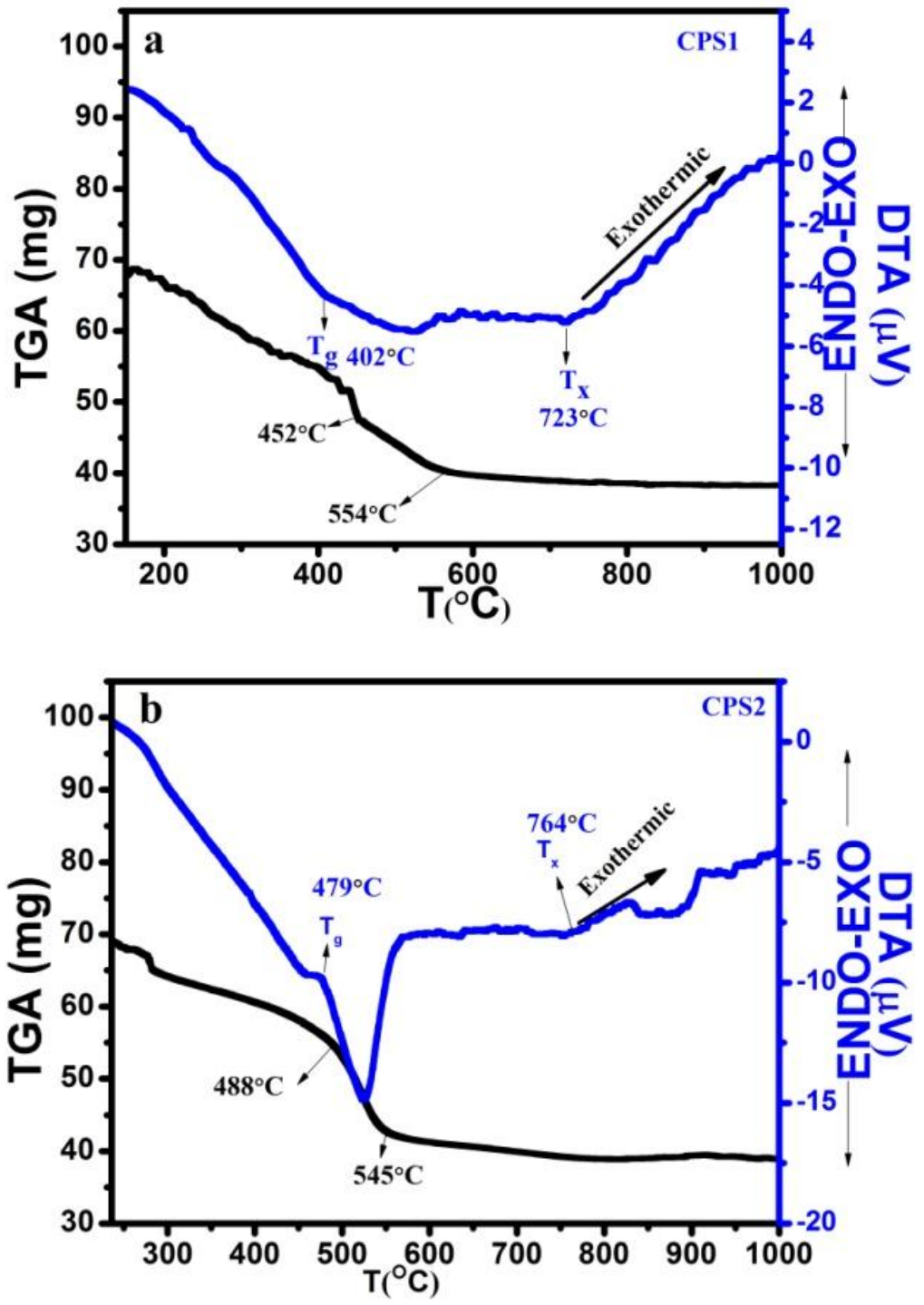

Figure 2.5 TGA/DTA curves of (a) CPS1, (b) CPS2 dried gels at 130°C.

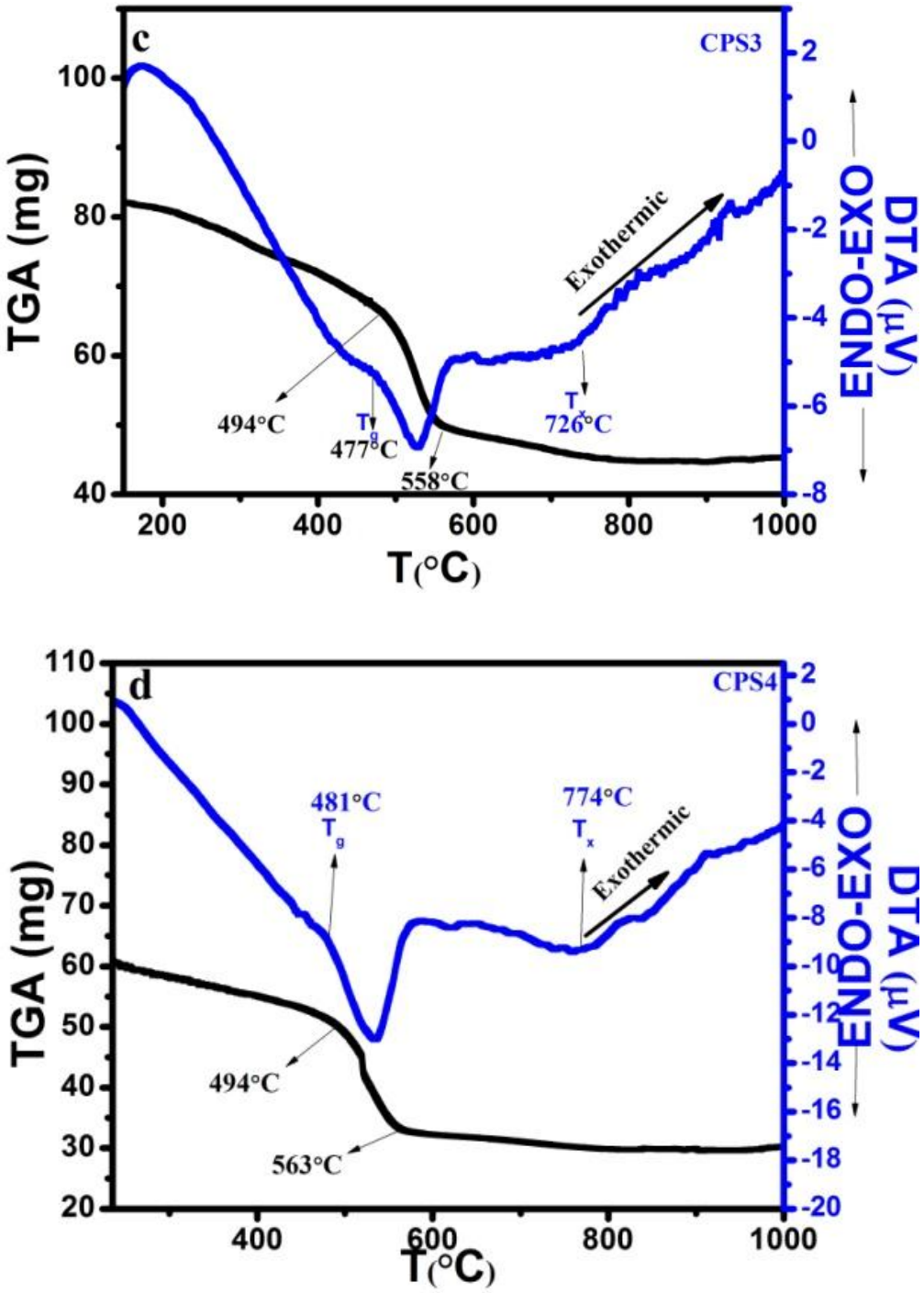

Figure 2.5 TGA/DTA curves of (c) CPS3 and (d) CPS4 dried gels at 130°C.

Table 2.3 TGA/DTA measurements for $58SiO_2$-(19-x) P_2O_5-(23+x) CaO glasses.

X mol%	Glass sample name	Fist weight loss (°C)	Second weight (°C)	T_g (°C)	T_x (°C)	ΔT T_x-T_g (°C)
0	CPS1	452	554	402	723	321
5	CPS2	488	545	479	764	285
10	CPS3	494	558	415	726	311
15	CPS4	494	563	481	774	293

Lucas-Girot et al. (2011) and Letaief et al. (2014) reported that for low P_2O_5 content, phosphorous is not considered as a glass former like silicon and it will be present in the glass structure as PO_4^{3-} ions acting like a glass modifier. Aguiar et al. (2008) observed that, in SiO_2-P_2O_5-CaO-Na_2O-MgO glasses, phosphorous does not act as a network former. Silicate glasses have enhanced bioactivity with inclusion of a small amount of P_2O_5. This remarkable inversion in the effect of P_2O_5 would be explained in the following way. Some of the phosphorous forms P-O-Si links and reduces the bioactivity (considered as negative effect) and some other is found as free orthophosphate, whose relatively fast initial release accelerates the HA deposition and boosts the bioactive process (considered as positive effect). The balance between these opposite effects decides the bioactivity of the P-containing composition. Based on the bioactivity data of the compositions modeled, Tilocca and Cormack (2007) concluded that the negative effect prevails for high P_2O_5 fractions, whereas positive effect prevails for that lower (below 10 mol % P_2O_5) fractions. From these literature supports, it could be concluded that P_2O_5 acts as a network former for CPS1 and CPS2 samples in the present study (with >10 mol % P_2O_5). For CPS3 and CPS4 samples P_2O_5 acts as a network modifier (with <10 mol % P_2O_5).

T_g and T_x values vary with P_2O_5 content. As the composition (x) increases from 0 to 5%, the T_g and T_x values increase. The observed P_2O_5 quantity is greater than 10 mol % in CPS1 and CPS2 samples and in this case, it (P_2O_5) acts as network former. P_2O_5

content is higher for CPS1 compared to CPS2 sample. Network former addition polymerizes the silicate network and decreases the required temperature to get glass formation as reported in the literature (Sun et al. 2015, Yang et al. 2012). As the P_2O_5 content is changing from 5 to 9 mol %, it acts as a network modifier. Compared to CPS2, CPS3 sample has less polymerization effect. In the network modifier case polymerization reduces and it leads to decrease in T_g and T_x values. As the mol% increases from 10 to 15% the T_g and T_x values increase. CPS3 and CPS4 samples have P_2O_5 less than 10 mol %. In this case, P_2O_5 acts as a network modifier and changes in T_g and T_x values depend on network modifier concentrations. Carta et al. (2007) reported that increase in network modifier content increases T_g, T_x values for soda lime phosphosilicate glasses. CaO (network modifier) content is more in CPS4 than CPS3 sample and P_2O_5 also acts as a network modifier for these samples. Depending on the network modifiers, increase in glass transition temperature and crystalline onset temperature takes place (Simon and Mocuta 2004). There is no significant weight loss above 700 °C in TGA curves. DTA curves show exothermic peaks above 700 °C. Due to this reason, 700 °C is considered as stabilization temperature for CPS samples (Masoud et al. 2010, Yang et al. 2012, Singh et al. 2009)

2.3.6 XRD analysis

The XRD pattern of CPS samples is shown in Figure 2.6 (a). The XRD pattern has broadband between the diffraction angles 20°-30°, indicating the amorphous nature. This occurs due to the internal disorders and glassy nature of the materials sintered at 700 °C. It was also confirmed by DTA analysis. The SBF treated samples show crystalline nature [as shown in Figure 2.6 (b)]. The dominant HA crystalite peak was identified at $2\theta = 32^{\circ}$ [(hkl) = (211)] corresponding to $Ca_5(PO_4)_3(OH)$ [HA] (JCPDS 01-074-0565). Calcite phase was also observed at $2\theta = 29°$ (JCPDS NO 01-081-2027). Another HA peak was observed at 38°. The intensities of three major reflections (211), (300), (002) increased from CPS1 to CPS4 sample.

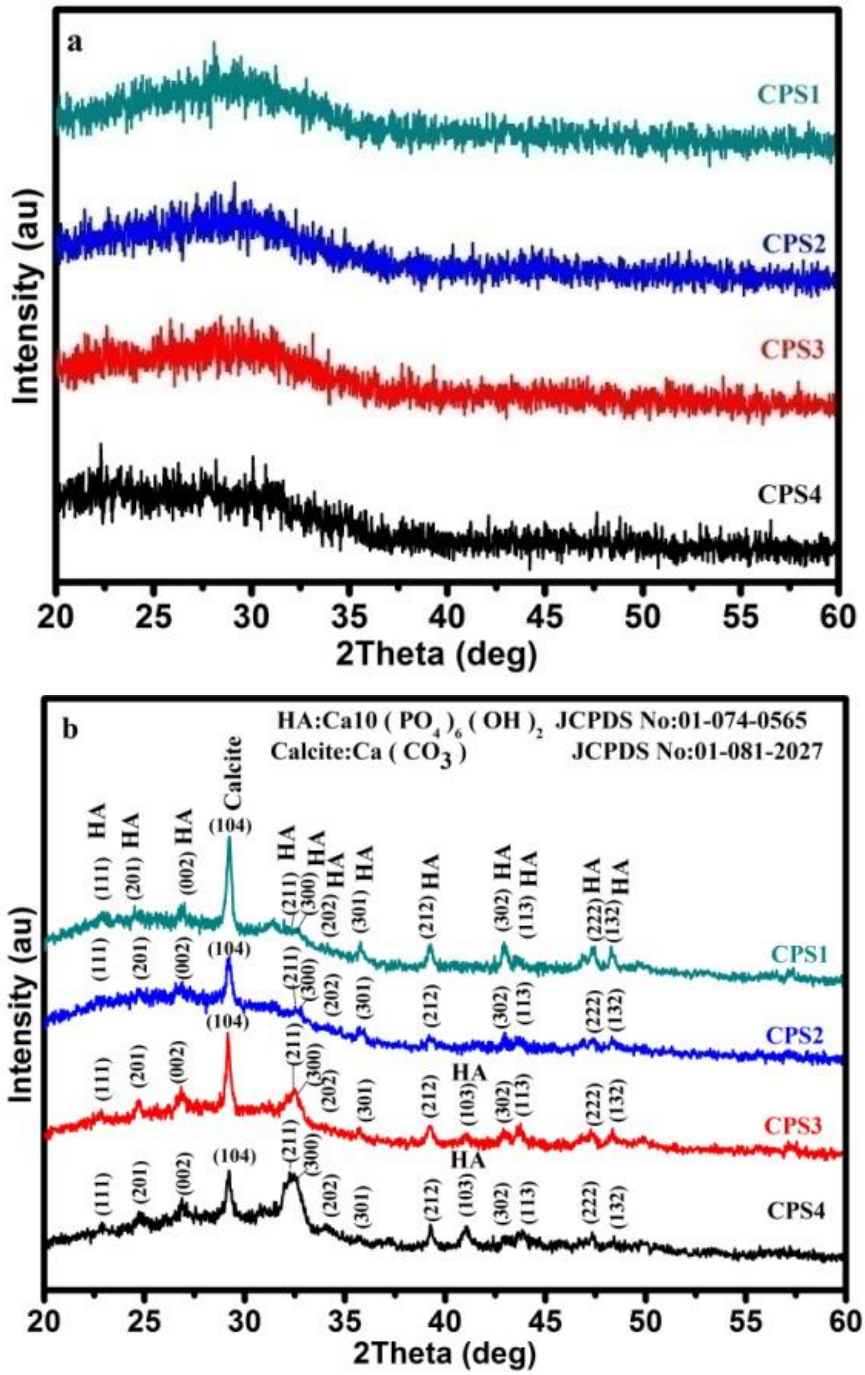

Figure 2.6 XRD pattern of CPS glass samples (a) before (b) after soaking in SBF.

During SBF treatment, a chemical reaction takes place on the sample surface. In this process calcium, phosphate ions migrate into SBF solution and form silanol groups. Due to polycondensation process silica gel layer forms on the sample surface. Calcium,

phosphate ions migrate through silica gel layer and form calcium phosphate (apatite) layer on the sample surface. Due to crystallization process between apatite layer and existing calcium, phosphate, hydroxyl ions in SBF solution, hydroxyapatite (HA) layer forms on the sample surface (Wu and Chang 2012, Catauro et al. 2014). HA layer growth depends on $Ca^{2+}$and PO_4^{3-} ion dissolution of the sample. Lower P_2O_5 content favors formation of more orthophosphate (PO_4^{3-}) units in the sample. Increase in CaO and decrease in P_2O_5 contents increase the Ca^{2+} and PO_4^{3-} ions which are released into SBF solution. This further leads to increase in HA layer formation on the sample surface (Singh et al. 2009). Due to this reason, the HA crystalline intensities have increased from CPS1 to CPS4 sample. CaO/P_2O_5 ratios for CPS1 to CPS4 samples are 1.2, 2, 3.6 and 9.5 respectively. From these observations, it can be confirmed that increase in CaO/P_2O_5 ratio increases the HA crystalinity for SBF treated samples.

HA formation is increased from CPS1 to CPS4 sample. Formed HA consumes Ca^{2+} ions and getting released into SBF solution, it leads to decrease in Ca^{2+} ion concentration in SBF solution and form $CaCO_3$ layer due to a chemical reaction between calcium and carbonate ions (Peitl et al. 2001). Due to this reason, calcite crystalline peak intensities have decreased from CPS1 to CPS2 samples (In this case P_2O_5 acts as network former).

The calcite intensities were increased from CPS2 to CPS3 sample, since the polymerization effect is more in CPS2 than CPS3 sample (In the case of CPS3, P_2O_5 acts as network modifier). The number of Ca^{2+} ions released by CPS2 samples is less and these Ca^{2+} ions react with PO_4^{3-} ions and form HA layer. Dissolution of $Ca^{2+}$and PO_4^{3-} ions is more in CPS3 sample and forms HA layer with less Ca^{2+} ions utilization of SBF. Calcite intensities were decreased from CPS3 to CPS4 sample, since formed HA consumes more Ca^{2+} ions.

2.3.7 Surface morphology

The surface morphology of CPS samples before and after SBF treatment is shown in Figure 2.7 and 2.8. For SBF untreated CPS samples EDX analysis confirmed that

elements present in the samples are Si, Ca, P and O as shown in Figure 2.7 (a, c, e and g). SBF untreated samples have a homogeneous surface morphology [Figure 2.7 (b, d, f and h)]. For SBF treated samples, the surface morphology [Figure 2.8 (a, c, e and g)] clearly exhibits the spherical shaped HCA nuclei formation on the sample surface. It is observed that the lower P_2O_5 concentration (increase in CaO) leads to increase in HCA nuclei progressively on the glass surface. For SBF treated samples, the EDX analysis of HCA layer has shown the presence of Ca, P, C and O elements on the sample surface [Figure 2.8 (b, d, f and h)]. The increase in Ca and P intensities of these samples indicates the increase in HA layer formation on the sample surface. In the previous section, it has been discussed that the crystallization process between apatite and existed calcium, phosphate and hydroxyl ions leads to HA formation on the sample surface. In this process, HA layer gets converted into as HCA layer in the presence of CO_3^{2-} (Jones and Clare 2012). All SBF treated samples show good homogeneity in particle size with the relevant HCA particle size distributions. HCA nuclei average sizes have increased from CPS1 to CPS4 samples as from 821nm to1259 nm [Figure 2.9 (a, b, c and d)]. It indicates that the average particle sizes of HCA nuclei have increased with increase in CaO/P_2O_5 ratio, similar studies have been reported in the literature (Zhao et al. 2010). CPS samples consist of CaO content in the increasing order from CPS1 to CPS4 samples. The increase in CaO content increases Ca^{2+} ions release into SBF solution and it leads to increase in HA layer formation on the sample surface. EDX analysis shows that Ca and P intensities [related to HA] increased from CPS1 to CPS4 sample.

2.3.8 Raman analysis

For CPS samples Si-O-Si asymmetric stretching (as s), Si-O-NBO asymmetric stretching (as s) modes were assigned at 1027-1080 cm^{-1} (Aguiar et al. 2009) and 961-967 cm^{-1}(Aguiar et al. 2009) wave number regions respectively as shown in Figure 4.6 (a) [Table 2.4]. Fivefold symmetric stretching [W_1] modes were also observed at 460-477 cm^{-1} (Aguiar et al. 2009). For the identification of NBO modes in silicate tetrahedra, the deconvolution process has been used in the wave number range of 800-1200 cm^{-1} [Figure

2.10 (b-e)]. Si-O-NBO (as s) intensity/ Si-O-BO (as s) intensity [NBO/BO] ratios have obtained using deconvolution process. The deconvoluted curve area is proportional to band intensities (Marsich et al. 2009). The obtained NBO/BO ratios of CPS1, CPS2, CPS3 and CPS4 samples are 0.58, 1.20, 1.46 and 1.78 respectively. Increase in CaO/P_2O_5 ratio increases NBO/BO ratio and increase in NBO/BO ratio decreases the degree of polymerization between silicate and phosphate tetrahedra. The electronegativity of Si^{4+} is predominated by the electronegativity of P^{5+} ion for CPS1 and CPS2 glasses. Due to this, NBOs of silicate tetrahedra get converted into as that of phosphate tetrahedra (Aguiar et al. 2009). Repolymerisation takes place between silicate and phosphate tetrahedra. Decrease in P_2O_5 decreases the polymerization, it leads to increase in the T_g, T_x values from CPS1 to CPS2 glass. CPS3 and CPS4 glasses have less P_2O_5 compared to CPS1 and

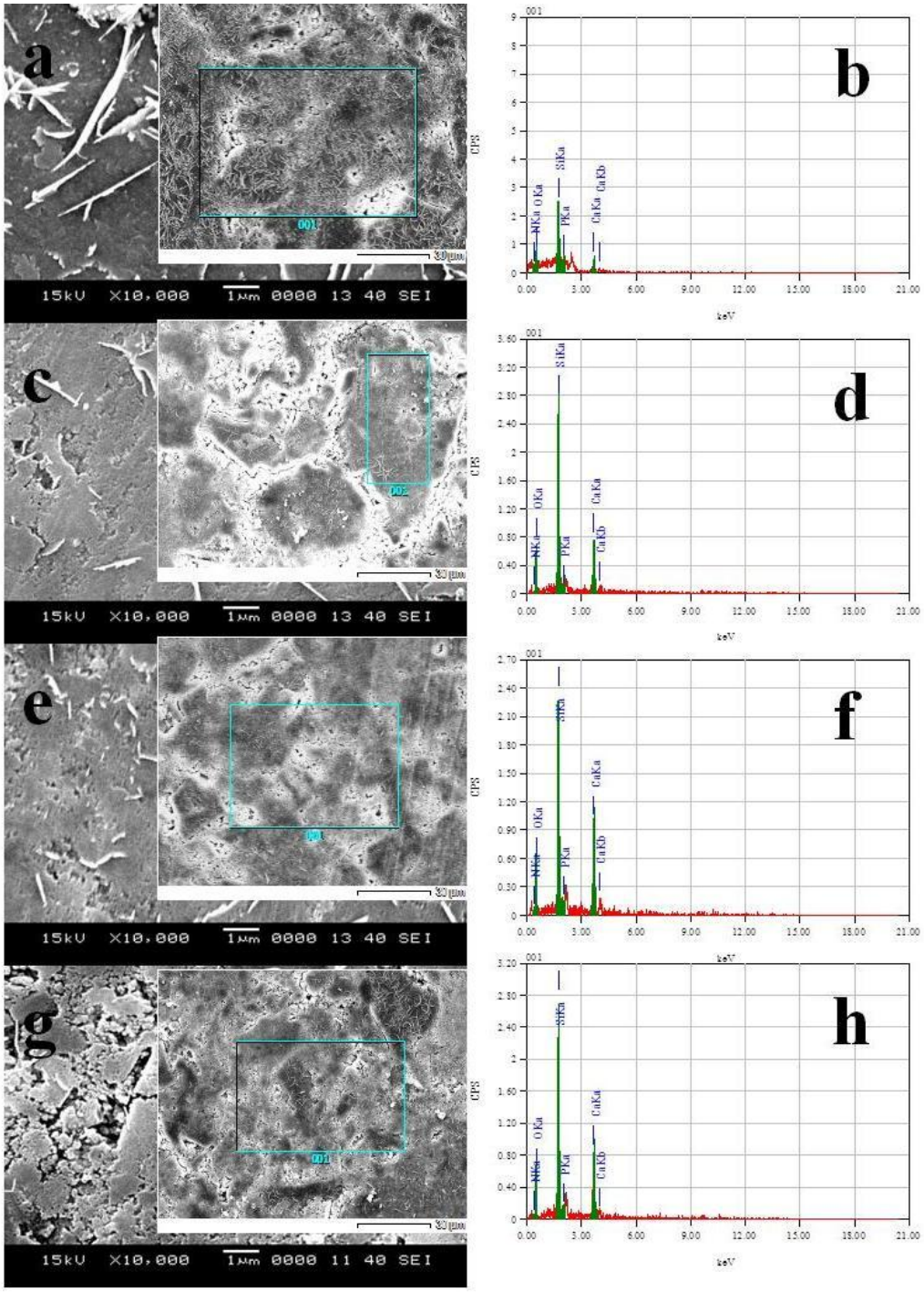

Figure 2.7 (a, c, e,g) SEM images and (b, d, f, h) EDX analysis of CPS1, CPS2, CPS3, CPS4 glasses.

CPS2 glasses, in this case electronegativity of Si^{4+} predominates the electronegativity of P^{5+} ion. The NBO conversion from silica tetrahedra to phosphate tetrahedra is very less for CPS3 compared to CPS2 sample, in this case phosphate phases form as clusters. Compared to CPS2, in CPS3 sample Phosphate phase size (cluster size) is more. O'DonnelI et al. (2012) reported that increase in Phosphate phase size decreases the T_g and T_x values. Due to this reason T_g and T_x values might have decreased from CPS2 to CPS3 glass. In the case of CPS3 and CPS4 samples, decrease in P_2O_5 content decreases the phosphate phase size. CPS4 sample has less P_2O_5 compared to CPS3 sample, due to this reason phosphate phase size decreases in CPS4 compared to CPS3 CPS2 glasses, in this case electronegativity of Si^{4+} predominates the electronegativity of P^{5+} ion. The NBO conversion from silica tetrahedra to phosphate tetrahedra is very less for CPS3 compared to CPS2 sample, in this case phosphate phases form as clusters. Compared to CPS2, in CPS3 sample Phosphate phase size (cluster size) is more. O'DonnelI et al. (2012) reported that increase in Phosphate phase size decreases the T_g and T_x values. Due to this reason T_g and T_x values might have decreased from CPS2 to CPS3 glass. In the case of CPS3 and CPS4 samples, decrease in P_2O_5 content decreases the phosphate phase size. CPS4 sample has less P_2O_5 compared to CPS3 sample, due to this reason phosphate phase size decreases in CPS4 compared to CPS3

For SBF treated samples CO_3^{2-} asymmetric stretching modes appeared in the wave number range of 1084-1086 cm^{-1} as shown in Raman spectra (Aguiar et al. 2009, Bellucci et al. 2014) [Figure 2.10 (f)]. PO_4^{3-} symmetric stretching modes were also observed at 954-965 cm^{-1} wave number region (Aguiar et al. 2009, Bellucci et al. 2014). For CP4 samples HA related crystalline PO_4^{3-} bending modes and fivefold symmetric stretching [W_1] modes were also observed at 591 cm^{-1} (Aguiar et al. 2009, Bellucci et al. 2014) and 433 cm^{-1} (Bellucci et al. 2014), respectively [Table 2.4]. Crystalline intensities of CO_3^{2-} modes increased from CPS1 to CPS4 sample. Due to this reason HCA formation also increases for CPS samples, and also that the HCA growth is carbonates depended (Rezwan et al. 2006). sample. Ca^{2+} ion effect is also more for CPS4 compared to CPS3 sample, it causes the increase in T_g and T_x values for CPS4 compared to CPS3 sample.

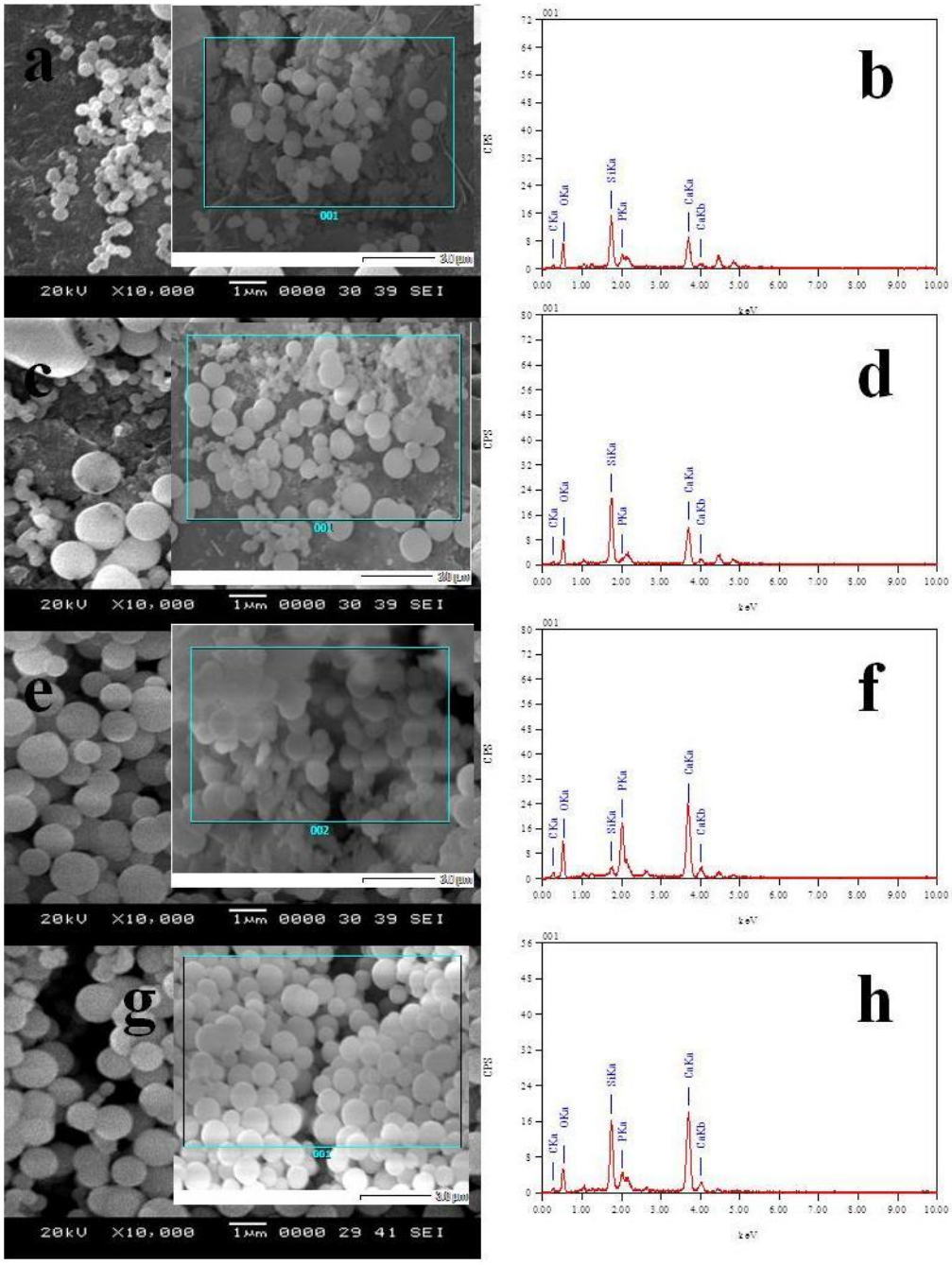

Figure 2.8 (a, c, e, g) SEM images and (b, d, f, h) EDX analysis of SBF treated CPS3, CPS4 glasses.

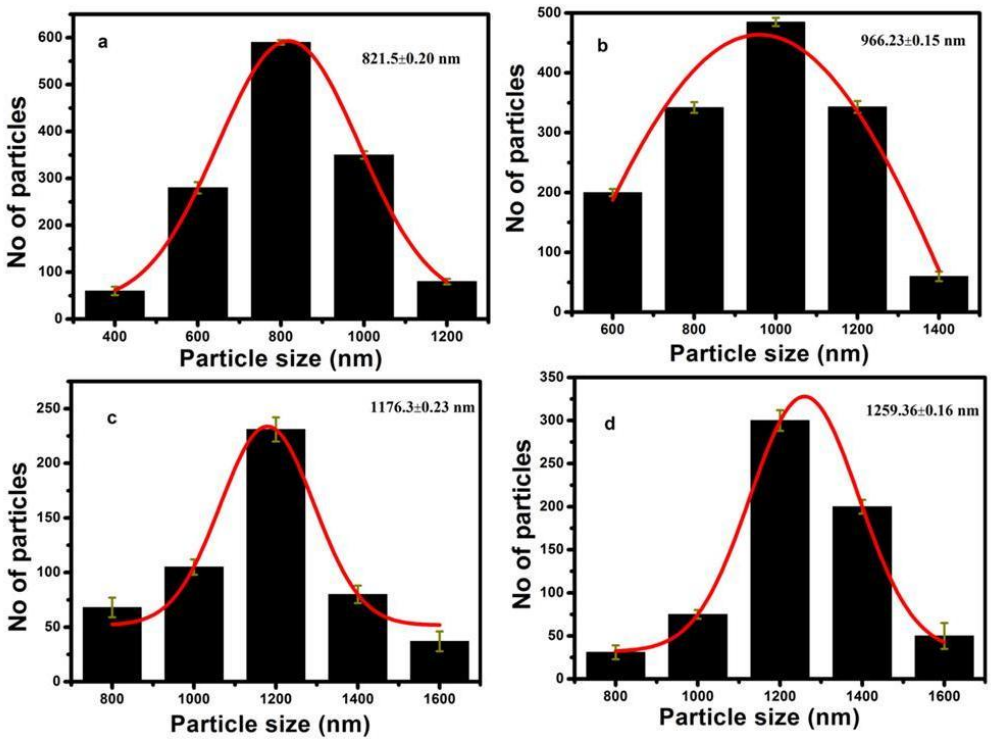

Figure 2.9 (a, b, c and d) HCA particle size distribution of SBF treated CPS1, CPS2, CPS3 and CPS4 glasses.

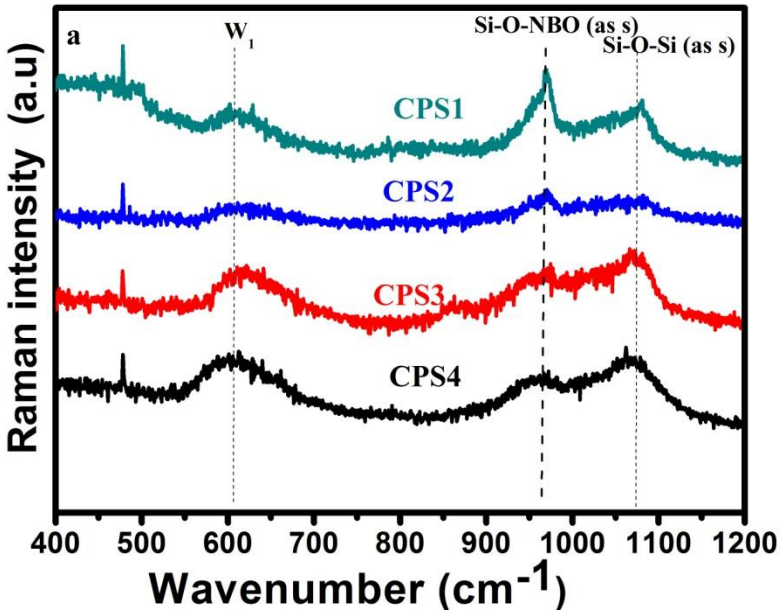

Figure 2.10 (a) Raman spectra of CPSN samples

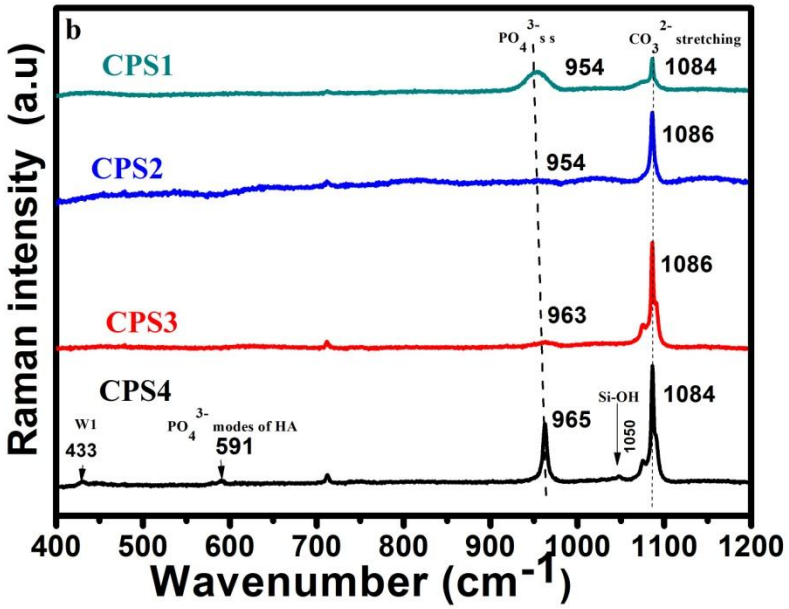

Figure 2.10 (b) Raman spectra of CPSN samples after SBF treatment

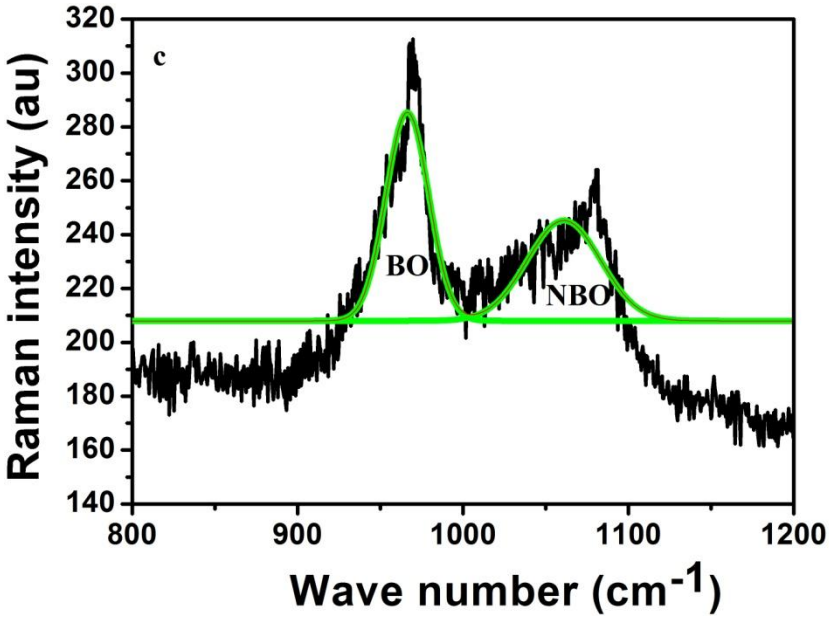

Figure 2.10 (c) Deconvoluted Raman spectra of CPS1 sample

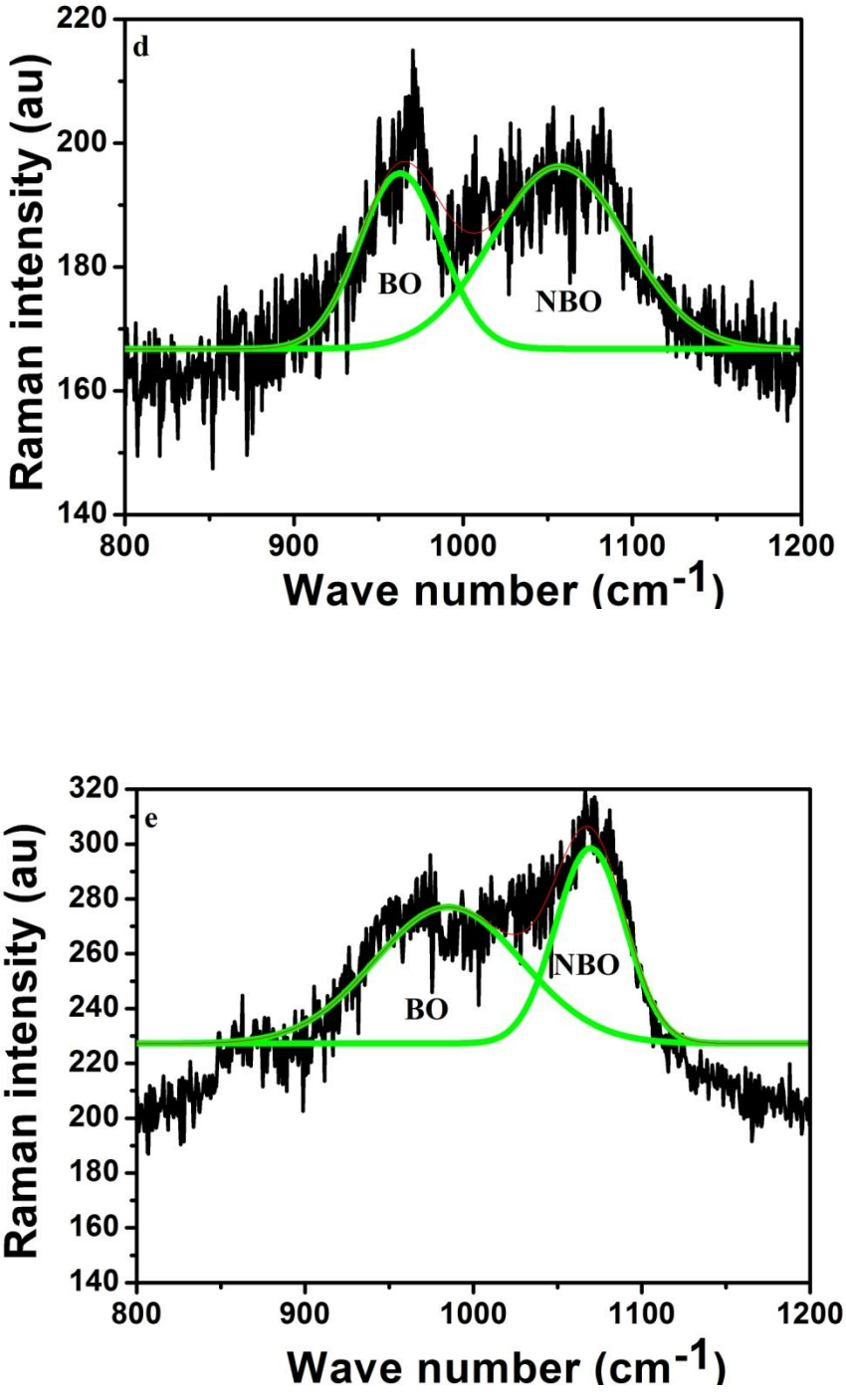

Figure 2.10 (d) and (e) are deconvoluted Raman spectra of CPS2and CPS3 samples respectively

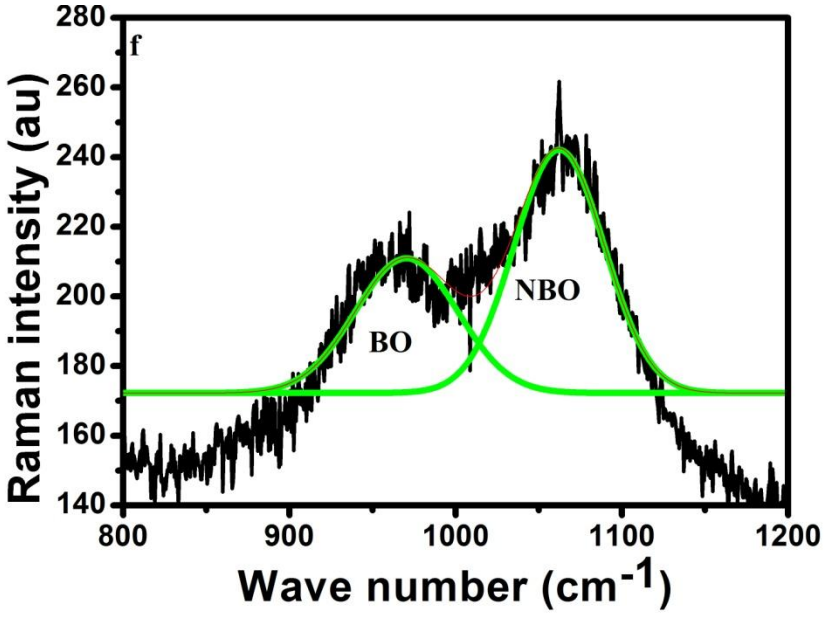

Figure 2.10 (f) Deconvoluted Raman spectra of CPS4 sample

Table 2.4 Raman band assignments of Calcium phosphosilicate glasses before and after soaking in SBF solution.

Raman absorption band in cm^{-1}.

Before soaking in SBF solution					**After soaking in SBF solution**				
CPS1	**CPS2**	**CPS3**	**CPS4**	**Assigned bands**	**CPS1**	**CPS2**	**CPS3**	**CPS4**	**Assigned Bands**
463	471	477	460	W1	-	-	-	433	W1
961	967	966	965	Si-O-NBO asymmetric stretching	-	-	-	591	PO_4^{3-} Modes of HA
1073	1027	1080	1076	Si-O-Si asymmetric stretching	954	954	963	965	PO_4^{3-} symmetric stretching
					1084	1086	1086	1084	CO_3^{2-} stretching

2.3.9 FTIR analysis

FTIR spectroscopic analysis of CPS samples is shown in Figure 2.11 (a). The transition bands observed at 1064-1187 cm^{-1}(Li et al. 2014) were assigned to the Si-O-Si asymmetric stretching (as s) and Si-O-NBO (as s) modes were assigned at 1026-1033 cm^{-1} (Aguiar et al. 2009). For CSP samples, different intensities occur at 466-478 cm^{-1} related to rocking modes of Si-O-Si (Li et al. 2014) [Table 2.5]. Si-O-Si bending modes were observed in the wave number region of 779-794 cm^{-1}(Sun et al. 2015). PO_4^{3-} asymmetric stretching mode of vibrations also were observed at 1222-1265 cm^{-1} (Sun et al. 2015). The decrease in P_2O_5 content decreases the degree of polymerization between silicate and phosphate tetrahedra, due to this reason phosphate tetrahedra have less prominence and silicate tetrahedra have more prominence supported by literature (Singh et al. 2009).

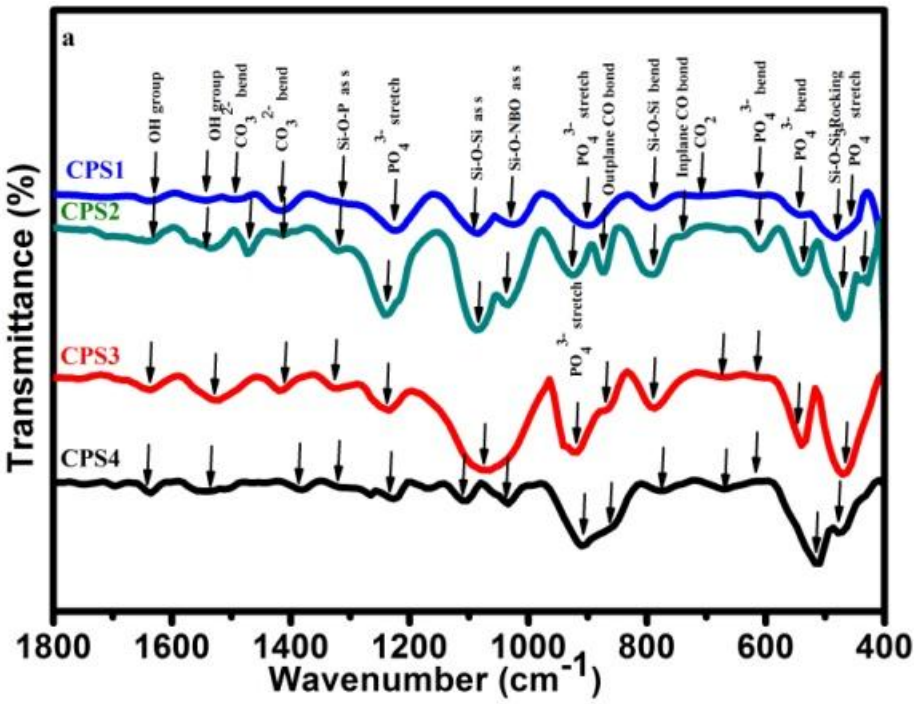

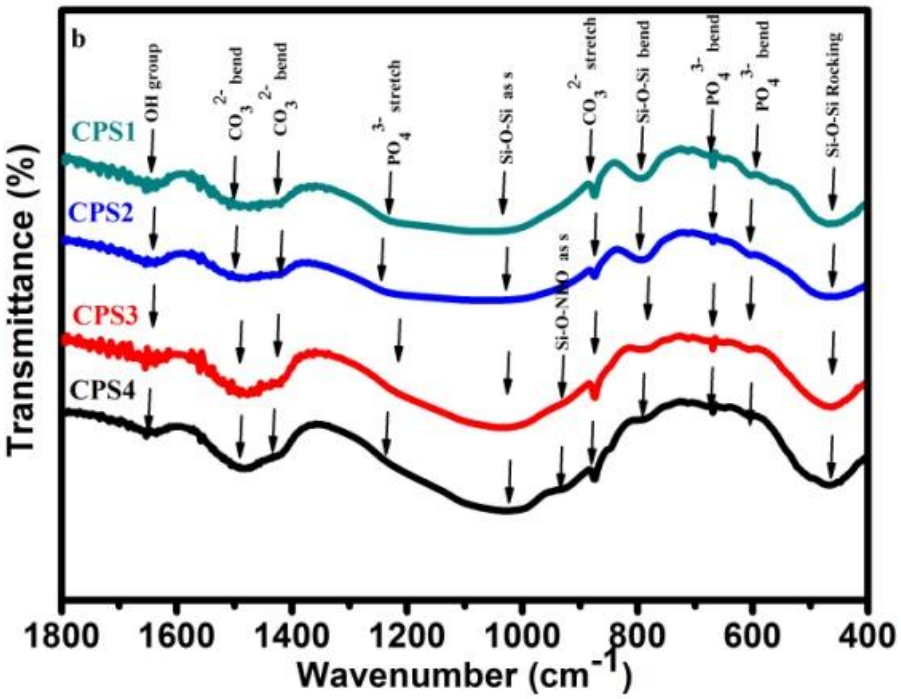

Figure 2.11 FTIR pattern of CPS glass samples (a) before (b) after soaking in SBF solution.

For SBF treated samples [Figure 2.11(b)] Si-O-Si asymmetric stretching mode became broader compared to SBF untreated samples in the FTIR spectra (1022-1087 cm^{-1}) [Sun et al. 2015], which is due to the formation of silica gel (amorphous) layer on the sample surface in the dissolution process. For SBF treated samples CO_3^{2-} bending (1413-1498 cm^{-1}) (Li et al. 2014) modes became broader and more prominent compared to SBF untreated samples. Sharp, intense CO_3^{2-} stretching modes (~873 cm^{-1}) (Notingher et al. 2002) were also observed for SBF treated samples compared to SBF untreated samples [Table 2.5]. For SBF treated samples PO_4^{3-} bending amorphous mode (601-605 cm^{-1}) (Peitl et al. 2001) broadness was decreased and sharpness was increased compared to SBF untreated samples. The increase in sharpness is related to the formation of PO_4^{3-} bending crystalline modes which are assigned at 669 cm^{-1}. From these observations, it can be concluded that during the crystallization process the HCA crystalline layer would be formed in the presence of carbonate groups. XRD, SEM/EDX and Raman

spectroscopic analysis confirmed the HCA crystal formation on the sample surface in the dissolution process.

It is also observed that the OH groups are also present in the FTIR spectra before and after SBF treatment at 1635-1643 cm^{-1} and 1641 cm^{-1} wave number regions, respectively (Bellucci et al. 2014). It may be due to absorbed water from the environment during the pelletization process (Bellucci et al. 2014). Si-O-Si rocking, bending modes were present in the wave number range of 464-470 cm^{-1} (Li et al. 2014) and 785-794 cm^{-1} (Sun et al. 2015) respectively after SBF treatment. Non-Bridging oxygen modes related to Si-O-Ca also observed for SBF treated CPS3 and CPS4 samples at 923-925 cm^{-1} (Aguiar et al. 2008).

2.3.10 TEM/SAED analysis

The TEM analysis revealed that SBF treated samples have spherical shaped particles as shown in Figure 2.12 (a, b, c and d). The d-spacing [for (211) plane] for spherical shaped particles are found using TEM/SAED pattern (Lu et al. 2013). The observed d-spaces for CPS1, CPS2, CPS3, CPS4 samples are 0.280 nm, 0.283 nm, 0.279 nm and 0.281 nm respectively. The observed $d_{(211)}$-spaces are in good agreement with standard JCPDS (24-0033) files of HCA layer. From these observations, it can be concluded that for SBF treated samples the crystals on the surface are HCA particles formed in the dissolution process.

2.3.11 pH measurement, Dissolution and Weight loss studies

In dissolution process, calcium and phosphate ions migrate into SBF solution, form silanol groups on the sample surface. In polycondensation process silanol groups form silica gel layer on the sample surface. Calcium and phosphate ions of glass matrix leach on the silica gel layer surface as amorphous calcium phosphate (apatite) layer, it changes the Ca^{2+} and PO_4^{3-} concentrations of SBF solution. Incorporation of Ca^{2+} and PO_4^{3-}, hydroxyl and carbonate ions from SBF solution into apatite layer leads to HCA formation on the sample surface in the crystallization process (Jones and Clare 2012).

Table 2.5 FTIR band assignments of Calcium phosphosilicate glasses before and after soaking in SBF solution.

Infrared vibration band in cm^{-1}.

Before soaking in SBF solution					**After soaking in SBF solution**				
CPS1	**CPS2**	**CPS3**	**CPS4**	**Assigned bands**	**CPS1**	**CPS2**	**CPS3**	**CPS4**	**Assigned bands**
474	466	470	478	Si-O-Si rocking	468	470	464	466	Si-O-Si rocking
536	540	540	516	PO_4^{3-} bending amorphous	601	605	603	601	PO_4^{3-} bending amorphous
613	609	617	-	PO_4^{3-} bending crystalline	669	669	669	669	PO_4^{3-} bending crystalline
794	790	786	779	Si-O-Si bending	794	792	792	785	Si-O-Si bending
1026	1033	1033	1033	Si-O-NBO (as s)	875	873	873	873	CO_3^{2-} stretching
1083	1187	1064	1103, 1172	Si-O-Si (as s)	-	-	925	923	Si-O-Ca (as s)
898	925	925	910	PO_4^{3-} (as s)	1078	1087	1035	1022	Si-O-Si (as s)
1415,1492	1411, 1472	1419, 1527	1380, 1465, 1512	CO_3^{2-} bending	1228	1236	1214	1228	PO_4^{3-} (as s)
					1419, 1498	1419, 1498	1413, 1481	1434, 1494	CO_3^{2-} bending
					1641	1641	1641	1641	-OH group

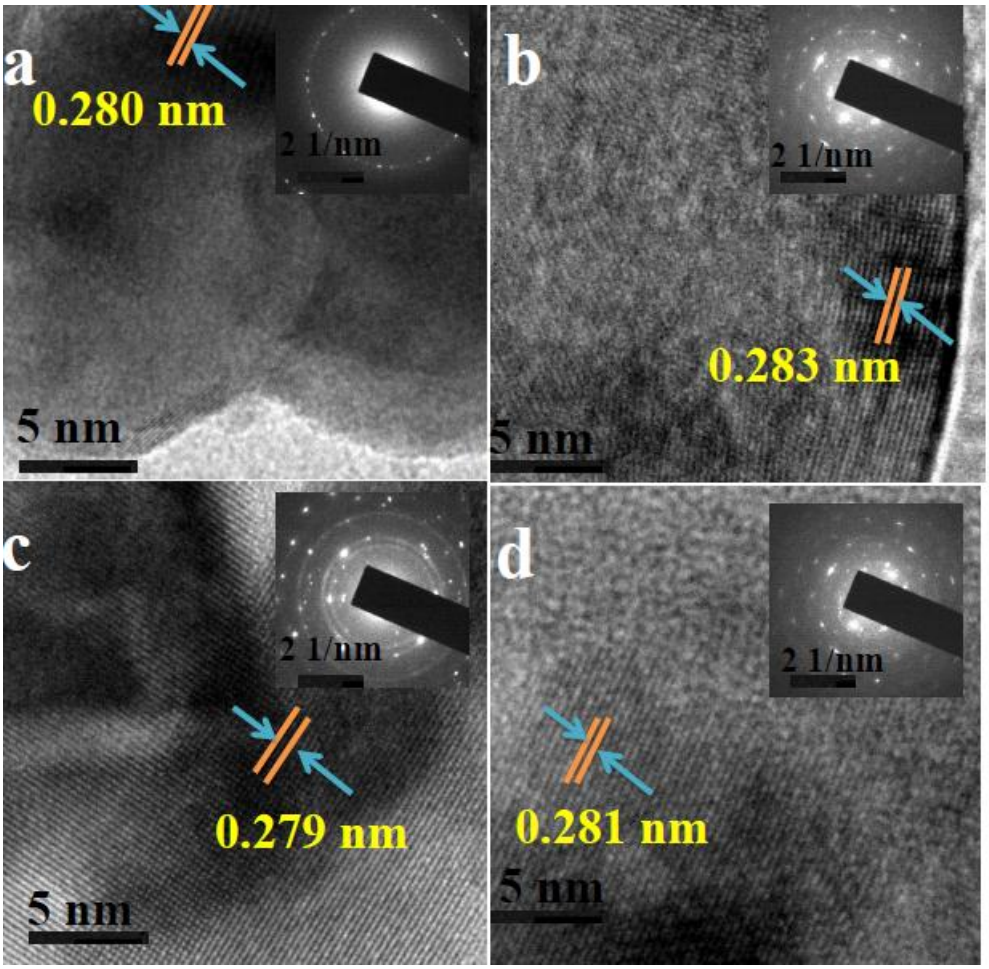

Figure 2.12 (a, b, c and d) TEM/SAED pattern of SBF treated CPS1, CPS2, CPS3 and CPS4 glasses.

The pH values are increased up to 24 hours of soaking time in the SBF solution as shown in Figure 2.13 (a). At this stage, due to the fast release of Ca^{2+} ions silanol groups have formed and it leads to the HA formation on the sample surface (Lukito et al. 2005, Masoud et al. 2010). The pH values are almost stabilized after 24 hours [Figure 2.13 (a^1)]. The pH values, Ca^{2+} and PO_4^{3-} ion concentrations of SBF solution are increased from CPS1 to CPS4 samples as shown in Figure 2.13 (b) and 2.13 (c). The weight loss of SBF treated CPS samples is also increased from CPS1 to CPS4 samples [Table 2.6].

Raman and FTIR spectroscopy analysis of CPS samples revealed that the non-bridging oxygens exist as Si-O-Ca asymmetric stretching modes. The Raman

spectroscopic analysis also revealed that NBO/BO ratio is increased for CPS samples with an increase in CaO/P_2O_5 ratio.

The Ca^{2+} and PO_4^{3-} ions release from glass matrix in the SBF solution depends on the Ca^{2+} and PO_4^{3-} ions in the glass matrix and degree of polymerization also. In the case of CPS1 and CPS2 samples, P_2O_5 acts as network former. Polymerization takes place between phosphate and silicate tetrahedra. P_2O_5 content is more and polymerization effect is also more for CPS1 than CPS2 sample, due to this reason CPS2 sample releases more PO_4^{3-} ions than CPS1 sample. NBO/BO ratio is more for CPS2 sample than CPS1 sample and NBOs are in Si-O-Ca form. Due to low polymerization and higher NBOs, the Ca^{2+} release also increased from CPS1 to CPS2 sample. CPS3 and CPS4 samples have less P_2O_5 content, in this case P_2O_5 acts as network modifier. Due to this reason polymerization effect is less for CPS3 and CPS4 samples, orthophosphate units form as clusters with very weak P-O bands (O'Donnell et al. 2012). Phosphate phase cluster size (with orthophosphate units) is less for CPS4 compare to CPS3 sample. Due to this reason, CPS4 glass can release more PO_4^{3-} ions than CPS3 sample. Due to increase in NBO/BO ratio, Ca^{2+} ion release also increase from CPS3 to CPS4 sample. From all these observations it can be concluded that the Ca^{2+} and PO_4^{3-} ion release from glass matrix in the SBF solution increases from CPS1 to CPS4 sample. The increase in NBO/BO ratio increases the dissolution of Ca^{2+} ions into SBF solution, it causes the increase in pH values of the SBF solution in the dissolution process for CPS samples. In dissolution process, HA layer formation on the sample surface not only depends on number of releasing Ca^{2+} and PO_4^{3-} ions from the sample, but also on the number of leaching Ca^{2+} and PO_4^{3-} ions from SBF solution. The increase in the Ca^{2+} ion release depends on an increase in NBO/BO ratio. The decrement in glassy nature is based on P_2O_5 content for CPS1 to CPS4 samples and it results in the increase in the dissolving PO_4^{3-} ions. The increase in weight loss of SBF treated samples [Table 2.6] in the dissolution process occurs from CPS1 to CPS4 samples based on the increment in number of dissolution of Ca^{2+} and PO_4^{3-} ions from the sample into SBF solution.

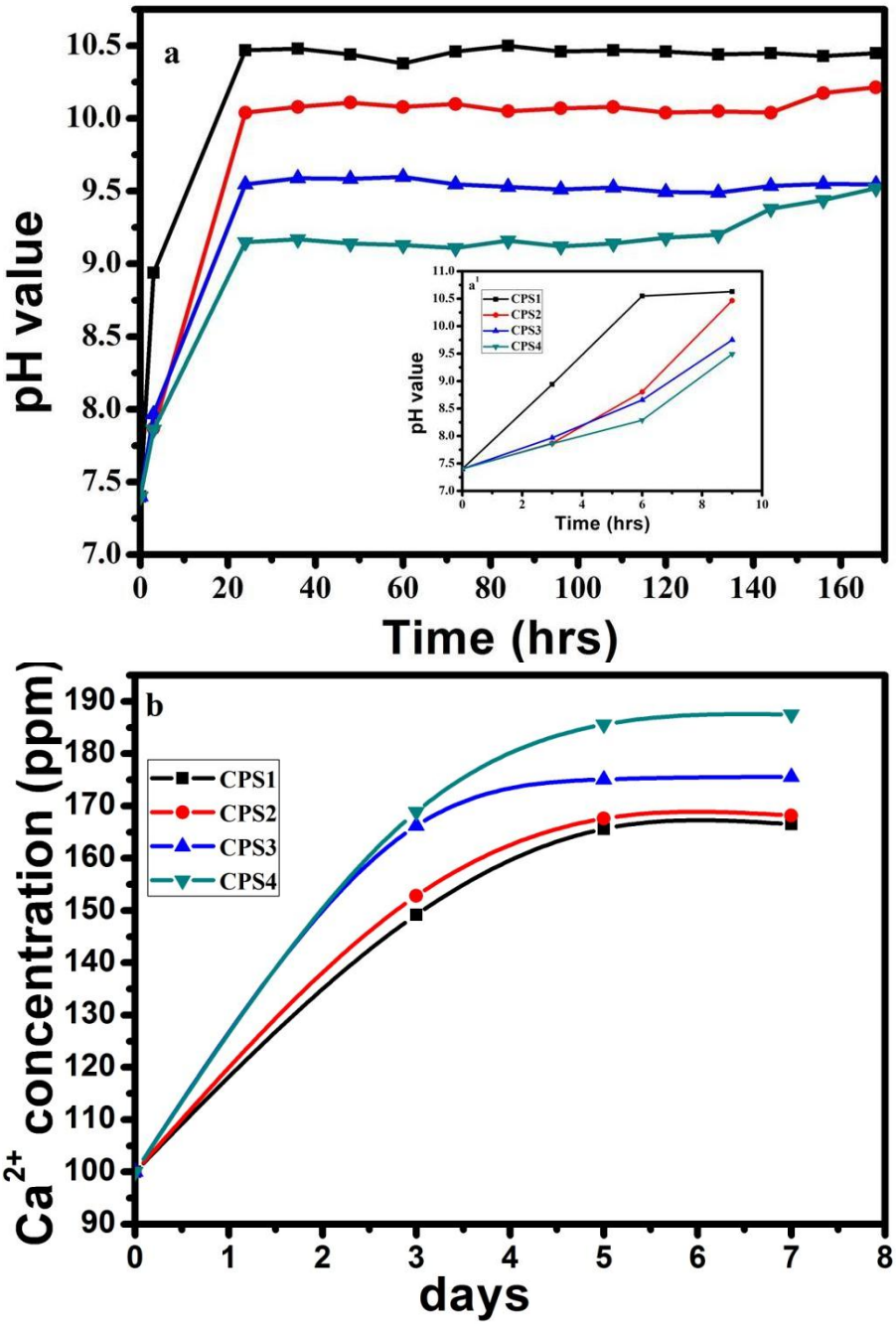

Figure 2.13(a) pH variation and (b) Ca^{2+} concentration variation SBF soaked CPS glasses with respect to soaking time.

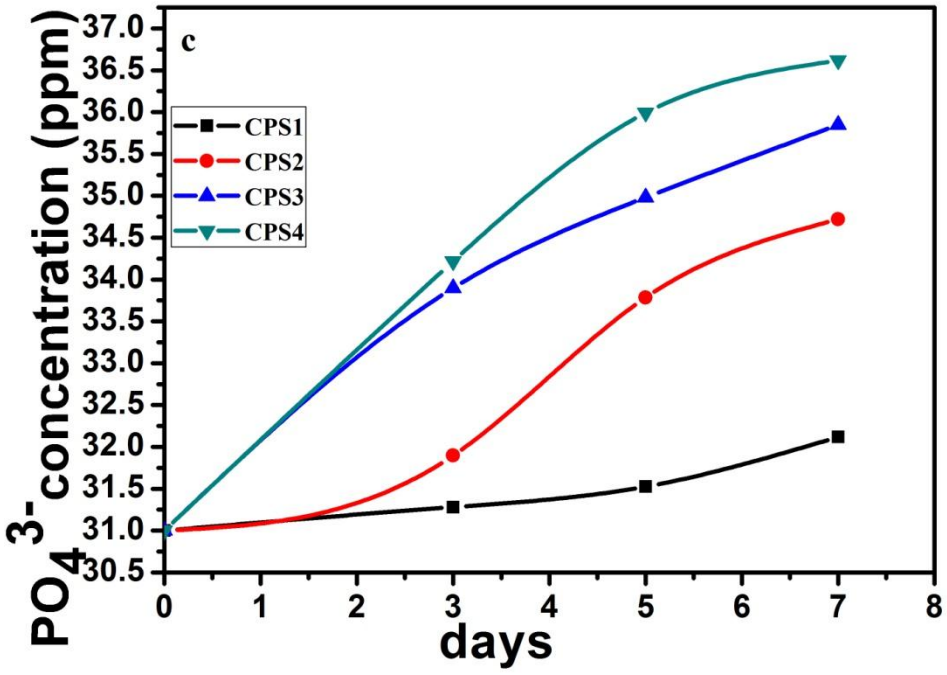

Figure 2.13 (c) PO_4^{3-} concentration of SBF solution for SBF soaked CPS glasses with respect to soaking time.

Table 2.6 HCA nuclei sizes, $d_{(211)}$-space of HCA and Weight loss % of SBF soaked $58SiO_2$-(19-x)P_2O_5-(23+x)CaO glasses with NBO/BO ratio.

x mol%	**NBO/BO ratio** **Raman**	**Nuclei average size (nm)** **SEM**	**Weight loss for SBF soaked samples (%)**
0	0.58	821	58
5	1.20	966	64
10	1.46	1176	83
15	1.78	1259	89

2.4 Conclusions

Synthesized dried gel samples have amorphous nature. Increase in P_2O_5 favors the orthophosphate structures where as decrease in P_2O_5 increases pore size of calcium phospho silicate dried gels. The glass transition and onset crystalline temperatures increase with increase in CaO/P_2O_5 ratio. The samples sintered at 700 °C have shown amorphous nature. CaO/P_2O_5 ratio is proportional to NBO/BO ratio for synthesized calcium phosphosilicate glass samples and also proportional to HCA particle size for SBF soaked glass samples. This study will be helpful to improve bone forming abilities in biomedical applications based on CaO/P_2O_5 and NBO/BO ratios.

CHAPTER 3

SYNTHESIS AND CHARACTERISATION OF SODA LIME PHOSPHOSILICATE GLASSES

Present chapter deals with the synthesis of soda lime phosphosilicate glasses and also includes thermal properties of soda lime phosphosilicate dried gels. Structural and surface morphological properties for synthesized and SBF treated glasses are studied through XRD, FTIR, Raman characterization techniques. HCA formation for SBF treated samples is confirmed by TEM/SAED analysis. Surface morphological properties were studied using SEM and EDX analysis. Based on composition variation HCA forming ability studies have been carried out by studying dissolution of phosphate and calcium ions SBF.

3.1. Introduction

The composite structure of bone matrix strongly influences the natural bone mechanical properties. Bioactive glass and glass ceramics are fillers for bioactive composites, since they can integrate into the body and can form biologically active apatite (Hydroxy apatite) layer at the bone/implant interface (Gerhardt and Boccaccini 2010, Bellucci et al. 2014). It is important to note that, bond between the bone and a glass material is the precipitation of an apatite layer on the surface of the glass material which is responsible for bioactivity. For tissue engineering applications it is essential that the nucleation and growth of hydroxy apatite (HA) layer be fast on the surface of the bioglass in a precise reaction time in the body environment (Bellucci et al. 2014, Yunos et al. 2008). The HA nucleation and growth rate are strongly influenced by the glass synthesis processes such as melt quenching, sol-gel processes, etc. Sol-gel glasses and glass-ceramics having good homogeneity can be produced at low temperature conditions. The sol-gel method offers potential benefits for obtaining the powdered materials with good control of composition (Lao et al. 2008), microstructure (Wu and Chang 2012) and wider range of bioactivity (Peitl et al. 2001). Compared to melt quenching technique, sol-gel

process is a more convenient technique to improve hydroxy carbonated apatite (HCA) layer growth rate in SBF solution based on dissolution property of synthesized glass matrix in SBF solution. The dissolution behavior depends on strength of glass material. In fact melt derived silicate glasses show high density with high strength and sol-gel derived silicate glasses show high porosity with low strength (Arcos et al. 2010, Siqueira and Zanotto 2013, Radev 2014, Catauro et al. 2014, Wang et al. 2011). Based on higher rate of dissolution in SBF solution, these glass samples have implications for biomedical applications such as bone bonding ability, tissue engineering, cancer therapy etc (De Groot et al. 1998, Onoki and Hashida 2006, Kobayashi et al. 2007).

The HCA formation on glass surface depends on process parameters such as glass composition, sintering temperature and bio active medium such as SBF solution. As reported by (Ohtsuki et al. 2009) glasses in CaO-SiO_2 binary system are important in the formation of apatite layer in the body environment, due to this reason CaO-SiO_2 particles are useful as inorganic fillers in novel bioactive composites for bone repair. CaO/P_2O_5 ratio influences the HCA growth rate in SBF solution for calcium phospho silicate glasses (Snyders et al. 2008, O'Kane et al. 2008). Network modifiers can break the glass ceramics structure and form non-bridging oxygens [NBO]. The formation of NBO results in the softening of the glass ceramic structure, especially the concentration of NBO effects its bio activity. Raman spectroscopy is the powerful tool for the identification of non bridging oxygens and for finding non bridging oxygen concentration. Based on the sintering temperature conditions, bio activity of sol-gel synthesized SiO_2-CaO-P_2O_5 bio glass can influence psudo-wollastanite or wollastonite structure formation after SBF treatment (Ma et al. 2010). Na_2O addition in calcium phosphosilicate glass system can overcome the problem of HCA layer growth rate resistance in SBF soaked calcium phosphosilicate glasses (Singh and Srinivasan 2010, Adams et al. 2013). Moreover, there are limited studies on role of Na_2O substitution for non bridging oxygen concentration and co-relation on apatite layer formation of phosphosilicate glasses. However influence of Na_2O addition on the structural properties and degradability for calcium silicate ceramics has been studied (Li et al. 2016).The present chapter is focused on the sol-gel

synthesis of [$58SiO_2$-(38-x)CaO-xNa_2O-$4P_2O_5$ bioactive (x= 5, 10, 15 and 20 mol %)] composition. Thermal, structural properties of synthesized glass samples were studied using TGA/DTA analysis and XRD techniques for the confirmation glass-ceramic nature of the material. The bridging oxygens (BO), non-bridging oxygens (NBO) in the synthesized composition were identified by FTIR spectroscopic technique and corresponding NBO/BO ratio were found using Raman spectroscopic analysis. Further the effect of NBO/BO ratio on early apatite layer formation for synthesized bioactive system has been investigated.

3.2. Materials and methods

3.2.1 Synthesis of soda lime phosphosilicate glasses

As discussed in section 2.2.1 sol was prepared in hydrolysis process and sodium nitrate were added and stirred well. The prepared sols were poured into teflon beakers, sealed with aluminum wrappers and kept inside hot air oven at 60 °C temperature for three days for aging purpose. Subsequently the aged gels were dried at 130 °C for 4 hours. The dried gels were ground, made into powders and heated at the rate of 5°C/min up to 700°C and stabilized at that temperature for 4 hours to obtain glass samples in the powder form. After getting powder samples, pellets have been prepared using KBR hydraulic press by applying 5 tons' of pressure for 5 minutes.

As discussed for CPS glasses in section 2.2.1 same characterization techniques were used for soda lime phosphosilicate glasses before and after SBF treatment.

Table 3.1 Batch composition of $58SiO_2$-(38-x)CaO-xNa_2O-$4P_2O_5$ glasses.

Glass sample	SiO_2 (mol%)	P_2O_5 (mol%)	Na_2O (mol%)	CaO (mol%)
CPSN1	58	4	5	33
CPSN2	58	4	10	28
CPSN3	58	4	15	23
CPSN4	58	4	20	18

3.3 Results and discussion

3.3.1 TGA/DTA analysis

In DTA curves T_g and T_x values related to primary crystalline phase are observed at 491 – 548 ˚C and 625 – 719 ˚C respectively as shown in Table 3.2 [Figure 3.1 (a-d)]. The thermal stability (ΔT) values are varying nonlinearly with Na_2O. Mixed alkali and alkaline effect leads to change in field strength of CPSN samples (Jones and Clare 2012). As shown in Figure 3.1 (e) CPSN samples show two weight losses in TGA curves. The first is at 462-566 ^{0}C and the second is at 606-640 ˚C. The first weight loss is related loss of organics (Ma et al. 2011, Masoud et al. 2010), the second is related to residual nitrates evaporation (Masoud et al. 2010, Yang et al. 2012).

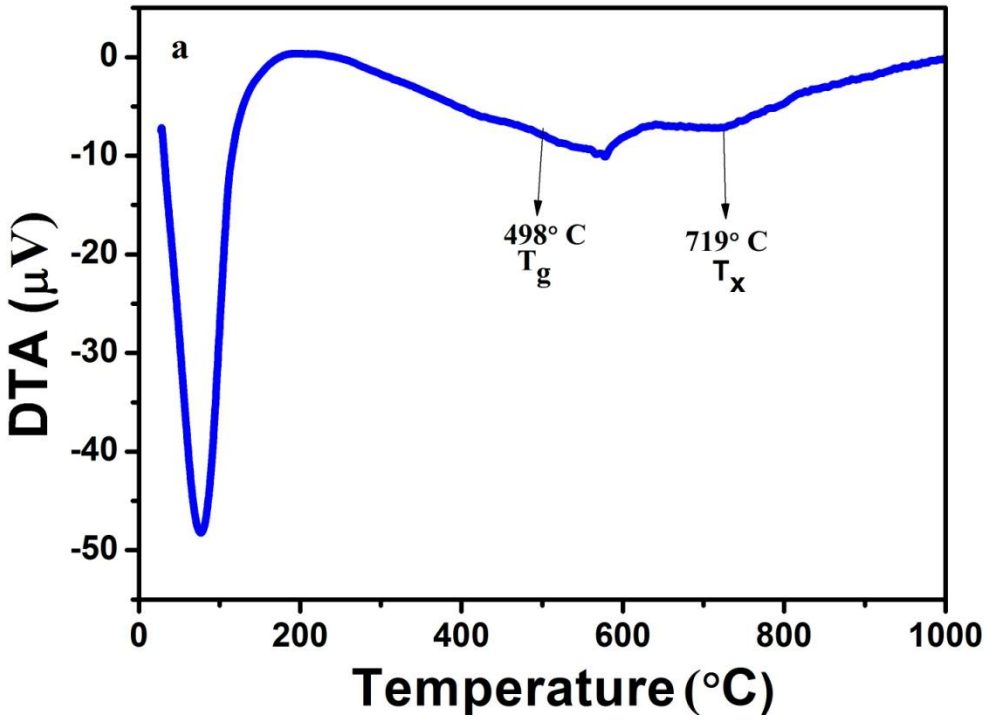

Figure 3.1(a) DTA curves of CPSN1 sample.

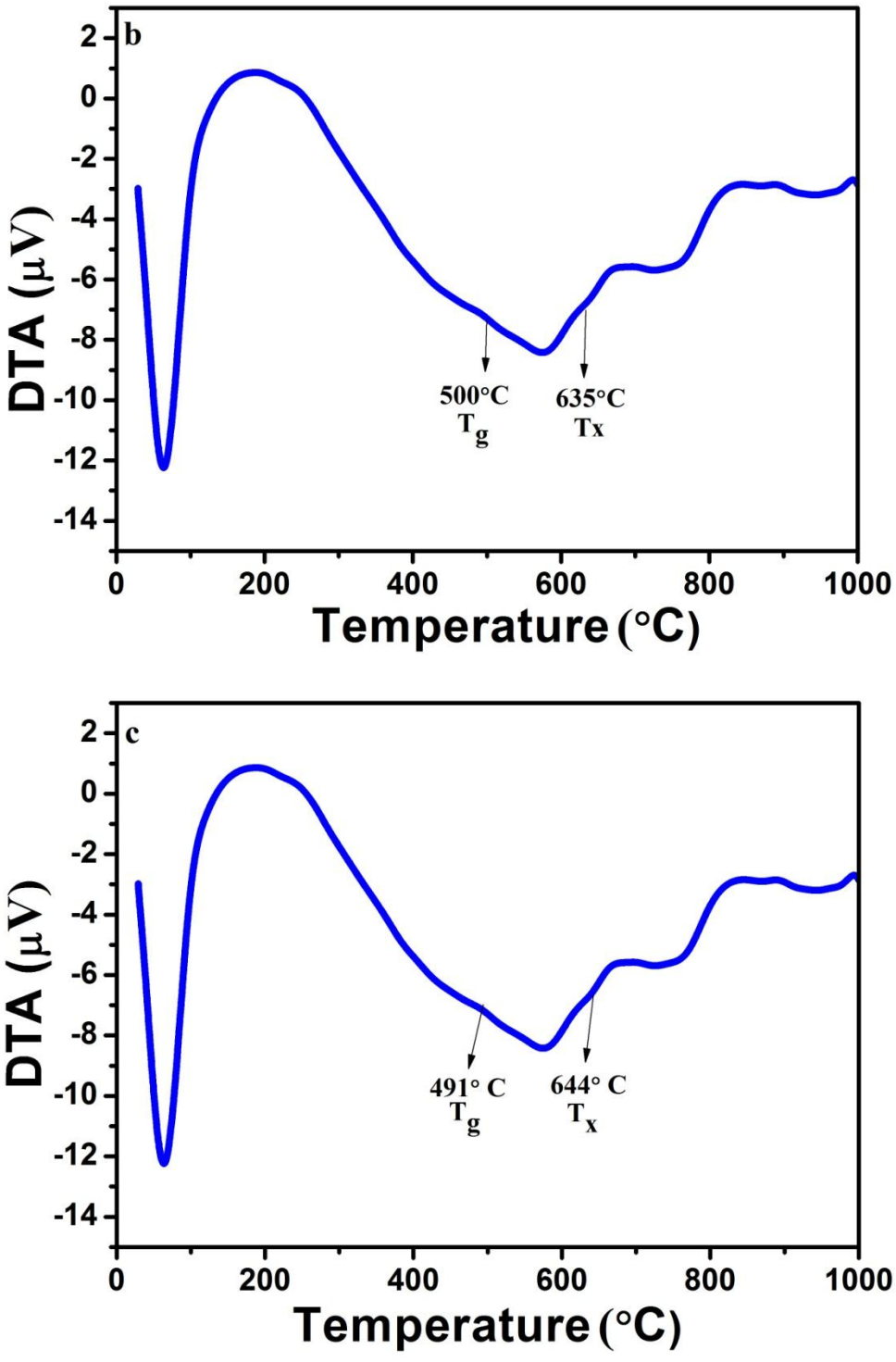

Figure 3.1 DTA curves of (b) CPSN2 and (c) CPSN3 samples

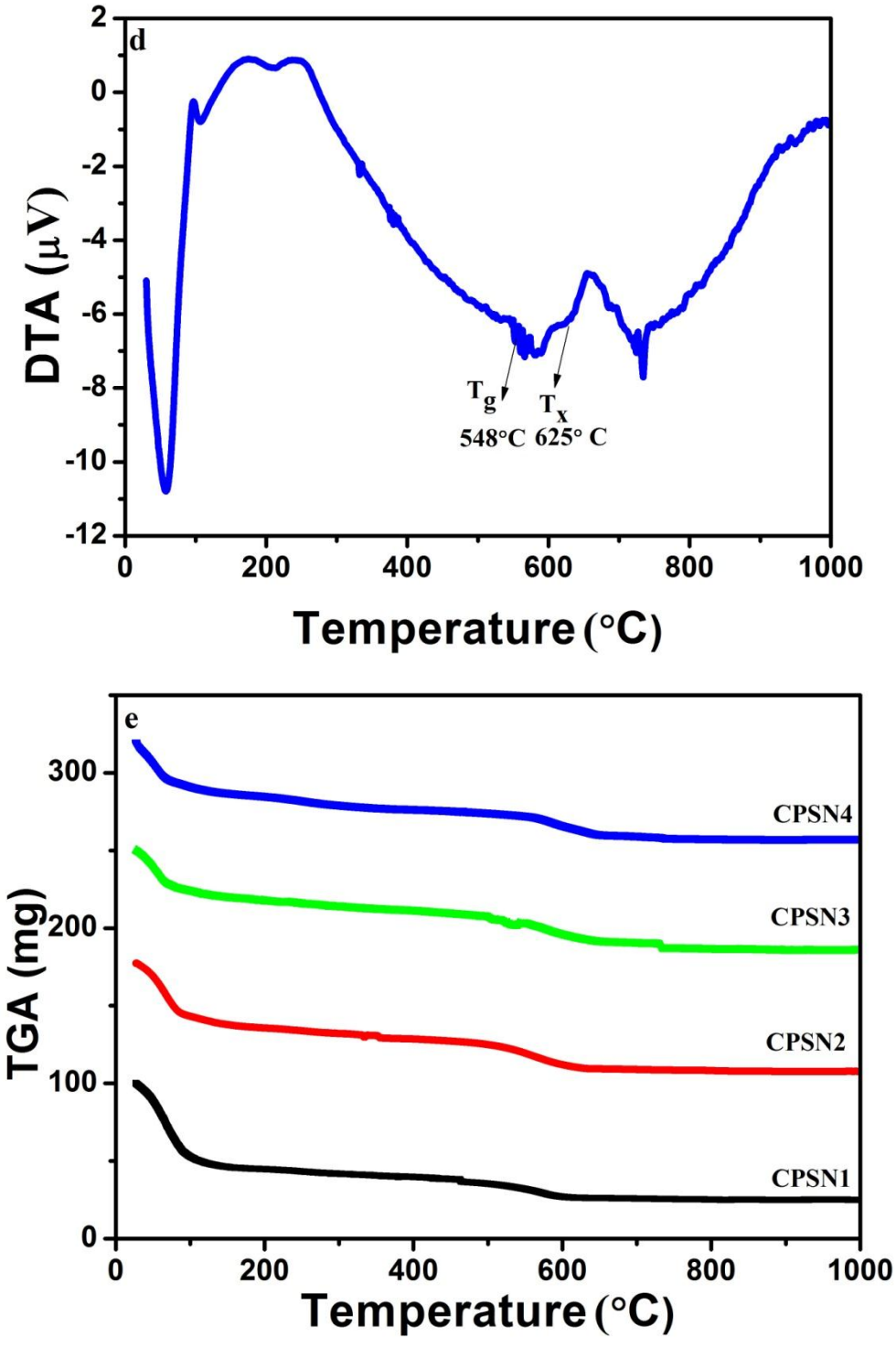

Figure 3.1(d) DTA curve of CPSN4 samples and (e) TGA curves of CPSN samples.

Table 3.2 Batch composition of $58SiO_2$-(38-x)CaO-xNa_2O-$4P_2O_5$ glasses with thermal properties.

X mol%	**Glass**	**First weight loss (°C)**	**Second weight (°C)**	**T_g °C**	**T_x °C**	**ΔT °C T_x-T_g (°C)**
5	CPSN1	462	606	498	719	221
10	CPSN2	522	619	500	635	135
15	CPSN3	534	640	491	644	153
20	CPSN4	566	640	548	625	77

3.3.2 XRD analysis

Figure 3.2 (a) shows the XRD pattern of CPSN samples. CPSN1 sample shows broad hump at 20°- 30°, it indicates that CPSN1 sample has amorphous nature. CPSN2, CPSN3 and CPSN4 show crystalline peaks. The crystalline intensity is increased from CPSN2 to CPSN3 samples, since thermal stability decreased. Due to increase in thermal stability the crystalline intensity is decreased from CPSN2 to CPSN3 samples whereas from CPSN3 to CPSN4 crystalline intensities are increased since thermal stability is decreased All crystalline peaks are related to sodium calcium silicate ($Na_2Ca_2Si_3O_9$) crystals as confirmed by standard JCPDS file no: (01-078-0364). The crystalline intensities vary nonlinearly from CPSN2 to CPSN4 sample with Na_2O. This variation occurs due to the light weight of Na_2O substitution (compared to weight of CaO). Also disrupt the glass network.

In SBF treatment, a chemical reaction occurs on the sample surface. In this process calcium ions migrate into SBF solution, form silanol groups. Due to polymerization and condensation process silica gel layer forms on sample. Calcium and phosphate ions migrate through silica gel layer and forms apatite (calcium phosphate) layer on the sample surface. Due to crystallization process between existed hydroxyl, calcium, phosphate ions in SBF and apatite layer, HA forms on sample surface. For SBF treated samples XRD pattern [Figure 3.2 (b)] show specific crystalline phases with

respect to composition changes. HA crystalline peaks also formed on the SBF treated CPSN sample surface. These crystalline peaks were matched with the standard JCPDS file with the number 01-089-6437. It was confirmed that $Na_2Ca_2Si_3O_9$ favoured to form HA for SBF treated samples in dissolution process (Wu and Chang 2012, Lukito et al. 2005, Singh et al. 2009). Calcite crystalline peak was also observed at 29° (JCPDS No: 01-085-1108). In dissolution process HA layer consumes the dissolution of Ca^{2+} ions (Lukito et al. 2005). HA layer may consume more Ca^{2+} ions for CPSN2 compared to CPSN1 sample, due to this reason calcite crystalline intensities were decreased from CPSN1 to CPSN2 sample. HA layer may consume less Ca^{2+} ions for CPSN3 compared to CPSN2 sample due to this reason, calcite crystalline intensities were increased from CPSN2 to CPSN3 sample. And also HA layer may consume more Ca^{2+} ions for CPSN4 compared to CPSN3 sample, due to this reason calcite crystalline intensities were decreased from CPSN3 to CPSN4 sample. From this observation it can be concluded that calcite crystalline intensities also showed nonlinear variation with CaO/Na_2O ratios.

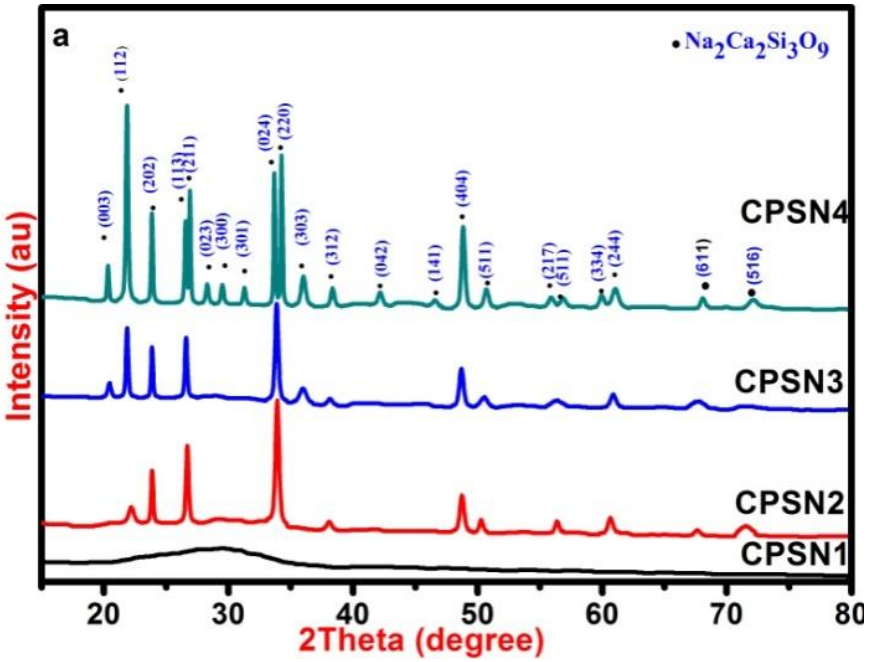

Figure 3.2(a) XRD patterns of CPSN samples

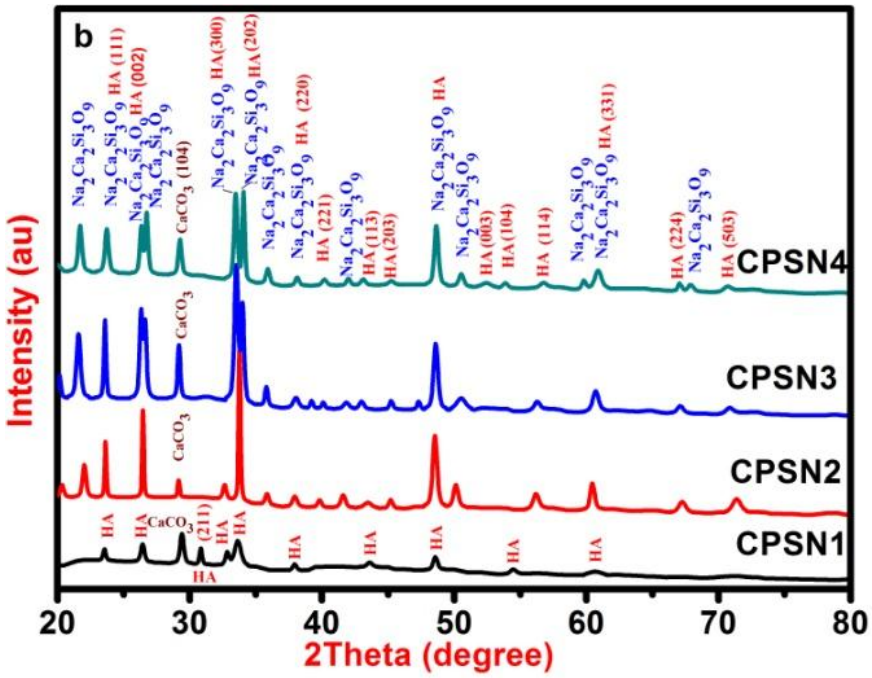

Figure 3.2(b) XRD patterns of CPSN samples after soaking in SBF.

3.3.3 SEM/EDX analysis

Surface morphology of CPSN samples is shown in Figure 3.3 (a, c, e and g). CPSN1 samples have no crystals on its surface. Further, it indicates CPSN1 is amorphous material as confirmed by XRD spectra. CPSN2 to CPSN4 samples show $Na_2Ca_2Si_3O_9$ crystalline morphology as can be seen from XRD spectra. EDX analysis confirms that CPSN samples have Si, Ca, Na, P and O elements on surface [Figure 3.3 (b, d, f and h)]. As discussed in the previous section the crystallization process between existing hydroxyl, calcium, phosphate ions

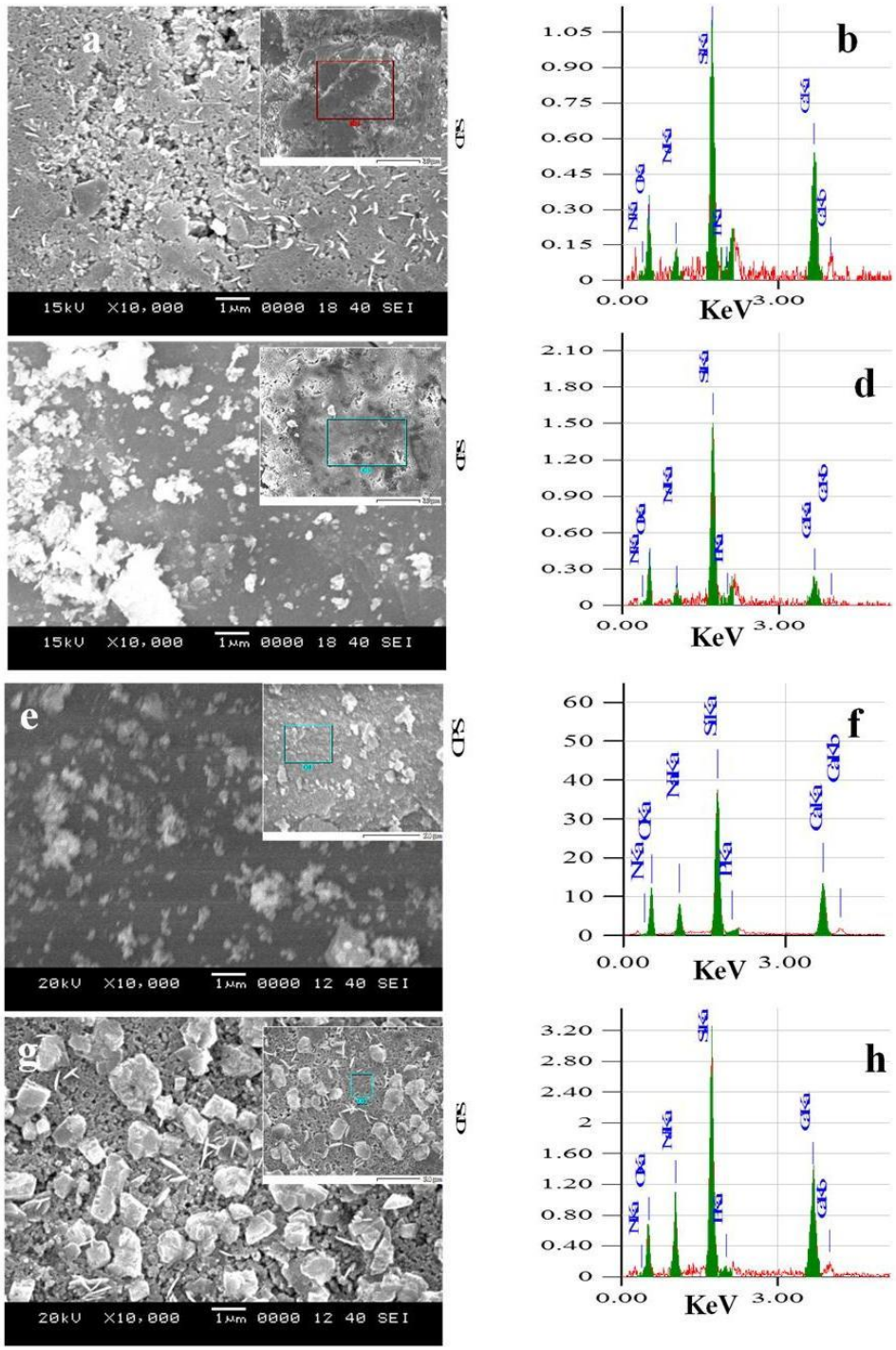

Figure 3.3 (a), (c), (e), (g) SEM images (b), (d), (f), (h). EDX analysis of CPSN1, CPSN2, CPSN3, CPSN4 glasses respectively.

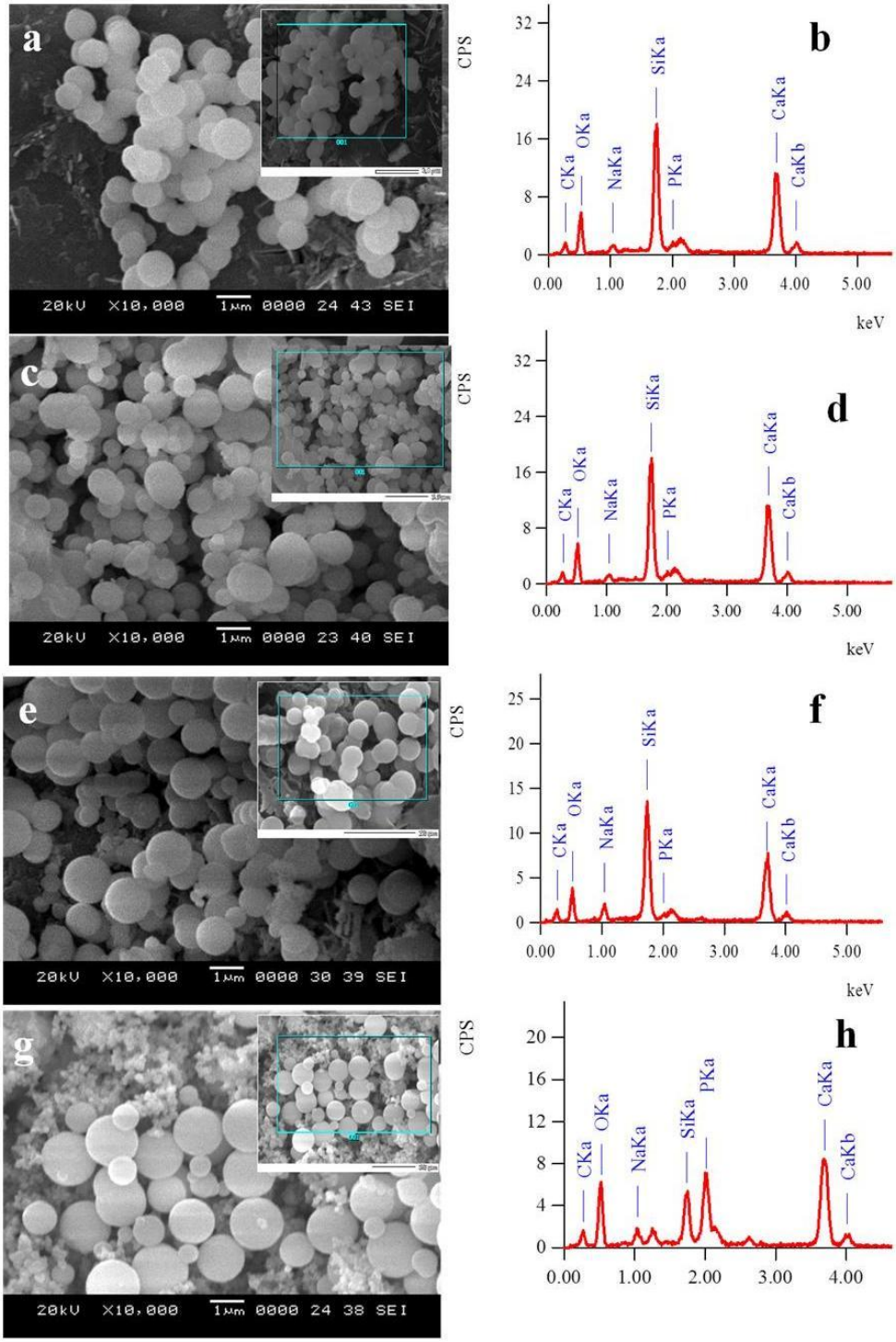

Figure 3.4 (a), (c), (e), (g) SEM images (b), (d), (f), (h) EDX analysis of SBF treated CPSN1, CPSN2, CPSN3 and CPSN4 glasses.

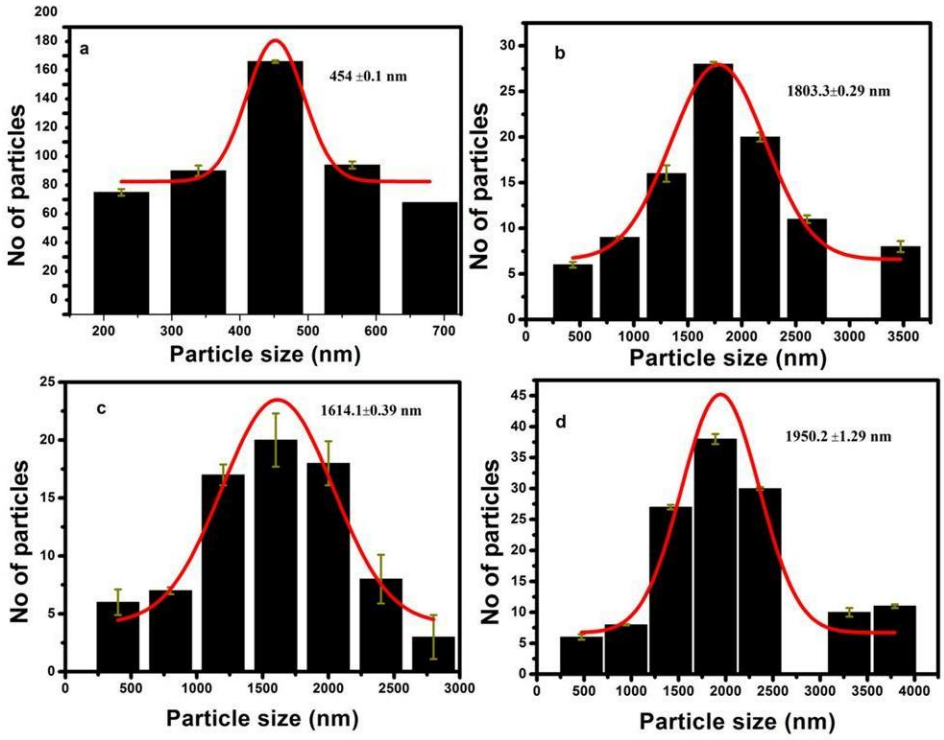

Figure 3.5 (a, b, c and d) HCA particle size distribution of SBF treated CPSN1, CPSN2, CPSN3 and CPSN4 glasses

and apatite layer leads to the formation of HA on sample surface. In this process, with the presence of CO_3^{2-}, HA is converted as HCA. SBF treated CPSN samples have spherical shaped HCA nuclei on their surfaces as shown in Figure 3.4 (a, c, e and g). Ca intensities also vary nonlinearly [Figure 3.4 (b, d, f and h)]**.** Also average HCA particle sizes (Figure 3.5) have increased from CPSN1 to CPSN2 decreased from CPSN2 to CPSN3 and again increased from CPSN3 to CPSN4 samples as shown in Table 3.5, it confirms that HCA nuclei size varies nonlinearly with Na_2O. From these observations it can be concluded that HCA formation varies nonlinearly with Na_2O (Zhao et al. 2010).

3.3.4 TEM/SAED analysis

Figure 3.5 (a, c, e and g) reports TEM images of SBF treated CPSN samples. Spherical shaped HCA crystals are observed in TEM images. Using SAED pattern [Figure 3.5 (b, d, f and h)] $d_{(211)}$-spaces of relevant TEM images were calculated by the

formula 2.4. Table 3.5 shows $d_{(211)}$-space of Hydroxyl apatite for CPSN samples by SAED analysis and these d-spaces were matched with the $d_{(211)}$-spaces of JCPDS file with Reference code: 01-089-6437.

3.3.5 Raman analysis

Figure 3.6 (a) shows the typical Raman spectra of CPSN samples. Si-O-Si asymmetric stretching modes were observed at 989-1070 cm^{-1} (Aguiar et al.2009) (Aguiar et al. 2009). A prominent Si-O-NBO asymmetric stretching mode was observed at 970-989 cm^{-1} (Aguiar et al.2009) . Raman spectra also displayed some discrete peaks emerging around 524-559 cm^{-1}, 588-600 cm^{-1}, 622-634 cm^{-1}as shown in Table 3.3 related to w_1 (≥5-fold rings) (Aguiar et al. 2009), D_1 (Four membered rings) and D_2 (three membered rings) (Aguiar et al. 2009), respectively. For SBF treated SN samples. Raman spectra showed peaks for PO_4^{3-}symmetric stretching, carbonate stretching modes were observed at 952-960 cm^{-1} and 1076-1086 cm^{-1}, respectively [Figure 3.6 (b)]. These studies confirmed that carbonates and phosphate groups were active for SBF treated SN samples

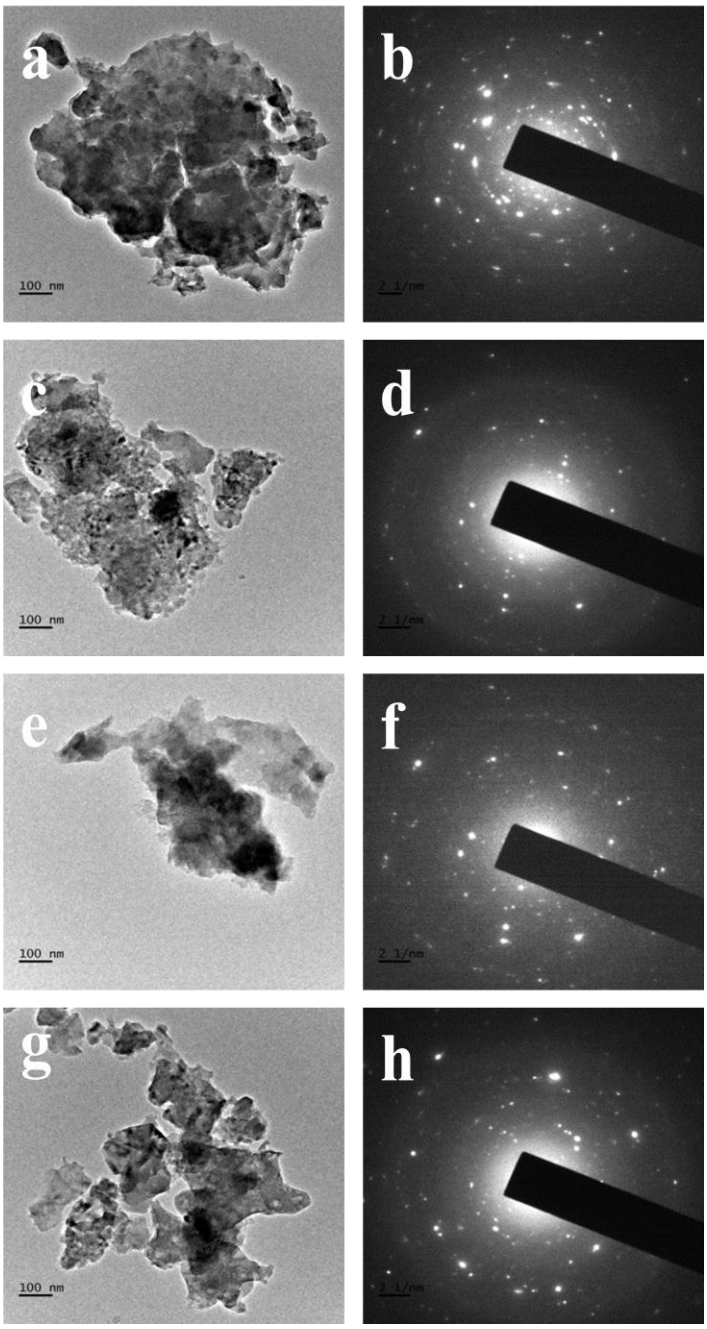

Figure 3.6 (a), (c), (e) and (g) TEM images of SBF treated CPSN1, CPSN2, CPSN3 and CPSN4 samples. (b), (d), (f) and (h) SAED pattern of SBF treated CPSN1, CPSN2, CPSN3 and CPSN4 samples.

Using de-convolution process non-bridging and bridging oxygen intensities were calculated. The obtained NBO/BO ratios for 5, 10, 15, 20 mol% Na_2O doped CPSN samples are 0.63, 0.79, 0.23 and 0.35 respectively. NBO/BO ratio was increased from 5 to 10 mol%, decreased from 10 to 15 mol% and increased from 15 to 20 mol% of Na_2O. It was observed that NBO/BO ratio varied nonlinearly with Na_2O [Figure 3.6 (c-f)]. CPSN1 sample showed broad bands, CPSN2 to CPSN3 samples show sharp peaks in Raman spectra. The peaks intensities (Related to Si-O-Si (as s), Si-O-NBO (as s), w_1, D_1 and D_2) decreased from CPSN2 to CPSN3, increased from CPSN3 to CPSN4. Thermal stabilities (ΔT) increased from CPSN2 to CPSN3, decreased from CPSN3 to CPSN4. Based on thermal stabilities (as discussed in TGA/DTA) in Raman spectra peak intensities are decreased from CPSN2 to CPSN3, increased from CPSN3 to CPSN4 samples (Marsich et al 2009, Lu et al. 2013).

Table 3.3 Raman band assignments of soda lime phosphosilicate glasses after soaking in SBF solution for 7 days.

Raman absorption band in cm^{-1}.

Before SBF treatment					After SBF treatment				
CPSN1	**CPSN2**	**CPSN3**	**CPSN4**	**Assigned bands**	**CPSN1**	**CPSN2**	**CPSN3**	**CPSN4**	**Assigned Bands**
-	524	559	533	W_1	955	960	952	952	PO_4^{3-} s s
600	590	588	591	D_1	1086	1086	1076	1076	CO_3^{2-} stretching
-	634	622	624	D_2					
970	986	989	988	Si-O-NBO as s					
1062	1064	1070	989	Si-O-Si as s					

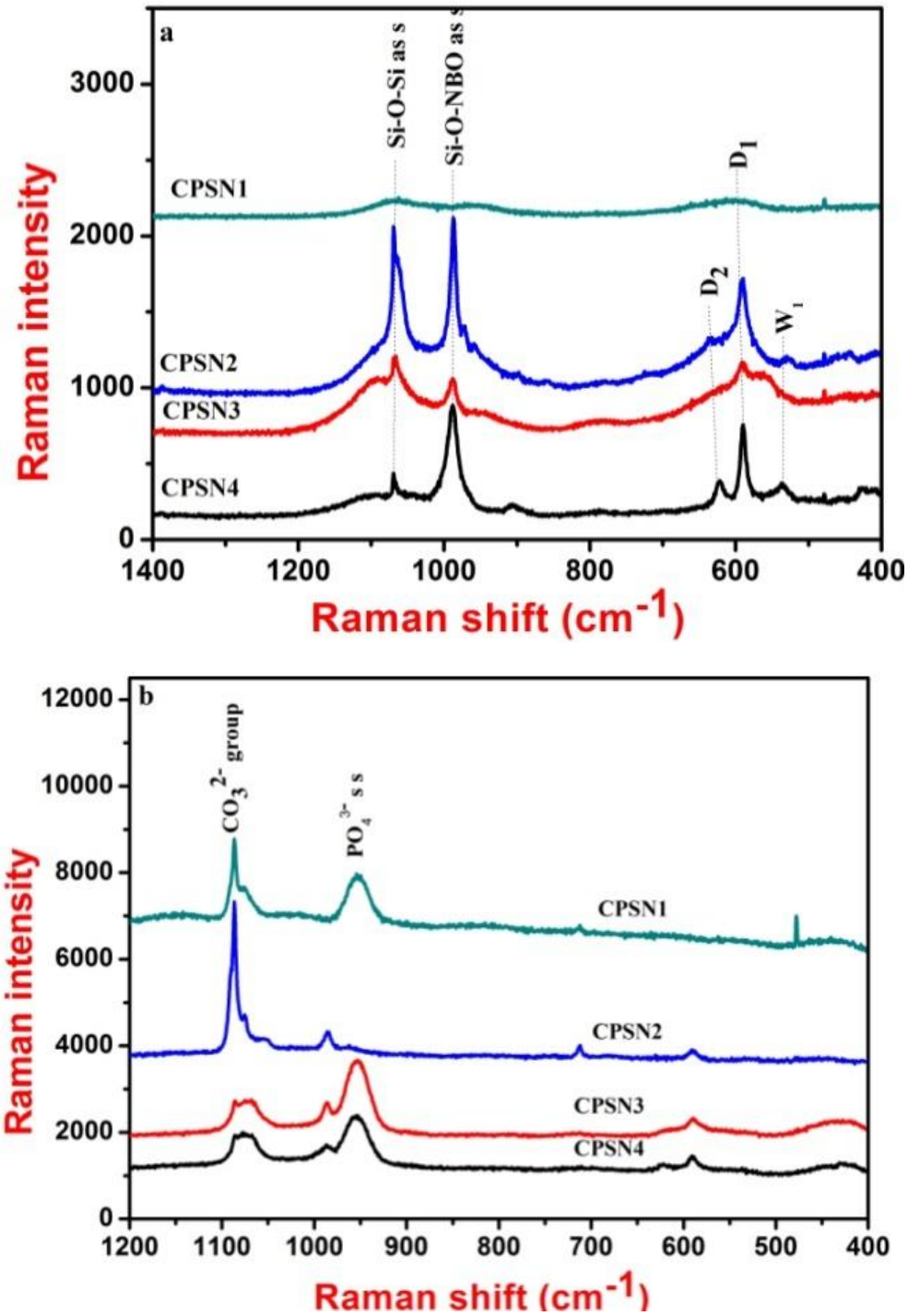

Figure 3.7 Raman spectra of (a) SBF un-treated and (b) SBF treated CPSN samples.

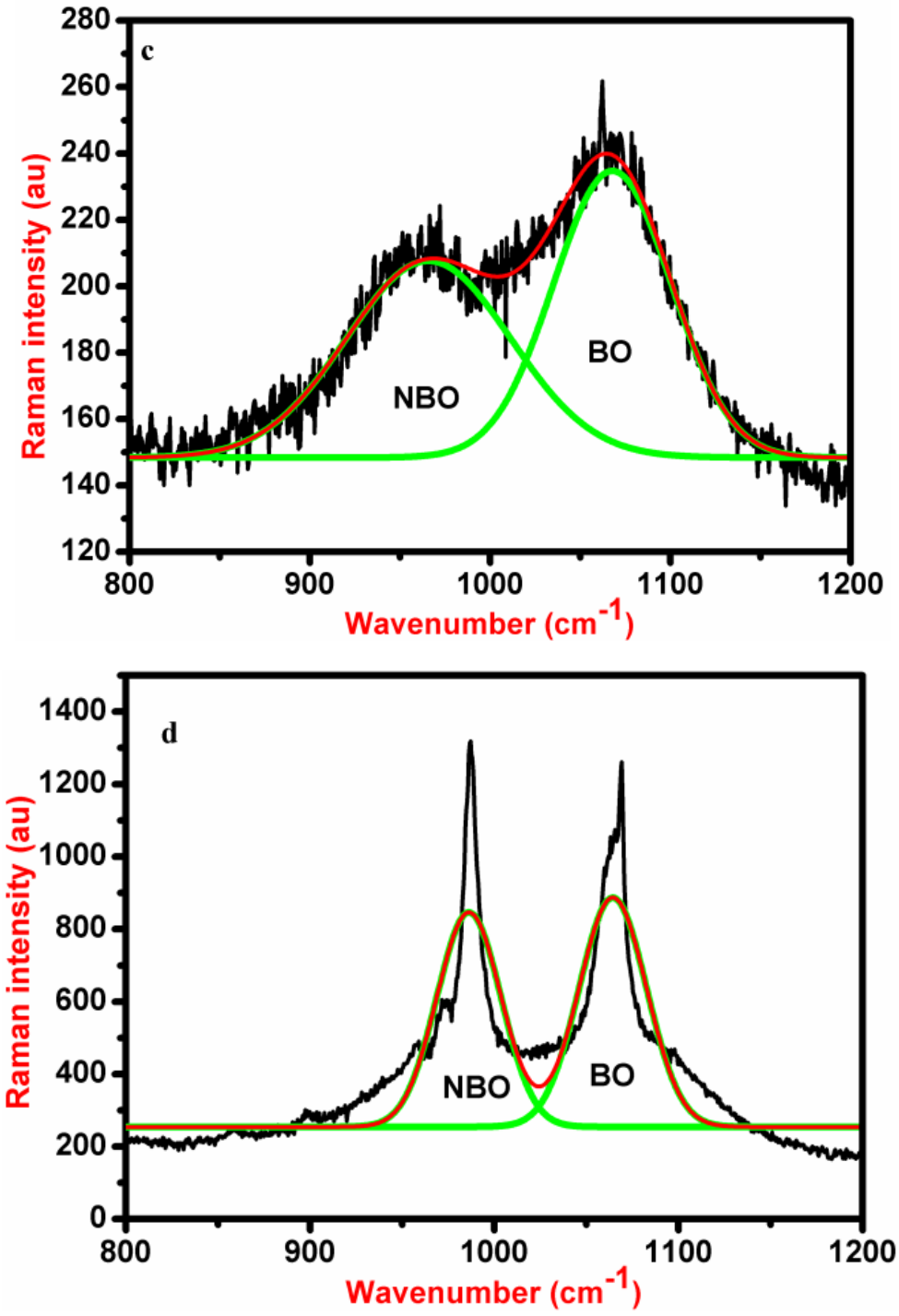

Figure 3.7 The de-convoluted results of the $58SiO_2$-(38-x) CaO-xNa_2O-4P_2O_5 system for (c) CPSN1, (d) CPSN2 samples.

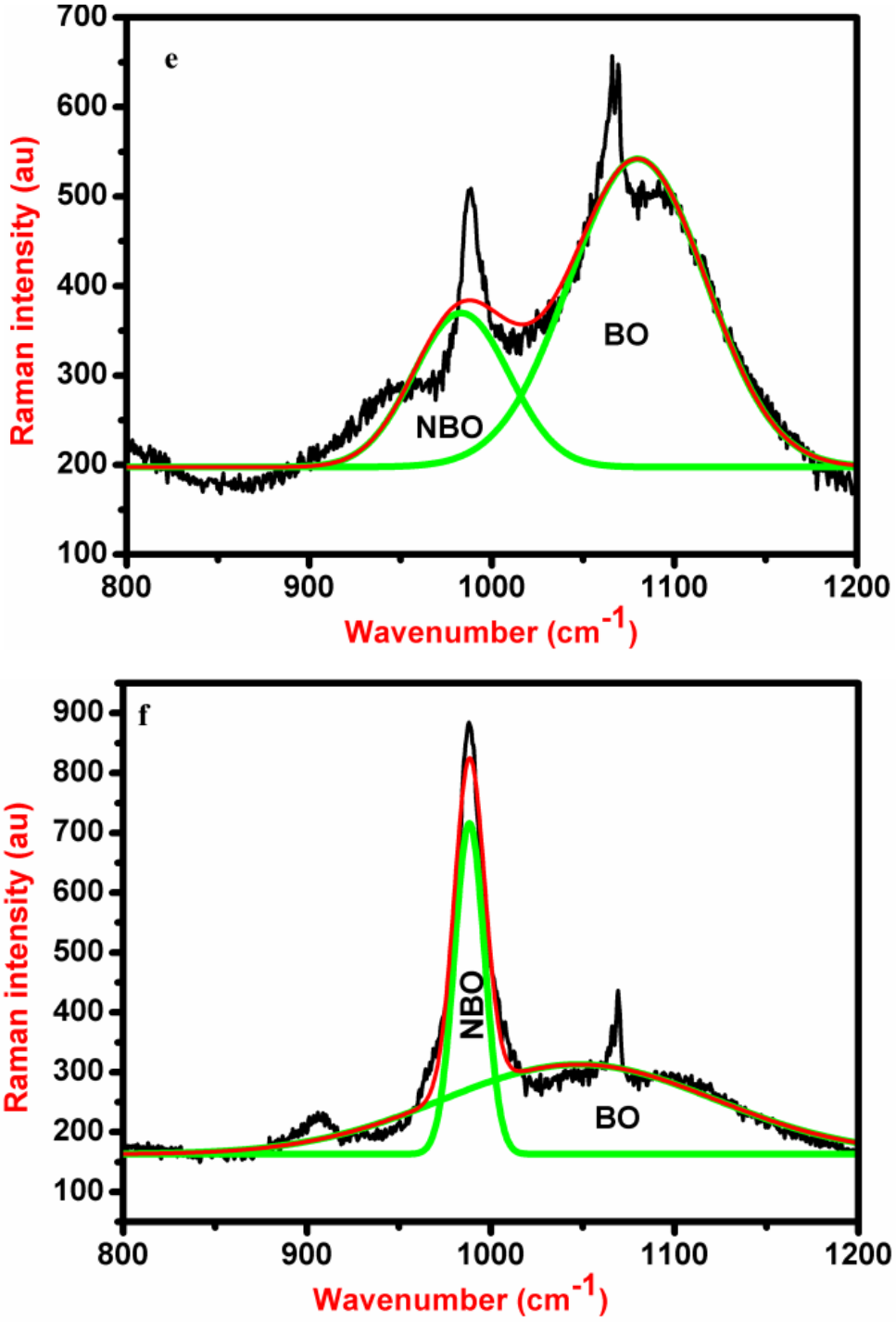

Figure 3.7 The de-convoluted results of the $58SiO_2$-(38-x) CaO-xNa_2O-4P_2O_5 system for (e) CPSN3 and (f) CPSN4 samples.

3.3.6 FTIR analysis

Figure 3.7 shows FTIR spectra of CPSN samples in the wave number range 400-3000 cm^{-1}. The assigned bands of Si-O-Si asymmetric stretching (as s) and Si-O-NBO asymmetric stretching (as s) modes related to silica matrix were observed at wave numbers 1094-1106 cm^{-1}(Li et al. 2014) and 1001-1024 cm^{-1} (Aguiar et al. 2008), respectively. Also Si-O-Si rocking, PO_4^{3-} bending and Si-O-Si bending modes were observed at 437-451 cm^{-1} (Li et al. 2014), 530-646 cm^{-1} (Aguiar et al. 2009, Bellucci et al. 2011) and 757-789 cm^{-1} (Aguiar et al. 2009), respectively [Table 3.4].

For SBF treated CPSN samples using FTIR spectroscopic analysis, assigned bands are observed in the wavelength region of 400 - 3000 cm^{-1}. As shown in Table 3.4 the assigned bands of Si-O-Si related to Si-O-Si rocking, bending and asymmetric stretching modes were observed at 457-466 cm^{-1}(Li et al. 2014), 774-792 cm^{-1} (Sun et al. 2015), 1011-1026 cm^{-1}(Sun et al. 2015), respectively [Figure 3.7 (a)]. For SBF treated samples broadness of Si-O-Si (as s) mode was increased and broadness of Si-O-Si bending mode was decreased (compared to FTIR spectra of SBF un-treated samples). It indicates that silica gel layer formed on glass surface. In dissolution process poly condensation of silanol groups lead to silica gel layer formation on sample surface (Yang et al. 2012, Marsich et al. 2009, Li et al. 2013, Aguiar et al. 2009). Calcium group was observed as Si-O-Ca (as Si-O-NBO) at 911-917 cm^{-1} (Aguiar et al. 2008). PO_4^{3-} bending crystalline modes (related to HA) were also observed at 623-698 cm^{-1}. [Figure 3.7(b)]. All bio active glass samples show the hydroxy carbonated apatite layer formation with the presence of corresponding Ca^{2+}, $CO_3^{2-}$and PO_4^{3-} groups.

3.3.7 pH assessment, Dissolution and Weight loss studies

In the dissolution process calcium ions get released into SBF solution, which led to silanol groups formation on sample surface. Due to the polymerisation and condensation process of silanol groups silica gel layer was formed on sample surface. Calcium and phosphate ions of sample leach on the silica gel layer surface leading to amorphous calcium phosphate (apatite) layer formation, it changes PO_4^{3-} and Ca^{2+} ion

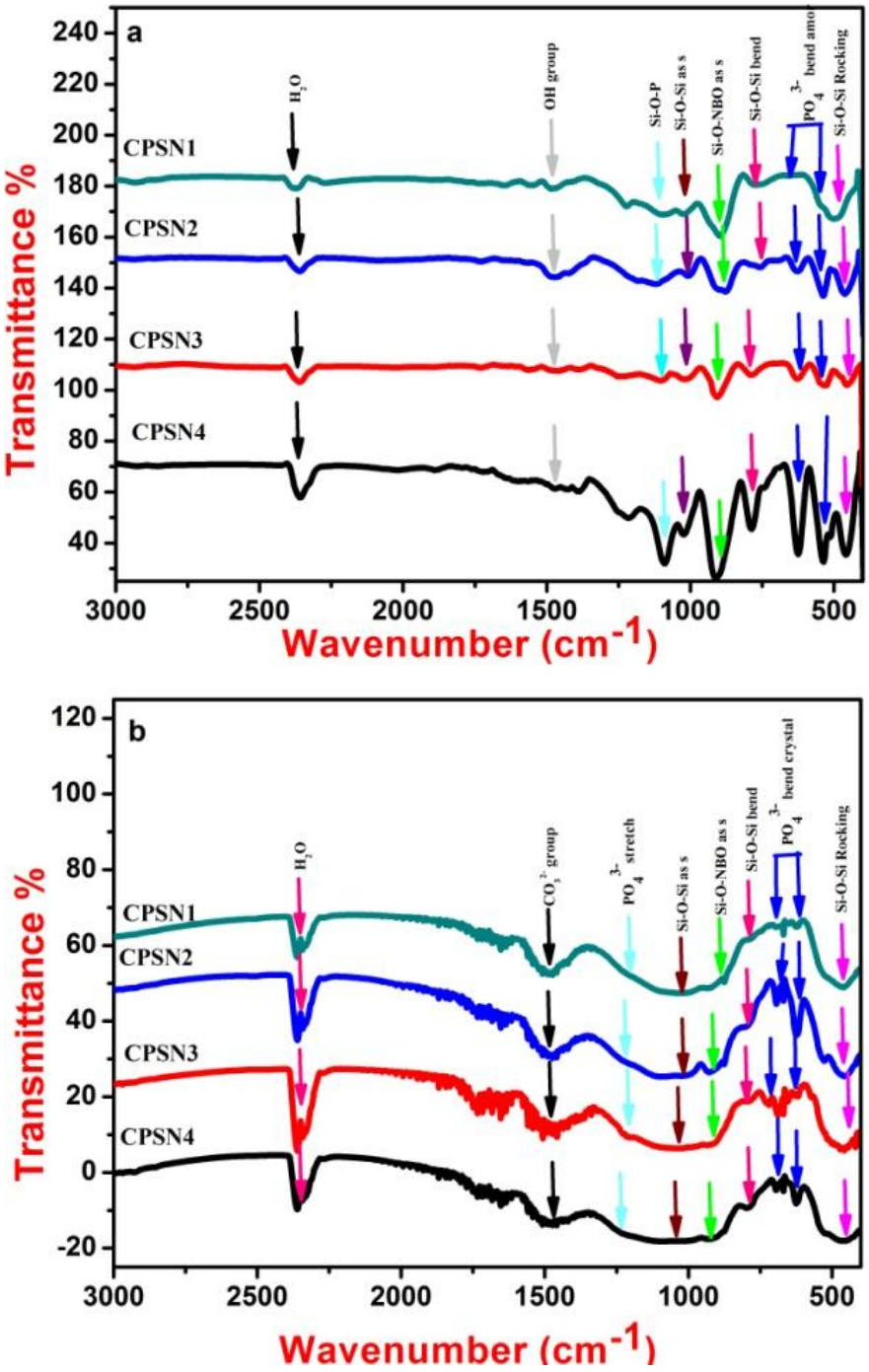

Figure 3.8 FTIR spectra of (a) SBF un-treated and (b) SBF treated CPSN samples.

Table 3.4 FTIR band assignments of soda lime phosphosilicate glasses before soaking in SBF solution.

Infrared transition band in cm^{-1}.

Before SBF treatment					**After SBF treatment**				
CPSN1	**CPSN2**	**CPSN3**	**CPSN4**	**Assigned bands**	**CPSN1**	**CPSN2**	**CPSN3**	**CPSN4**	**Assigned Bands**
437	451	448	451	Si-O-Si Rocking	457	460	463	466	Si-O-Si Rocking
530	533	536	539	PO_4^{3-} bending	626	623	623	629	PO_4^{3-} bending
646	626	626	623	PO_4^{3-} bending	681	690	690	698	PO_4^{3-} bending
777	757	789	786	Si-O-Si bending	774	786	792	786	Si-O-Si bending
1024	1001	1016	1022	Si-O-NBO (as s)	911	917	917	911	Si-O-NBO (as s)
1094	1106	1103	1094	Si-O-Si (as s)	1026	1011	1018	1026	Si-O-Si (as s)

concentrations of SBF solution. Incorporation of hydroxyl, PO_4^{3-}, Ca^{2+} and carbonate ions from SBF solution into apatite layer led to HCA formation on the sample surface (in the crystallization process) (Yang et al. 2012).

As shown in Figure 3.8 (a) the pH values increased till 10 hours of soaking time of the sample in SBF solution, which is due to the fast release of Ca^{2+} ions into SBF solution forming silanol. After 10 hours, pH values were slightly increased and almost stabilized [Figure 3.8 (a)]. As shown in Table 5.5 weight loss measurements confirmed that HCA formation increased from CPSN1 to CPSN2, decreased from CPSN2 to CPSN3 and increased from CPSN3 to CPSN4 samples.

Raman and FTIR spectroscopy analysis of CPSN samples revealed that the non-bridging oxygens existed as Si-O-Ca asymmetric stretching modes. The Raman

spectroscopic analysis also revealed that NBO/BO ratio increases for CPSN glasses from CPSN1 to CPSN2, decreases from CPSN2 to CPSN3 and increases from CPSN3 to CPSN4 sample. From this observation, it can be concluded that NBO/BO ratio varied nonlinearly with Na_2O.

HA layer formation on sample surface depends on Ca^{2+} and PO_4^{3-} ion release, as well as depends on the number of leaching Ca^{2+} and PO_4^{3-} ions also. The increase in NBO/BO ratio increases Ca^{2+} ion release. NBO/BO ratio showed nonlinear variation with Na_2O. Due to this reason the number of releasing Ca^{2+} ions also show nonlinear variation with Na_2O [Figure 3.8 (b)]. Ca^{2+} ion release leads to the HA formation on sample surface. From these observations, it can be concluded that HA formation show nonlinear variation with Na_2O. In dissolution process HA layer consumes the dissolution of Ca^{2+} ions (Lukito et al. 2005). Ha formation is more for CPSN2 compared to CPSN1 sample, due to this reason calcite crystalline intensities were decreased from CPSN1 to CPSN2 sample. Ha formation is less for CPSN3 compared to CPSN2 sample due to this reason calcite crystalline intensities were increased from CPSN2 to CPSN3 sample. HA formation is less for CPSN3 compared to CPSN4 sample, due to this reason calcite crystalline intensities were decreased from CPSN3 to CPSN4 sample. From this observation it can be concluded that calcite crystalline intensities also showed nonlinear variation with CaO/Na_2O ratios as discussed in XRD spectra. All synthesized glass samples have 4 mol% P_2O_5 content. CPSN1 sample has amorphous nature. HA formation depends on the number of leaching PO_4^{3-} ions on glass surface. Crystalline nature has increased from CPSN2 to CPSN4 samples and glass strength also increases. Increase in glass strength reduces the dissolution of glass, it causes the decrease in PO_4^{3-} ion release into SBF solution. SBF solution need to utilize PO_4^{3-} ions for HA formation based on PO_4^{3-} ion release from glass matrix. Due to this reason PO_4^{3-} ions concentration is decreased from CPSN1 to CPSN4 sample in dissolution process as shown in Figure 3.8 **(c)** (Wu and Chang 2012).

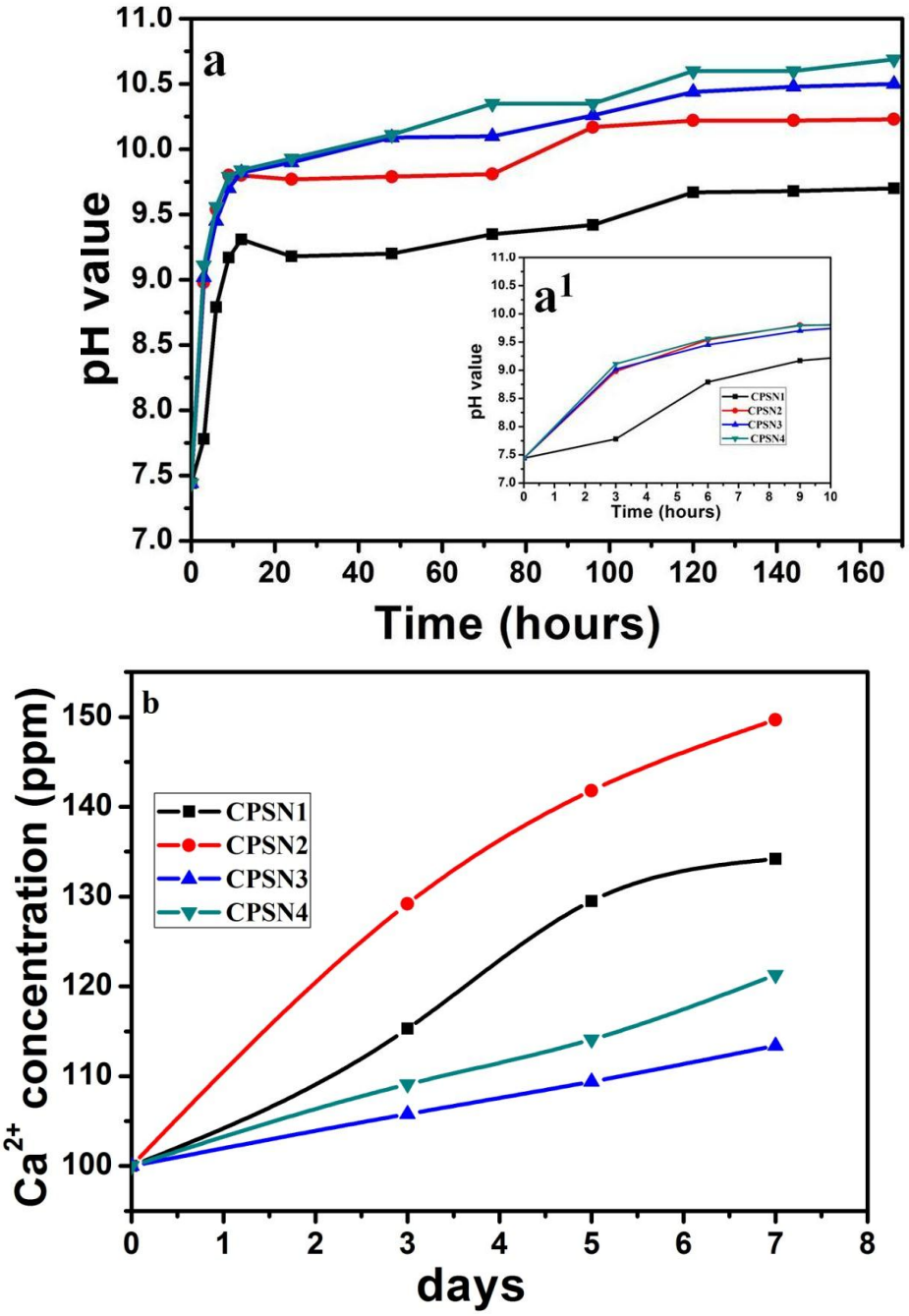

Figure 3.9 Variation of SBF solution (a) pH, (b) Ca concentration values with respect to CPSN glass soaking time in SBF solution.

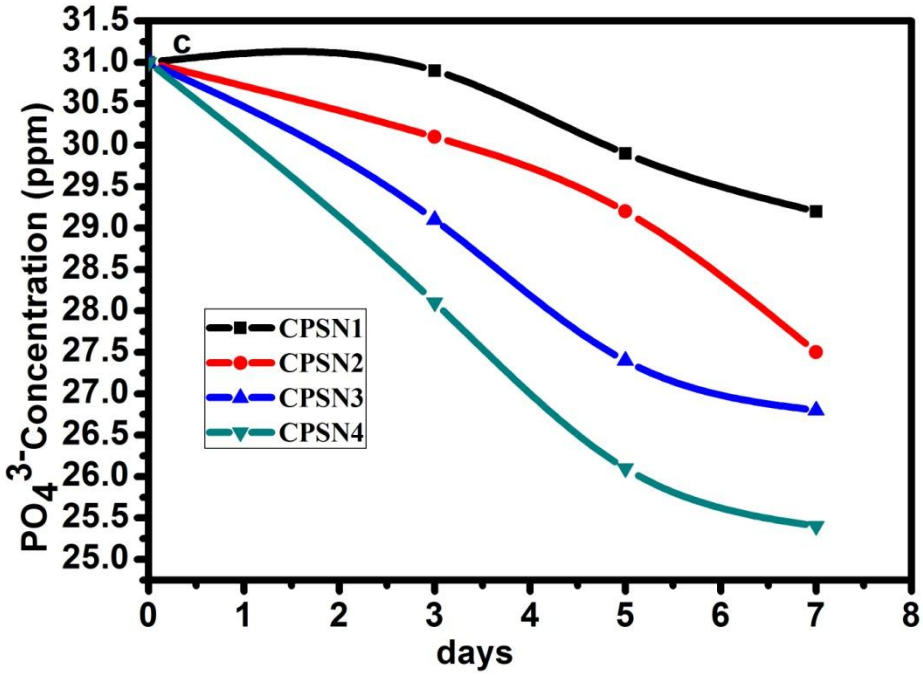

Figure 3.9 (C)Variation of SBF solution P concentration values with respect to CPSN glass soaking time in SBF solution.

Table 3.5 Weight loss % of SBF soaked $58SiO_2$-(38-x)CaO-xNa_2O-$4P_2O_5$ glasses with NBO/BO ratio and HCA particle sizes. d-space for Hydroxyl apatite by SAED analysis for CPSN samples.

x mol %	**(Raman) NBO/BO ratioa1**	**(SEM) Particle size (nm)**	**$d_{(hkl)}$ (TEM/SAED) (nm)**	**Weight loss for 7days SBF soaking %**
5	0.6293	454	0.2793	55.32
10	0.7917	1803	0.2812	69.13
15	0.2264	1614	0.2799	18.09
20	0.3513	1950	0.2787	20.08

The weight loss of SBF treated samples in the dissolution process increases from sample CPSN1 to CPSN2, decreases from CPSN2 to CPSN3 and increases from CPSN3 to CPSN4 sample. It indicates that weight losses of CPSN samples vary nonlinearly with

increasing Na_2O. This observation also confirmed that CaO/Na_2O ratio leads to the nonlinear variation of HA formation for SBF treated soda lime phosphosilicate glasses.

NBO/BO ratio and dissolution of SN samples vary nonlinearly with Na_2O. Weight losses of CPSN samples also vary nonlinearly with Na_2O. Spherical shaped HCA nuclei were observed by SEM images, confirmed by the identification of C, Ca, P elements using EDX analysis. HCA nuclei sizes also vary nonlinearly with Na_2O.

3.4 Conclusions

Thermal stability, NBO/BO ratio of soda lime phosphosilicate glasses vary nonlinearly with Na_2O. Sample with 5 mol% Na_2O, shows the amorphous nature whereas with 10–20 mol% Na_2O shows crystalline nature with $Na_2Ca_2Si_3O_9$ phase. The $Na_2Ca_2Si_3O_9$ crystalline intensities vary nonlinearly with Na_2O content. HCA particle size for SBF soaked samples also vary nonlinearly with Na_2O.

This study will be helpful to know the difference in HCA formation for amorphous and different crystalline glass materials. Based on this, bone forming abilities can be improved in biological fluids in bio medical applications.

CHAPTER 4

SYNTHESIS AND CHARACTERISATION OF BARIUM SODALIME PHOSPHOSILICATE GLASSES

Chapter-4 deals with the synthesis of barium soda lime phosphosilicate glasses and includes of barium soda lime phosphosilicate dried gels the thermal properties. Structural properties of synthesized and SBF soaked barium soda lime phosphosilicate glasses are studied through FTIR, XRD, Raman spectrometry techniques. For SBF treated samples TEM/SAED analysis confirmed the HCA particles presence on sample surface. Hydroxy carbonate apatite forming ability studies have been done by dissolution studies of phosphate and calcium ions in SBF solution.

4.1. Introduction

Bioactive glass and glass ceramics are well known reactive materials and can be integrated in to human body where they can form biologically active apatite (Hydroxy apatite) layer at the bone/implant interface. Due to this reason they act as the fillers for bioactive composites (Yousefi et al. 2014, Greenspan et al. 1994, Greenspan et al. 1997, Greenspan et al. 1998). It is important to note that, bond between a glass material and the bone is a precipitation of an apatite layer on the surface of the glass material which is responsible for bioactivity. For tissue engineering applications, it is essential that the nucleation and growth of hydroxy apatite (HA) layer be fast on the surface of the bioglass surface in a precise reaction time in body environment (Kokubo et al. 1990, Sooksaen et al. 2015, Yousefi et al. 2014).

The HA growth rate is strongly influenced by the glass synthesis processes such as sol-gel processes, melt quenching technique, etc (Al-Noaman et al. 2012, Catauro et al. 2016). Sol-gel glasses can be produced at low temperature conditions with good homogeneity. The sol-gel method offers potential benefits for obtaining the powdered materials with good control of composition, microstructure and wider range of bioactivity (Al-Noaman et al. 2012, Bellucci et al. 2014, Goller et al. 2004, Arcos and Vallet-Regí

2010). Sol-gel process is a more convenient technique than melt quenching technique to improve HCA layer growth rate in SBF solution based on dissolution property of synthesized glass-ceramics in SBF solution. Based on higher rate of dissolution in SBF solution these glass samples have implications for biomedical applications such as, tissue engineering, bone bonding ability, cancer therapy etc (Hashmi et al. 2013, Peitl et al. 2001, Lukito et al. 2005, Sooraj Hussain et al. 2004, Laczka et al. 1999). The HCA growth rate in SBF solution is influenced by CaO/P_2O_5 ratio for calcium phospho silicate glasses (Sopcak et al. 2015, González et al. 2003,Marsich et al. 2009).

Network modifiers lead to change in the structure of glass ceramics with non-bridging oxygens [NBO] formation, this formation causes the softening of the glass ceramic. The bio activity strongly effected by NBO/BO ratio (Marsich et al. 2009). Raman spectroscopy is a powerful tool for non bridging oxygen identification and for finding the concentration of non bridging oxygens in glass matrix (González et al. 2003). Based on the sintering temperature, bio-activity of sol-gel SiO_2-CaO-P_2O_5 bio glass can influence the wollastonite or psudo-wollastanite structures formation after SBF treatment (Ma et al. 2010). The problem of HCA layer growth rate resistance in SBF soaked calcium phosphosilicate glasses can overcome by Na_2O addition (Siqueira and Zanotto 2013, Lusvardi et al. 2009, Al-Noaman et al. 2012) reported that melt quenched 47S SiO_2-CaO-P_2O_5-Na_2O bio active glass form HCA crystalline layer on glass surface after 30 days of SBF soaking time for pelletized glass samples. HCA layer formation for sol-gel derived SiO_2-CaO-P_2O_5-Na_2O bio glass, strongly influenced by precursors such as Tri ethyl phosphate (TEP) or phosphoric acid (H_3PO_3) (Siqueira and Zanotto 2013). Based on CaO quantity, lower P_2O_5 content and higher molar SiO_2 content sol-gel derived calcium phosphosilicate glasses exhibit good bioactivity. Higher CaO content leads to amorphous nature of glasses before SBF treatment. Recent study shows that barium with low concentrations in the glasses, acts as a muscle stimulant and is found in human teeth (Carta et al. 2007). Bone stimulating property can be improved by incorporation of bone stimulator ions into their chemical compositions. Moreover, there are limited studies on the role of CaO substitution on apatite layer formation of barium doped phosphosilicate

glasses (Shelby 2005, Arepalli et al. 2015, Zhao et al. 2010) and on the importance of higher BaO contents on HCA forming ability for sol-gel derived soda lime phospho silicate glass system.

The present chapter is concentrated on synthesis of [58SiO_2-(32-x)BaO-xCao-6Na_2O-4P_2O_5 bioactive (x= 15, 20, 25 and 30 mol %)] composition by sol-gel method. Thermal and structural properties were studied using TGA/DTA analysis and XRD techniques. Using FTIR, Raman spectroscopic techniques the non-bridging oxygens (NBO) and bridging oxygens (BO) were identified in the synthesized composition. NBO/BO ratios were found using Raman spectroscopic analysis. NBO/BO ratio effect on apatite layer formation for synthesized bio-active system has been investigated.

4.2. Materials and methods

4.2.1 Synthesis of tertiary calcium phosphosilicate glasses

As discussed in section 2.2.1 sol was prepared by hydrolysis process and for prepared sol sodium nitrate and barium nitrate were added and stirred well. The prepared sols were poured into teflon beakers, sealed with aluminum wrappers and kept inside hot air oven at 60 °C temperature for three days for aging purpose. Subsequently the aged gels were dried at 130 °C for 4 hours. The dried gels were ground, made into powders and heated at the rate of 5°C/min up to 700°C and stabilized at that temperature for 4 hours to obtain glass samples in the powder form. After getting powder samples, pellets have been prepared using hydraulic press by applying 5 tons' of pressure for 5 minutes.

As mentioned for CPS glasses in section 2.2.1 same characterization techniques were used for tertiary calcium phosphosilicate glasses before and after SBF treatment.

Table 4.1 Batch composition of $58SiO_2$-(32-x)BaO-xCaO-6Na_2O-4P_2O_5 glasses.

Glass sample	SiO_2 (mol%)	P_2O_5 (mol%)	Na_2O (mol%)	BaO (mol%)	CaO (mol%)
CPSNB1	58	4	6	17	15
CPSNB2	58	4	6	12	20
CPSNB3	58	4	6	7	25
CPSNB4	58	4	6	2	30

4.3. Results and discussion

4.3.1. TGA/DTA analysis

TGA/DTA curves were recorded to find the thermal behavior of CPSNB glasses. Three weight losses were observed in TGA curves as shown in Figure 4.1 (a-d). The first weight loss was at 108 – 123 $^{\circ}$C related to the evaporation of organics. The second weight loss was at 497 – 535 $^{\circ}$C related to the elimination of water caged in pores and third was at 598-627 $^{\circ}$C related to the organic residues from precursors used for sample synthesis and to the dehydration process [Table 4.2]. The glass transition temperatures were observed using DTA curves. These results dictated that CaO incorporation increases all the three temperatures, namly (1) The nucleation temperature (T_g) at 294-340 $^{\circ}$C (2) The onset stabilisation temperature (T_x) at 400 – 428 $^{\circ}$C (3) The crystallisation temperature (T_{c1}) at 420 – 472 $^{\circ}$C range. These three temperatures were known to be related to primary crystalline phase (Shelby 2005).Thermal stabilization temperature (ΔT) were calculated using formula 2.1. The calculated ΔT values are in in the range 78-106 °C. Second, third, fourth and fifth crystalline temperatures were also observed for CPSNB1, CPSNB2, CPSNB3 and CPSNB4 samples as shown in Table 4.3 (Arepalli et al. 2015). From these observations it was concluded that mixed alkaline earth oxide effect favors the crystalline nature of the glass samples.

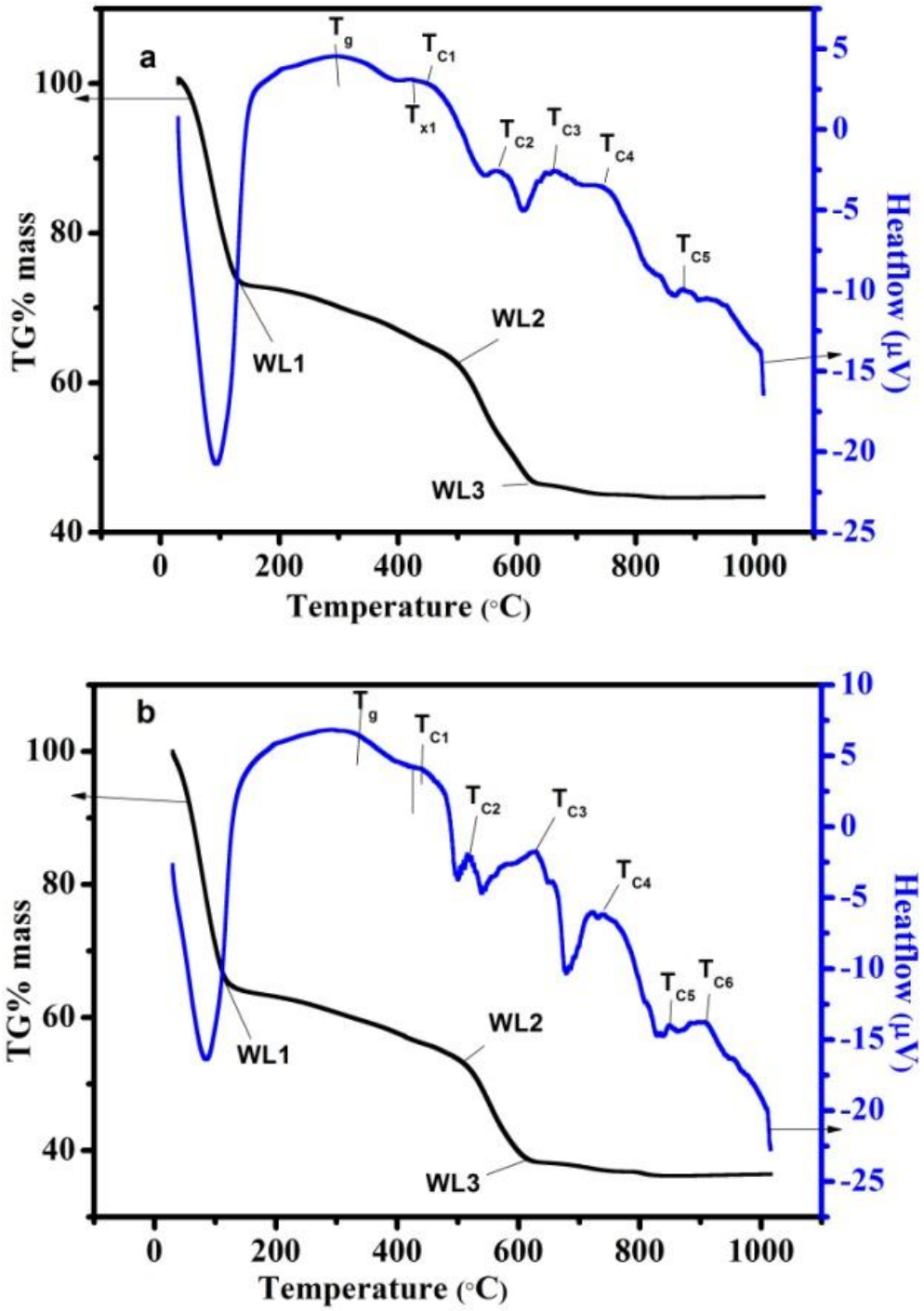

Figure 4.1 TGA/DTA curves of (a) CPSBN1, (b) CPSBN2 dried gels at 130°C.

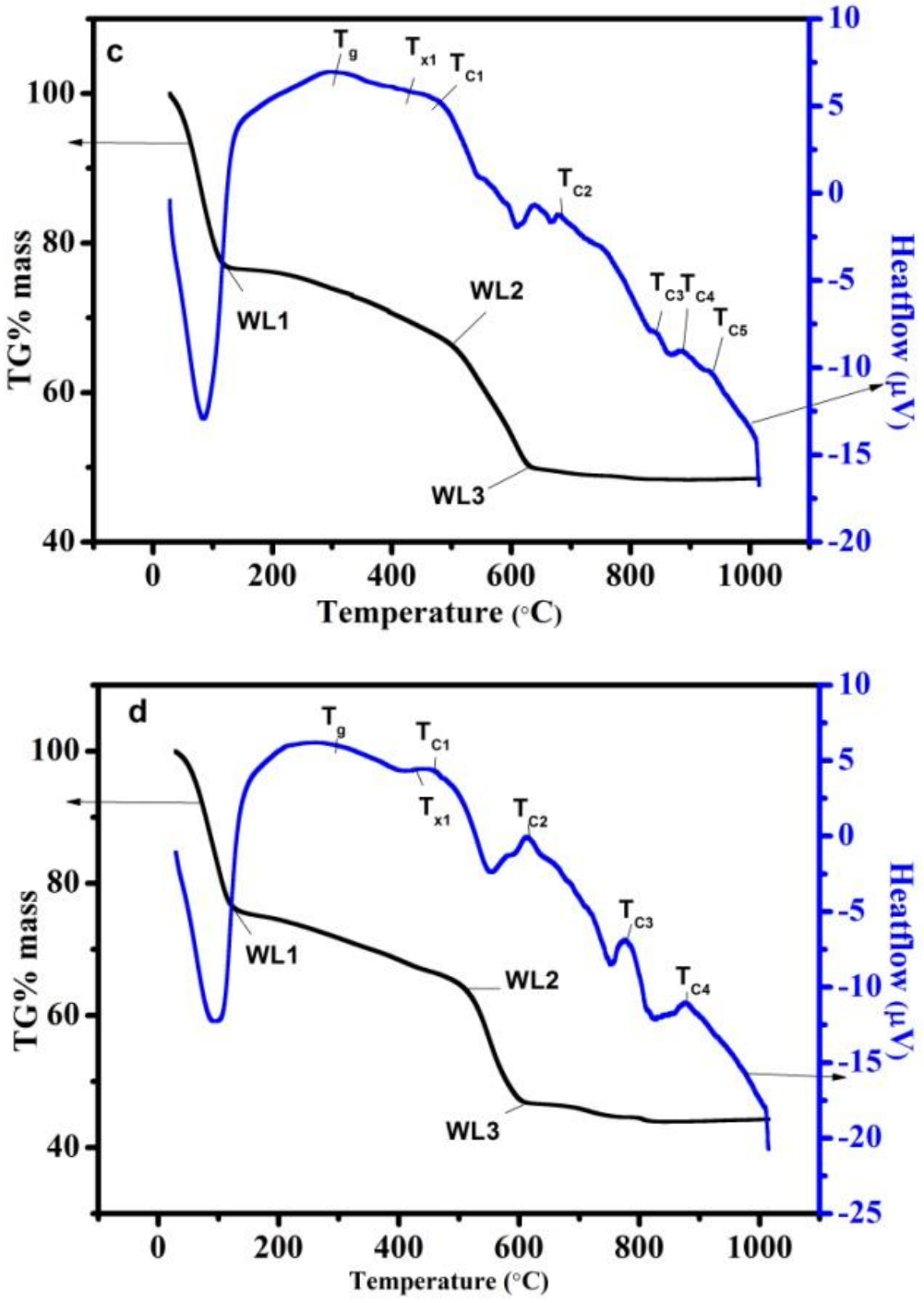

Figure 4.1 TGA/DTA curves of (c) CPSBN3 and (d) CPSBN4 dried gels at 130°C.

Table 4.2 Batch composition of $58SiO_2$-(32-x)BaO-xCaO-$6Na_2O$-$4P_2O_5$glasses with thermal properties.

Glass sample name	**Fist weight loss (°C)**	**Second weight loss (°C)**	**Third weight Loss (°C)**	**T_g (°C)**	**T_x (°C)**	**ΔT T_x-T_g (°C)**
CPSNB1	113	528	603	294	400	106
CPSNB2	123	497	622	327	405	78
CPSNB3	108	511	627	333	425	92
CPSNB4	111	535	598	340	428	88

Table 4.3 TGA/DTA related temperature values of $58SiO_2$-(32-x)BaO-xCaO-$6Na_2O$-$4P_2O_5$ glasses.

Glass	**T_{C1}(°C)**	**T_{C2}(°C)**	**T_{C3}(°C)**	**T_{C4}(°C)**	**T_{C5}(°C)**
CPSNB1	420	581	649	767	881
CPSNB2	446	521	627	741	849
CPSNB3	456	753	884	888	934
CPSNB4	472	610	779	876	-

4.3.2. XRD analysis

XRD patterns of CPSNB samples shown in Figure 4.2 (a) All samples show broad hump at 20 - 30° with some sharp intense peaks, indicating that all CPSNB samples had glass-ceramic in nature. Crystalline peak intensities decreased for CPSNB samples with increasing CaO content from 15 to 30 mol %. All glass samples were sintered at 700 °C. Sintering temperature was higher than the onset crystalline temperature (As discussed in DTA curves). Due to this reason all glass samples showed crystalline peaks. The difference between sintering and onset crystalline temperatures was in decreasing order from CPSNB1 to CPSNB4 glass and leading to decrease in crystalline nature with CaO addition.

For SBF treated CPSNB samples XRD pattern [Figure 4.2 (b**)**] showed HA crystalline peaks. The major diffraction peak was identified at $2\theta=32^0$ [(hkl) = (211)]. d-spacing of crystalline peaks were matched with the standard JCPDS file with number 01-074-0565. Calcite phase was also observed at 29° (JCPDF NO 01-081-2027). In SBF treatment, a chemical reaction occurs on sample surface. In this process Ca^{2+} ions migrate into SBF solution and forms silanol (Si-OH) groups. Due to poly-condensation process silica gel layer forms on sample surface. Phosphate and calcium ions migrate through silica gel layer and forms apatite layer on the sample surface. Due to crystallization process between apatite layer and prevalent hydroxyl, calcium, phosphate ions in SBF, HA layer forms on sample surface. CPSNB1 sample has more BaO content than CPSNB2. BaO addition decreases the glass strength, increases the dissolution in SBF and it leads increase HA formation on sample surface. For SBF treated samples crystallite sizes were calculated for (211) and (132) planes using formula 2.3. HA crystallite sizes were decreased with increasing CaO content from 15 to 20 mol % . It corroborates that HA forming ability is more for CPSNB1 compared to CPSNB2 sample. HA crystallite sizes were increased from 20 to 30 mol% of CaO. HA layer formation depends on Ca^{2+} ions dissolution in SBF solution. CaO quantity increases from CPSNB2 to CPSNB4 sample. Due to this reason Ca^{2+} ions dissolution increases from CPSNB2 to CPSNB4 sample, it led to increase in HA crystalline intensity from CPSNB2 to CPSNB4 sample. It corroborates that HA forming ability increases from CPSNB2 to CPSNB4 sample. From all these observations it was concluded that both the conditions, namely (i) higher BaO content and (ii) increase in CaO content favour the HA formation.

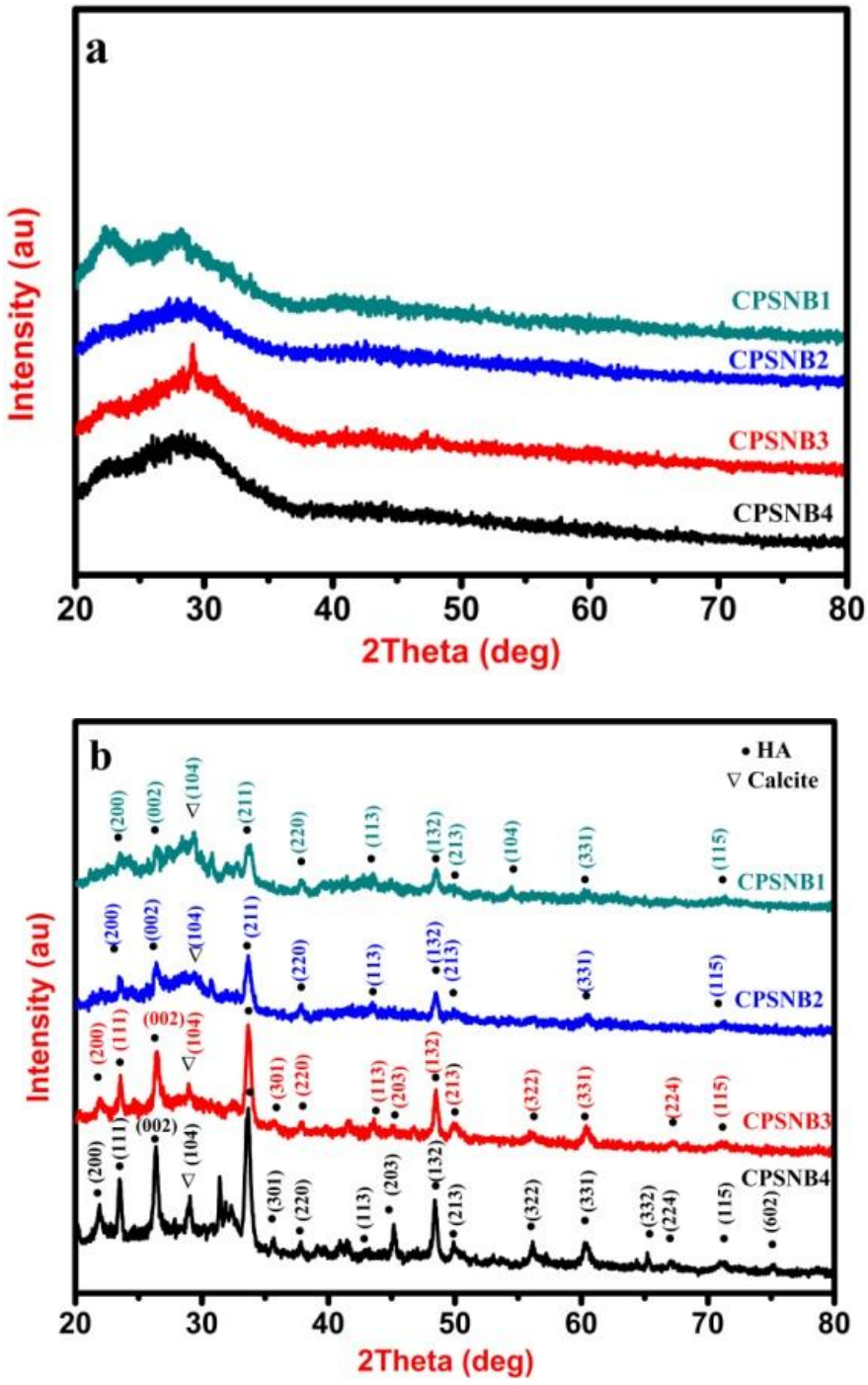

Figure 4.2 XRD pattern of CPSNB samples (a) before SBF treatment (b) after SBF treatment.

4.3.3. Surface morphology

The surface morphology of CPSNB samples before and after SBF treatment is as shown in Figure 4.3 and 4.4. Before SBF treatment [Figure 4.3 (a, c, e and g)] all CPSNB samples had not shown any spherical shaped crystalline particles and corresponding EDX analysis confirmed that elements present in sample were Ba, Si, Ca, Na, P and O [Figure 4.3 (b, d, f and h)]. After SBF treatment the SEM images [Figure 4.4 (a, c, e and g)] clearly exhibited the spherical shaped nuclei on the sample surface. As discussed in the previous section the crystallization process between apatite layer and existing hydroxyl, calcium, phosphate ions led to the formation of HA on the sample surface. In this process, with the presence of CO_3^{2-}, HA gets converted into as HCA. EDX analysis also supports the HCA layer formation on the CPSNB sample surfaces by identifying elements as Ca, P, C and O [Figure 4.4 (b, d, f and h)]. EDX spectra show that Ca intensity decreased for CPSNB samples with increase in CaO content from 15 to 20 mol %. All SBF treated CPSNB samples show good homogeneity in particle size and smooth spherical morphology with HCA particles. For CPSNB1 samples HCA average size is 1517 nm. For CPSNB2, CPSNB3 and CPSNB4 sample, average HCA particle sizes are 1355 nm, 1587 nm and 1605 nm, respectively [Figure 4.5]. This shows that average particle size decreases with increase in CaO content from 15 to 20 mol% and increases with increase in CaO content from 20 to 30 mol % (Zhao et al. 2010). From these observations it could be concluded that HCA Forming ability is more for CPSNB1 compared to CPSNB2 sample and HA forming ability is in increasing order from CPSNB2 to CPSNB4 sample as observed in XRD analysis.

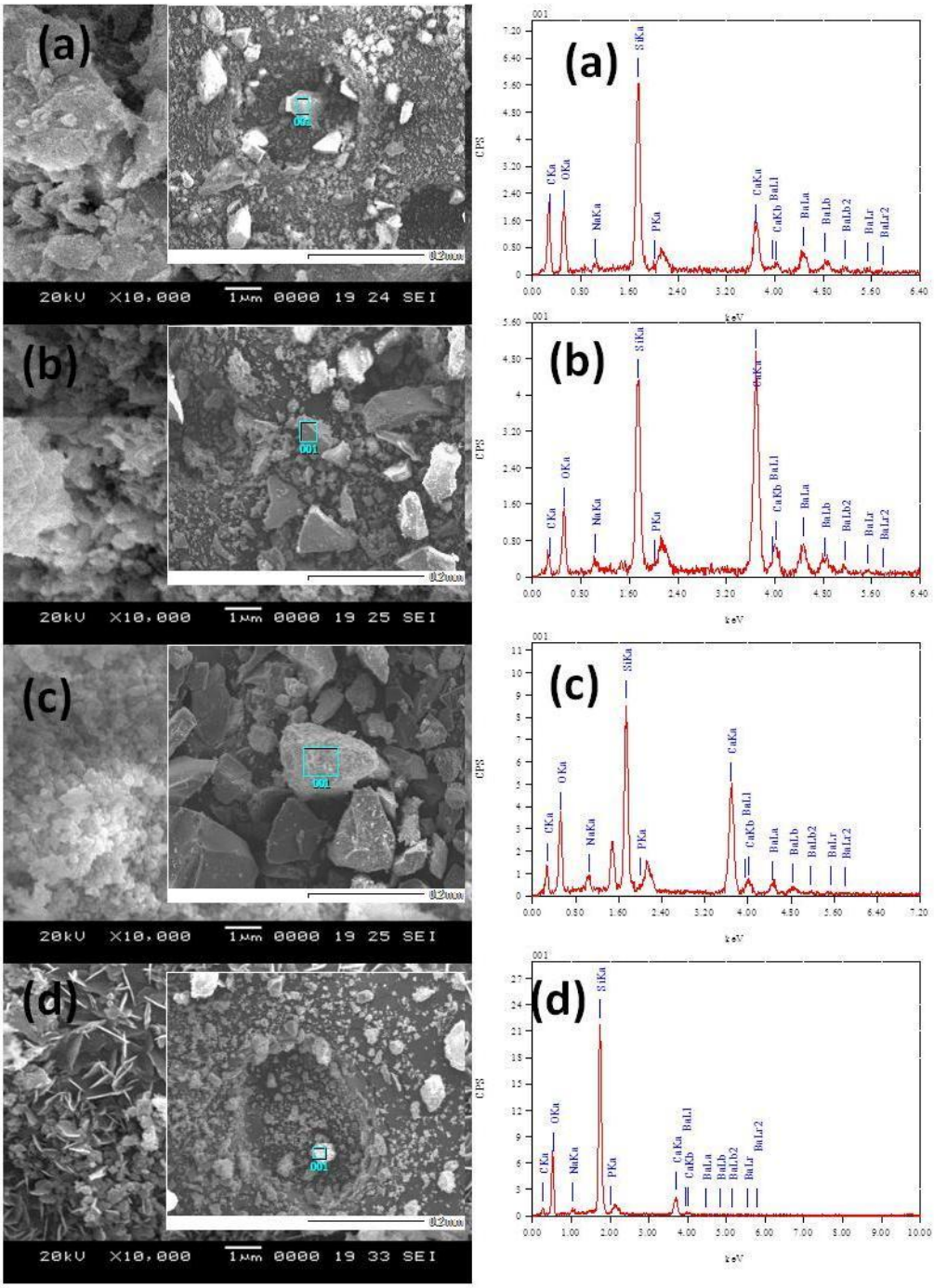

Figure 4.3 (a), (b), (c) and (d) SEM images and EDX analysis of CPSNB1, CPSNB2, CPSNB3 and CPSNB4 glasses.

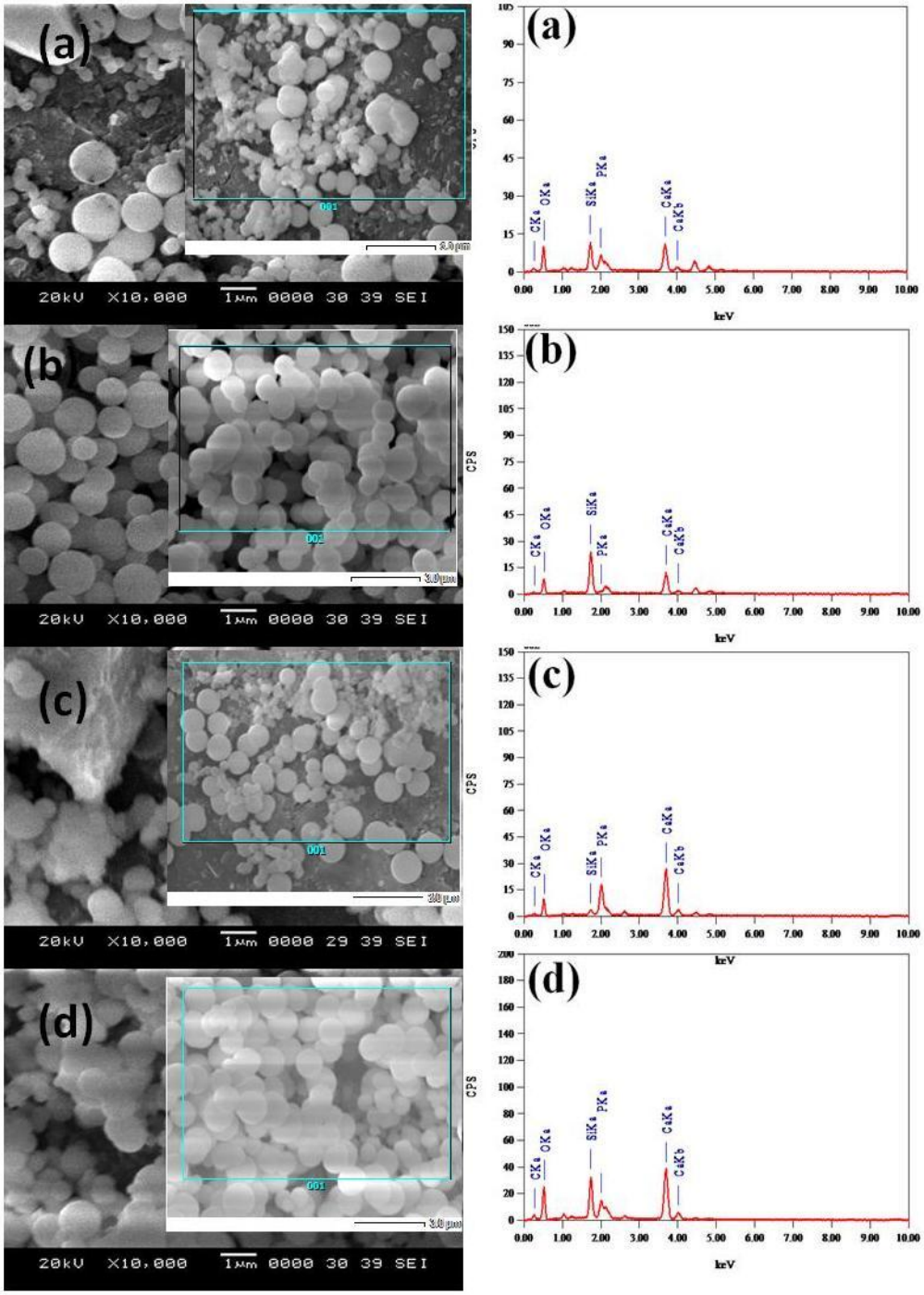

Figure 4.4 (a), (b), (c) and (d) SEM images and EDX analysis of SBF treated CPSNB1, CPSNB2, CPSNB3 and CPSNB4 glasses.

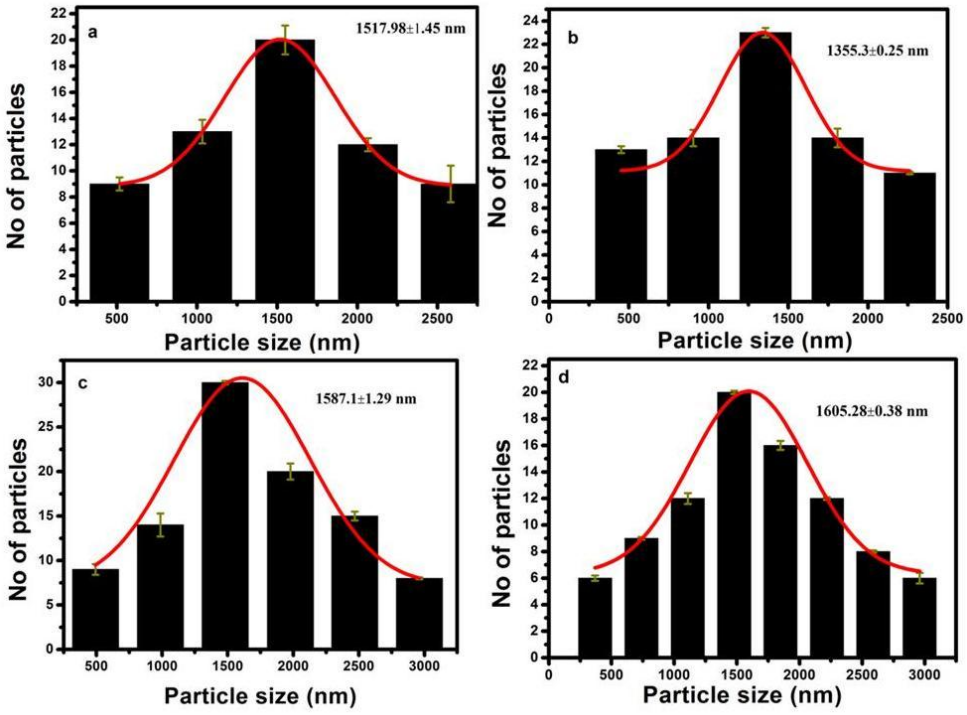

Figure 4.5 particle size distribution of SBF treated (a) CPSNB1, (b) CPSNB2, (c) CPSNB3 and (d) CPSNB4 glass samples

4.3.4. Raman analysis

Figure 4.6 (a) shows Raman spectra of CPSNB samples. For all CPSNB samples assigned D_2 modes were observed at the wave number range of 565-593 cm^{-1} (Aguiar et al. 2008, Notingher et al. 2002). Si-O-NBO (Aguiar et al. 2009), Si-O-Si asymmetric stretching modes were observed at 956-965 cm^{-1}(Aguiar et al. 2009) and 1058-1068 cm^{-1}(Aguiar et al. 2009), respectively as shown in Table 4.4 Using de-convolution process, non-bridging and bridging oxygen intensities were calculated (intensities were considered as corresponding fitted areas of Si-O-NBO, Si-O-Si asymmetric stretching modes) (Marsich et al. 2009, Zhao et al. 2010). NBO/BO ratio varies with CaO as shown in (as shown in Figure 4.6 (b-e)). The obtained NBO/BO ratios for CPSNB1, CPSNB2, CPSNB3 and CPSNB4 samples were 0.36, 0.23, 0.27 and 0.47, respectively. It indicates that NBO/BO ratio decreased with increase in CaO from 15 to 20 mol% and increased with increase in CaO from 20 to 30 mol% (Zhao et al. 2010). Wollstonite crystalline phase was also observed in the wave number region 1044-1051 cm^{-1} (Yadav and Singh 2015).

Table 4.4 Raman absorption bands for $58SiO_2$-(32-x)BaO-xCaO-$6Na_2O$-$4P_2O_5$ glasses (a) before and (b) after soaking in SBF solution.

(a) Before SBF treatment				
CPSNB1	**CPSNB2**	**CPSNB3**	**CPSNB4**	**Assigned bands**
565	578	593	592	D_2
962	956	957	965	Si-O-NBO as s
1058	1068	1061	1058	Si-O-Si as s

(b) After SBF treatment				
CPSNB1	**CPSNB2**	**CPSNB3**	**CPSNB4**	**Assigned bands**
958	952	986	952	PO_4^{3-} s s
1081	1084	1083	1076	CO_3^{2-} stretching

For SBF treated CPSNB samples, wollstanite crystalline phase has not been observed. It gave evidence to the fact that the wollstanite dissolved in SBF. Phosphate symmetric stretching, carbonate stretching vibrational modes were observed at 952-986 cm^{-1} (Aguiar et al. 2009) and 1076-1084 cm^{-1} (Rezwan et al. 2006), respectively as shown in Figure 4.6 (f) [Table 4.4]. CaO addition led to the deformation of Si-O-Si asymmetric stretching mode and formation of non-bridging oxygen modes. Si-O-Si stretching deformation causes not only for Si-O-NBO formation, but also for D_2 mode formation. For SBF treated CPSNB samples XRD pattern confirmed the HA formation. Raman spectroscopic analysis confirmed that carbonate groups were present. From these observations it was concluded that HCA layer formation was complete. SEM/EDX analysis also confirmed the HCA formation. Raman spectra confirmed that NBO/BO ratio decreased with CaO from 15 to 20 mol% and increased from 20 to 30 mol%. SEM/EDX analysis confirmed that HCA particle sizes decreased with CaO in the range 15 to 20 mol % and increased in the range from 20 to 30 mol %. From all these observations, it was concluded that NBO/BO ratio was proportional to HCA particle sizes of SBF treated CPSNB samples.

4.3.5. FTIR analysis

Figure 4.7 (a) shows FTIR spectra of CPSNB samples in the wave number range 400-3500 cm^{-1}. Si-O-Si and Si-O-NBO asymmetric stretching modes related to silica matrix were observed at 1033-1103 cm^{-1}(Rezwan et al. 2006) and 925-948 cm^{-1} (Rezwan et al. 2006), respectively. Si-O-Si rocking, bending modes were observed at 478-486 cm^{-1} (Rezwan et al. 2006), 771-779 cm^{-1} (Rezwan et al. 2006), respectively. PO_4^{3-} and CO_3^{2-} bending modes were also observed at 594-624 cm^{-1} (Kokubo and Takadama 2006) and 1427 cm^{-1} (Notingher et al.2002, Rezwan et al. 2006), respectively. The vibration

mode due to deformation of –OH groups was assigned at 1650-1658 cm^{-1} (Notingher et al.2002) Table 4.5.

For SBF treated CPSNB samples Si-O-Si modes were related to Si-O-Si rocking, bending and asymmetric stretching modes are observed at 458-473 cm^{-1}(Rezwan et al. 2006), 729-786 cm^{-1}(Rezwan et al. 2006) and 1097-1243 cm^{-1} (Rezwan et al. 2006), respectively [Figure 4.7 (b)]. Calcium group was observed as Si-O-Ca (as Si-O-NBO) at 879-928 cm^{-1}(Rezwan et al. 2006). CO_3^{2-} bending mode was also observed at1471-1491cm^{-1}(Aguiar et al. 2008). PO_4^{3-} bending modes with amorphous and crystalline nature were observed at 599-661 cm^{-1}(Kokubo and Takadama 2006) and 679-692 cm^{-1} (Kokubo and Takadama 2006), respectively. Si-O-Si asymmetric stretching mode broadness was increased for SBF treated samples compared to synthesized samples, it shows that silica gel layer formed on the sample surface in poly condensation process. From these observations, it can be confirmed that HCA layer was completely formed in SBF treatment. OH groups were observed at 1637-1718 cm^{-1} (Kokubo and Takadama 2006) respectively.

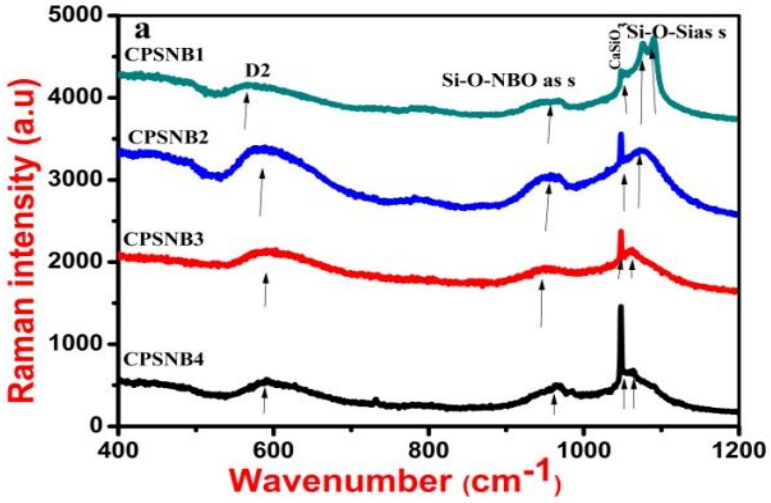

Figure 4.6 (a) Raman spectra of $58SiO_2$-(32-x) BaO-xCaO-$6Na_2O$-$4P_2O_5$system

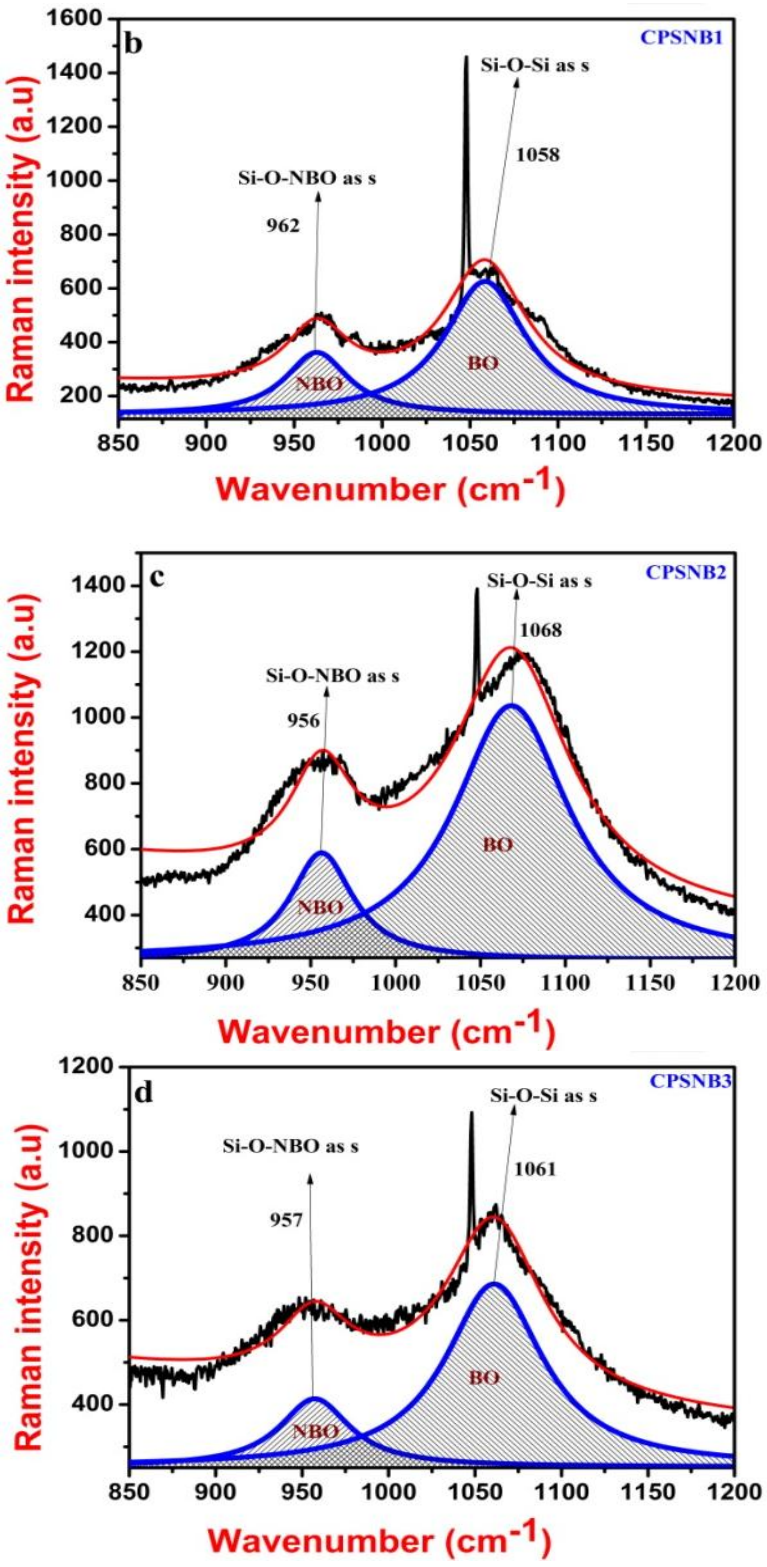

Figure 4.6 (b, c, d) Deconvoluted results of the sample CPSNB1,CPSNB2 and CPSNB

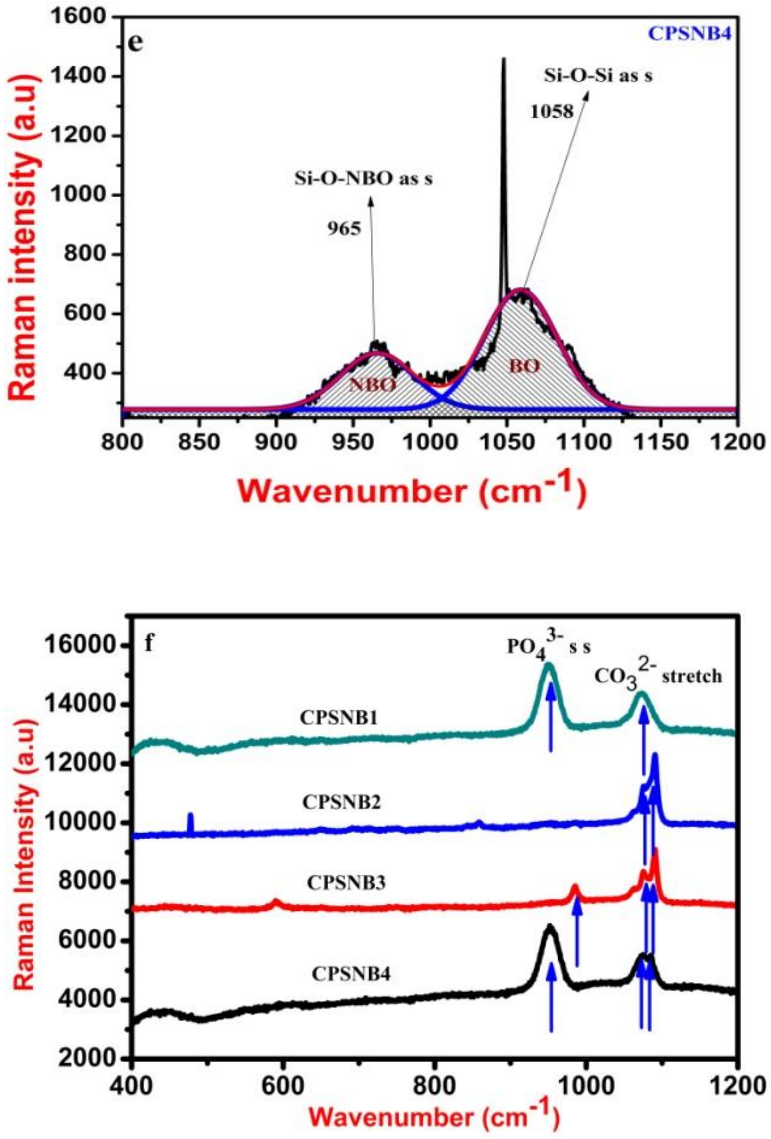

Figure 4.6 (e) deconvoluted results of the sample CPSNB4 (f) Raman spectra of SBF treated $58SiO_2$-(32-x) BaO-xCaO-$6Na_2O$-$4P_2O_5$ system.

Table 4.5 FTIR band assignments of barium doped soda lime phosphosilicate glasses before soaking in SBF solution.

Before soaking in SBF solution				
CPSNB1	**CPSNB2**	**CPSNB3**	**CPSNB4**	**Assigned bands**
486	486	478	478	Si-O-Si Rocking
594	609	624	624	PO_4^{3-} bending
779	771	771	771	Si-O-Si bending
925	948	933	925	Si-O-NBO As s
1087	1041	1033	1103	Si-O-Si as s
1427	1427	1427	1427	C-O bending
1650	1658	1650	1650	-OH group

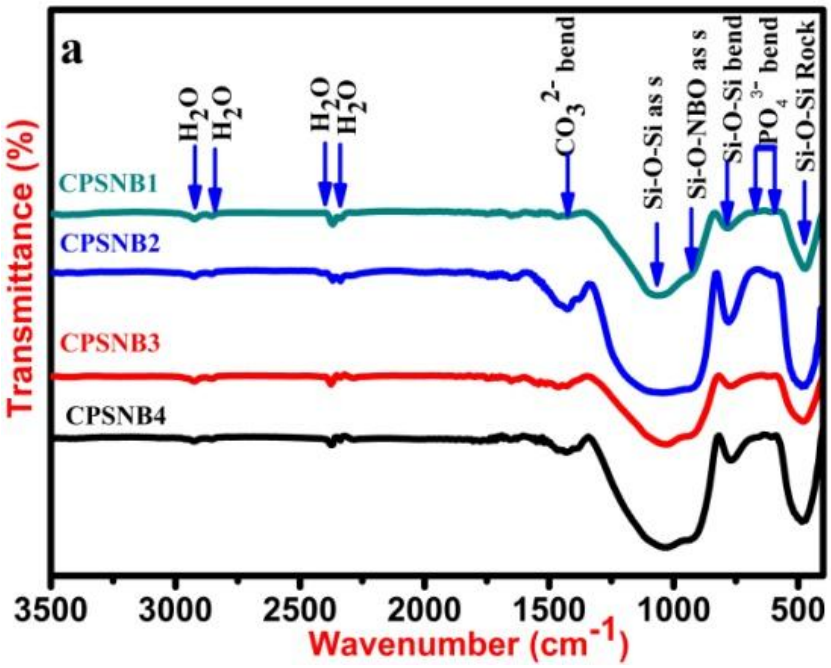

Figure 4.7 (a) FTIR spectra of CPSNB samples

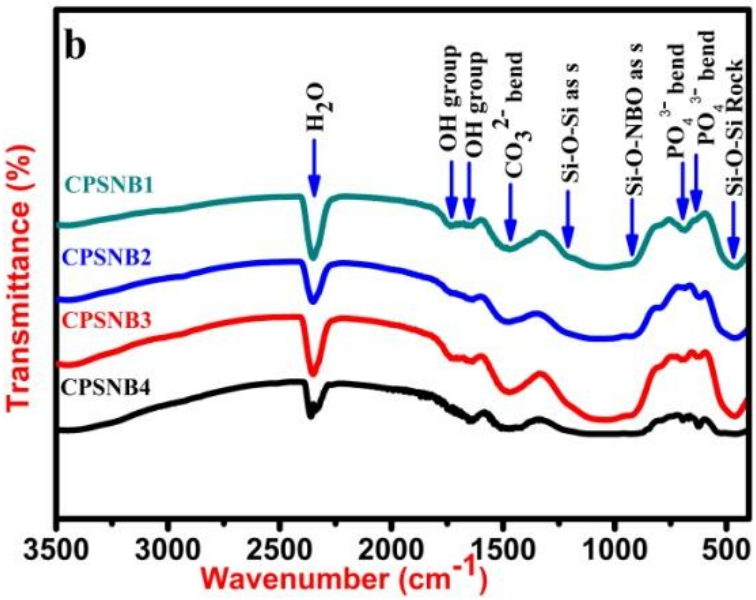

Figure 4.7(b) FTIR spectra of CPSNB samples after SBF treatment.

Table 4.6 FTIR band assignments of barium doped soda lime phosphosilicate glasses after soaking in SBF solution.

After soaking in SBF solution				
CPSNB1	**CPSNB2**	**CPSNB3**	**CPSNB4**	**Assigned bands**
460	463	473	458	Si-O-Si rocking
661	614	599	614	PO_4^{3-} bending
				Amorphous
687	692	679	687	PO_4^{3-} bending crystalline
786	769	774	729	Si-O-Si (bending)
928	879	909	920	Si-O-NBO (as s)
1192	1185	1243	1097	Si-O-Si (as s)
1472	1491	1489	1471	C-O bending
1718	1637	1688	1699	-OH group

4.3.6. TEM/SAED analysis

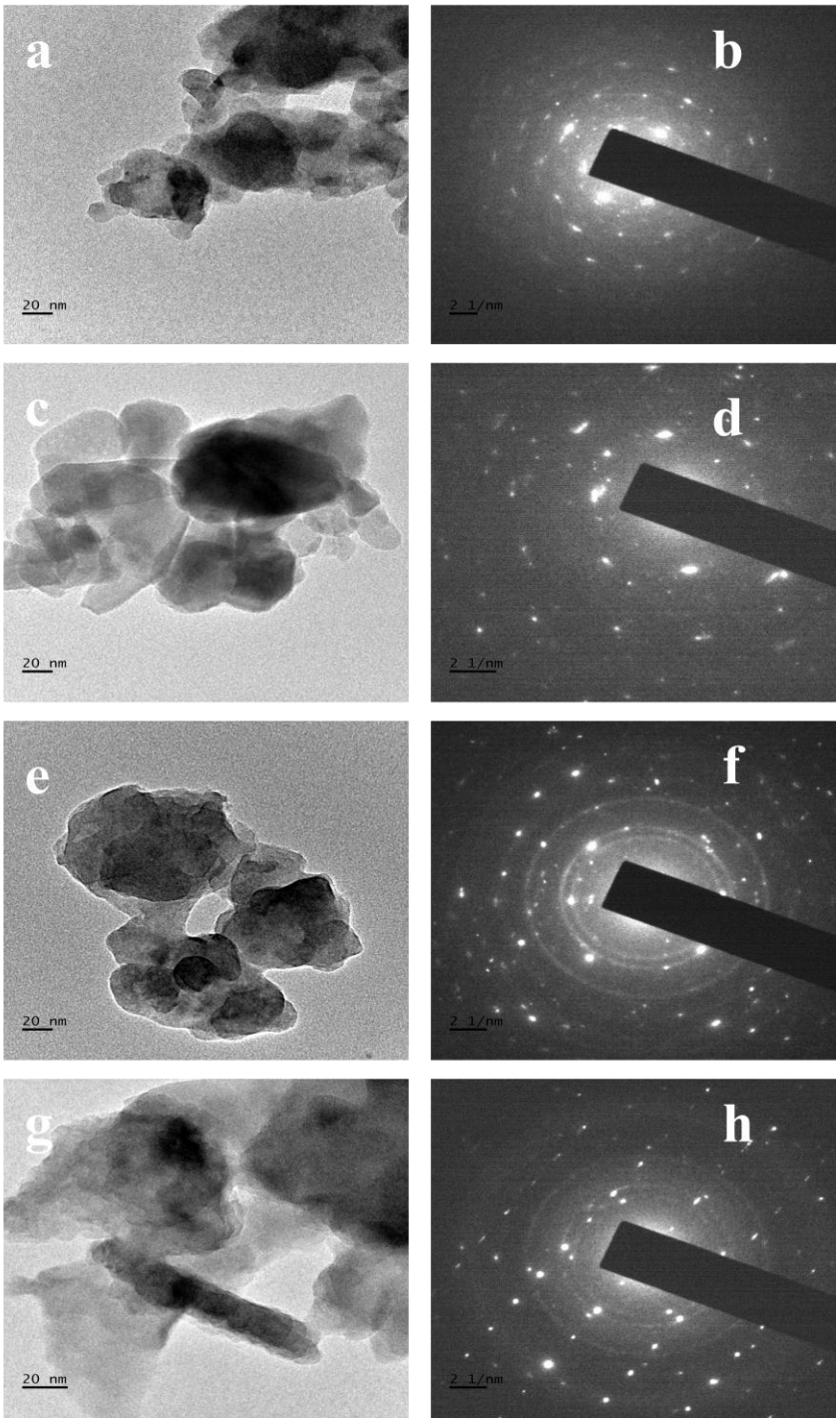

Figure 4.8 (a,c,e,g) TEM images (b,d,f,h) SAED pattern of SBF treated CPSNB1, CPSNB2, CPSNB3 and CPSNB4 glass samples

Figure 4.8 (a, c, e and g**)** reported the TEM images of SBF treated CPSNB samples. Spherical shaped particles have been observed in TEM images. Using SAED pattern [Figure 4.8 (b, d, f and h)] d-spacing of relevant TEM images were calculated using the formula 2.2. The calculated d-spacings were matched with the d-spaces of HA layer (Standard JCPDS card no.09-0432) [Table 4.7]. Hence, it was concluded that the spherical shaped particles were HCA particles.

Table 4.7 comparision of d-space for Hydroxyl apatite by SAED analysis and JCPDS file with Reference code: 01-086-0740.

D_{hkl} (TEM)	**CPSNB1**	**CPSNB2**	**CPSNB3**	**CPSNB4**	**d_{hkl} (JCPDS-01-086-0740)**
$d_{(002)}$	0.3368 nm	0.3349 nm	0.3356 nm	0.3372 nm	0.3441
$d_{(202)}$	0.2649 nm	0.2639 nm	0.2651 nm	0.2669 nm	0.2622
$d_{(301)}$	0.2528 nm	0.2498 nm	0.2512 nm	0.2531 nm	0.2513
$d_{(213)}$	0.1817 nm	0.1805 nm	0.1811 nm	0.1829 nm	0.1835

4.3.7. pH assessment, Dissolution and weight loss studies

pH values of SBF solution values were measured before and after soaking CPSNB samples in SBF for 7 days. pH values were found to increase till 10 hours [Figure 4.9 (a)], which was due to the fast release of calcium ions into SBF forms Si-OH groups (Arepalli et al. 2015). After 10 hours pH values were almost stabilized [Figure 4.9 (a)].

For CPSNB1 sample, NBO/BO ratio is high compared to CPSNB2 sample. NBOs are in the form of Si-O-Ca. HA layer formation on sample surface depends on calcium, phosphate ions dissolution of glass in SBF solution. NBO/BO ratio is also in the order CPSNB4> CPSNB1> CPSNB3> CPSNB2. All CPSNB samples have 4 mol% P_2O_5. So, for SBF treated samples CaO content plays major role for HA formation. Releasing Ca^{2+} ions into SBF for CPSNB samples are in the sample order of CPSNB4> CPSNB1> CPSNB3> CPSNB2 and HA formation was also in the same (decreasing order) order Figure 4.9 (b). From all these observations, it can be concluded that HCA formation is

NBO/BO ratio dependent. Same observations were supported in XRD, SEM and EDX analyses also. Due to this, CPSNB samples weight loss also changed (decreased) in the order of CPSNB4> CPSNB1> CPSNB3> CPSNB2 [Table 4.8] (Sooraj Hussain et al. 2004). Ba^{2+} ionic radius is more than Ca^{2+}. So, increase in BaO addition decreases the local field strength, leading to increase in dissolution of CPSNB sample. Compared to CPSNB2, CPSNB1 has more Ba^{2+} ions and it leads to increase in Ca^{2+} and PO_4^{3-} ion dissolution in SBF. The number of Ba^{2+} ions is less, number of Ca^{2+} ions is more in CPSNB3 compared to CPSNB2 sample, leading to increase in local field strength for CPSNB3 sample.

Due to this reason PO_4^{3-} ion release decreases in the dissolution process for CPSNB3 compared to CPSNB2 sample. With low BaO, the field strength is high for CPSNB4 compared to CPSNB3 sample. Due to this reason CPSNB4 sample releases less PO_4^{3-} ions into SBF solution compared to CPSNB3 sample. From these observations it could be concluded that the decrease in BaO reduces the PO_4^{3-} dissolution. PO_4^{3-} ions dissolution decreased from CPSNB1 to CPSNB4 sample. SBF also need to utilize PO_4^{3-} ions in HCA formation in the increasing order from CPSNB1 to CPSNB4 sample. So, the phosphate ion concentration of SBF solution decreased for CPSNB1 to CPSNB4 sample as shown in Figure 4.9 (c).

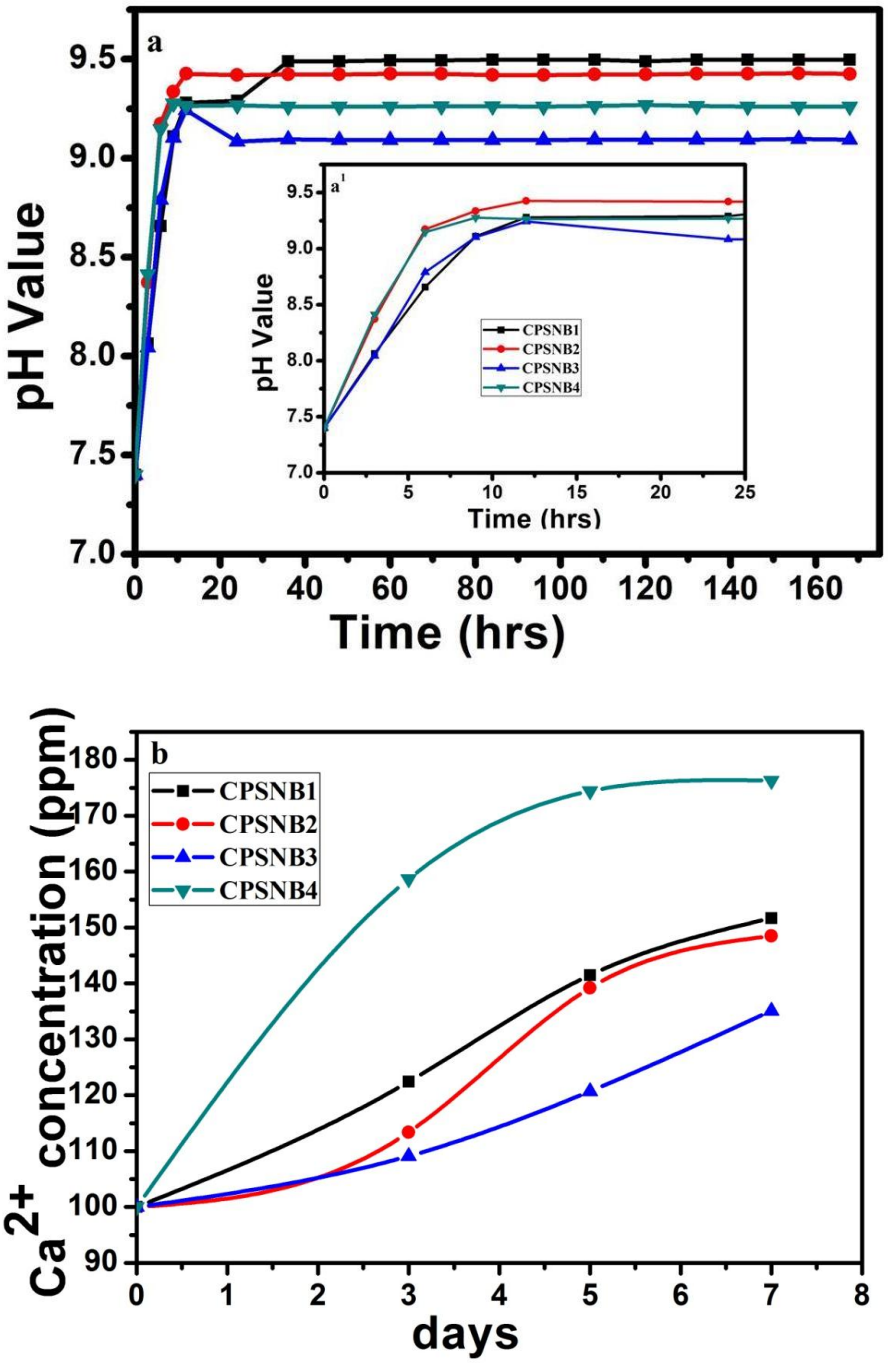

Figure 4.9 Variation of SBF solution (a) pH, (b) Ca concentration values with respect to CPSN glass soaking time in SBF solution.

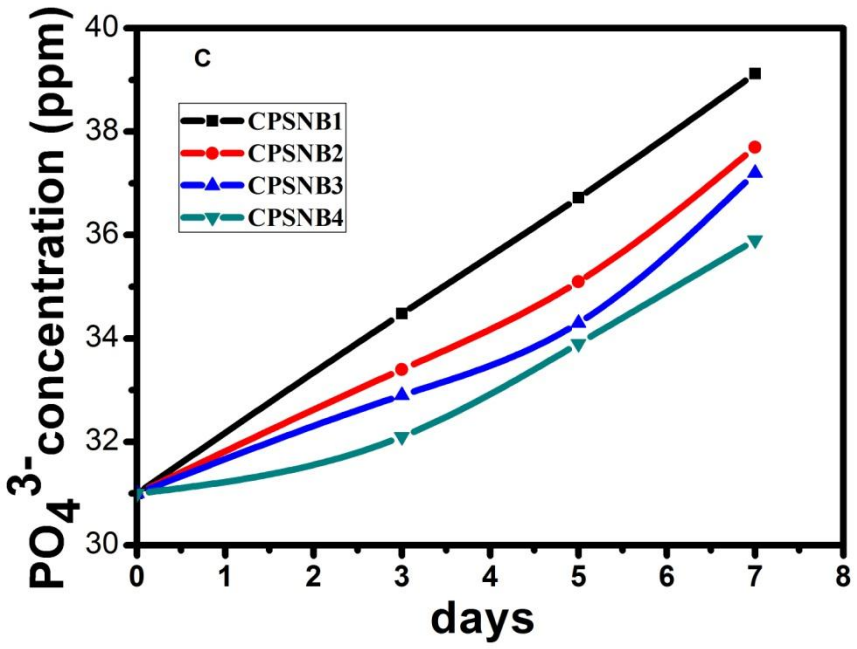

Figure 4.9 (c) Variation of SBF solution P concentration values with respect to CPSN glass soaking time in SBF solution.

Table 4.8 Weight loss % of SBF soaked $58SiO_2$-(32-x)BaO-xCaO-$6Na_2O$-$4P_2O_5$ glasses with NBO/BO ratio and HCA particle sizes.

x mol%	**(Raman) NBO/BO ratio**	**(SEM) Particle size (nm)**	**Weight loss for 7days SBF soaking %**
15	0.36	1517	35.47
20	0.23	1355	29.39
25	0.27	1587	39.12
30	0.47	1605	52.33

4.4. Conclusions

Increase in CaO content increases the nucleation and crystallization temperature. Increase in CaO content increases amorphous nature. NBO/BO ratio decreased with increase in CaO content from 15 to 20 mol% and increased with increase in CaO content from 20 to 30 mol%. NBO/BO ratio is proportional to Weight loss of SBF-treated samples as well as HCA particle size. From these observations it was concluded that both network modifiers (CaO and BaO) play important roles in the formation of HCA layer in SBF treatment. It is helpful to improve bone forming ability based on dissolution of glass in SBF with BaO/CaO in biomedical applications.

CHAPTER 5

SUMMARY AND SCOPE FOR FUTURE WORK

Summary

This chapter summarizes the work carried out in the thesis and presents important findings along with future scope of the work. $58SiO_2$-$(19-x)P_2O_5$-$(23+x)CaO$ (x=0, 5, 10 and 15 mol %) dried gels were synthesized at 130 °C using sol-gel method. XRD pattern confirmed that all gel samples have amorphous nature. FTIR analysis shows that increase in P_2O_5 increases the degree of polymerization. Raman spectroscopic analysis proved that increase in P_2O_5 decreases the orthophosphate structural units. From FESEM analysis it was observed surface pore size increased with increases in P_2O_5.

Above dried gels were sintered at 700 °C, at this stage dried gels got converted into calcium phosphosilicate glasses. Quaternary (soda lime phosphosilicate) and tertiary (barium soda lime phosphosilicate) glasses were also synthesized at 700 °C sintering temperature. All synthesized glass samples were soaked in the SBF for 7 days. Comparative studies have been done for synthesized and SBF treated glass samples, for these studies structural, morphological and dissolutions characterizations were used. XRD, FTIR, Raman, SEM/EDX and TEM/SAED characterizations confirmed the HCA formation for SBF treated samples. Dissolution properties were studied using changes in pH, calcium and phosphate ion concentrations of SBF, based on dissolution and weight loss of SBF treated samples were carried out. HCA formation strongly depends on changes in calcium ion concentration in dissolution process.

The obtained NBO/BO ratios of $58SiO_2$-$(19-x)P_2O_5$-$(23+x)CaO$ (x=0, 5, 10 and 15 mol %) glasses were 0.58, 1.20, 1.46, and 1.78, respectively. For 7 days SBF treated samples the weight losses were found as 58%, 64%, 83%, and 89% respectively for corresponding NBO/BO ratios. In the same way calcium ion concentration of SBF also increased as NBO/BO ratio with CaO. Increases in weight loss percent are an indication

of increase in HCA layer formation. From this, it was confirmed that increase in HCA layer formation is proportional to NBO/BO ratio.

The obtained NBO/BO ratios of $58SiO_2$-(38-x)CaO-xNa_2O-4P_2O_5 (x=5, 10, 15 and 20 mol %) glasses were obtained as 0.63, 0.79, 0.23 and 0.35, respectively. It means NBO/BO ratio shows nonlinear variation with increase in Na_2O. After 7 days SBF treatment the weight losses were found as 55%, 69%, 18%, and 20% respectively for corresponding NBO/BO ratios. In the same way calcium ion concentration of SBF also varied nonlinearly as NBO/BO ratio with CaO. From this, it was confirmed that change in HCA layer formation is proportional to NBO/BO ratio.

The obtained NBO/BO ratios of $58SiO_2$-(32-x)BaO-xCao-6Na_2O-4P_2O_5 [where x=15, 20, 25 and 30 mol %] were 0.36, 0.23, 0.27and 0.47, respectively. It means NBO/BO ratio decreased with increase in CaO from 15 to 20 mol% and again NBO/BO ratio increased with increase in CaO from 20 to 30 mol%. After 7 days SBF treatment the weight losses were observed as 35%, 29%, 39%, and 52% respectively for corresponding NBO/BO ratios. In the same way calcium ion concentration of SBF also show similar variation as NBO/BO ratio with CaO. From this, it was confirmed that change in HCA layer formation is proportional to NBO/BO ratio.

For ternary calcium phosphosilicate glasses NBO/BO ratio is proportional to CaO content. For quaternary soda lime phosphosilicate glasses NBO/BO ratio shows nonlinear variation with CaO content. For tertiary barium soda lime phosphosilicate glasses NBO/BO ratio decreased with increase in CaO from 15 to 20 mol% and increased with increase in CaO from 20 to 30 mol%. For all SBF treated samples HCA formation is proportional to NBO/BO ratio. Among all glass samples, high CaO concentrated sample (ternary system) show more HCA forming ability. Calcium phosphosilicate glasses with less concentrations of BaO and Na_2O at higher CaO concentration favors the HCA formation in tertiary glass system.

Future work

Bio compatibility properties may be studied for *in vitro*/*in vivo* biomedical applications for ternary, quaternary and tertiary calcium phosphosilicate glasses based on NBO/BO ratio.

References

Adam, J.L. (2001). "Non-oxide glasses and their application in optics." *J. Non-Cryst. Solids.*, 287, 401-404.

Adams, L. A., Essien, E.R., Shaibu, R. O., and Oki, A. (2013). "Sol-Gel Synthesis of SiO_2-CaO-Na_2O-P_2O_5 Bioactive Glass Ceramic from Sodium Metasilicate." *New Journal of Glass and Ceramics*, 2013, 3, 11-15.

Aguiar, H., Serra, J., González, P., and León, B. (2009). "Structural study of sol–gel silicate glasses by IR and Raman spectroscopies." *J. Non-Cryst. Solids*, 355(8), 475–480.

Aguiar, H., Solla, E.L., Serra, J., González, P., León, B., Almeida, N., Cachinho, S., Davim, E.J.C., Correia, R., Oliveira, J.M., and Fernandes, M.H.V. (2008). "Orthophosphate nanostructures in SiO_2–P_2O_5–CaO–Na_2O–MgO bioactive glasses." *J. Non-Cryst. Solids*, 354(34), 4075–4080.

Aguiar, He´ lio., Serra, Julia., Gonza´ lez, P1´o., and Betty Leo´n., (2010). "Influence of the Stabilization Temperature on the Structure of Bioactive Sol–Gel Silicate Glasses." *J. Am. Ceram. Soc*., 93, 2286–2291.

Aguiar, He´lio., Serra, Julia., and Gonza´lez, and P1´o., (2011). "Nano structural Transitions in Bioactive Sol–Gel Silicate Glasses." .*Int. J. Appl. Ceram. Technol*., 8, 511–522.

Ahsan, M.R., and Mortuza, M.G. (2005). "Infrared spectra of $xCaO(1 - x - z)SiO_2zP_2O_5$ glasses." *J. Non-Cryst. Solids*, 351(27–29), 2333–2340.

Al-Noaman, A., Rawlinson, S.C.F., and Hill, R.G. (2012). “The role of MgO on thermal properties, structure and bioactivity of bioactive glass coating for dental implants.” *J. Non-Cryst. Solids*, 358(22), 3019–3027.

Anjaneyulu, U., and Vijayalakshmi, U. (2017). “Preparation and characterization of novel sol-gel derived hydroxyapatite/Fe 3 O 4 composites coatings on Ti-6Al-4V for biomedical applications.” *Mater. Lett.*, 189, 118–121.

Ankan M (2015), “Measurement of magnetic hysteresis loops in continuous and patterned ferromagnetic nanostructures by static magneto-optical kerr effect magnetometer.”

Arcos, D., and Vallet-Regí, M. (2010). “Sol–gel silica-based biomaterials and bone tissue regeneration.” *Acta Biomater.*, 6(8), 2874–2888.

Arepalli, S.K., Tripathi, H., Vyas, V.K., Jain, S., Suman, S.K., Pyare, R., and Singh, S.P. (2015). “Influence of barium substitution on bioactivity, thermal and physico-mechanical properties of bioactive glass.” *Mater. Sci. Eng. C*, 49, 549–559.

Bellucci, D., Bolelli, G., Cannillo, V., Cattini, A., and Sola, A. (2011). “In situ Raman spectroscopy investigation of bioactive glass reactivity: Simulated body fluid solution vs TRIS-buffered solution.” *Mater. Charact.*, 62(10), 1021–1028.

Bellucci, D., Sola, A., Salvatori, R., Anesi, A., Chiarini, L., and Cannillo, V. (2014). “Sol–gel derived bioactive glasses with low tendency to crystallize: Synthesis, post-sintering bioactivity and possible application for the production of porous scaffolds.” *Mater. Sci. Eng. C*, 43, 573–586.

Brow, R.K., Click, C.A. and Alam, T.M. (2000). “Modifier coordination and phosphate glass networks.” *J. Non-Cryst. Solids.*, 274, 9-16.

Carta, D., Knowles, J.C., Smith, M.E., and Newport, R.J. (2007). "Synthesis and structural characterization of P_2O_5–CaO–Na_2O sol–gel materials." *J. Non-Cryst. Solids*, 353(11–12), 1141–1149.

Catauro, M., Bollino, F., Papale, F., Mozetic, P., Rainer, A. and Trombetta, M. (2014). "Biological response of human mesenchymal stromal cells to titanium grade 4 implants coated with PCL/ZrO_2 hybrid materials synthesized by sol–gel route: in vitro evaluation." *Mater. Sci. Eng. C*, 45, 395–401.

Catauro, M., Dell'Era, A. and Ciprioti, S.V. (2016). "Synthesis, structural, spectroscopic and thermoanalytical study of sol–gel derived SiO_2–CaO–P_2O_5 gel and ceramic materials." *Thermochim. Acta*, 625, 20–27.

Daguano, Juliana, K.M.F., Suzuki, Paulo A., Strecker, Kurt. and Fernandes, Maria H.F.V., (2012). "Evaluation of the micro-hardness and fracture toughness of amorphous and partially crystallized $3CaO{\cdot}P_2O_5$–SiO_2–MgO bio glasses". *Mater. Sci. Eng., A*, 533, 26– 32.

Fujibayashi, S., Neo, M., Kim, H.-M., Kokubo, T., and Nakamura, T. (2003). "A comparative study between in vivo bone ingrowth and in vitro apatite formation on Na_2O–CaO–SiO_2 glasses." *Biomaterials*, 24(8), 1349–1356.

Gerhardt, L.C., and Boccaccini, A.R. (2010). "Bioactive Glass and Glass-Ceramic Scaffolds for Bone Tissue Engineering." *Materials*, 3(7), 3867–3910.

Goller, G., Oktar, F.N., Ozyegin, L.S., Kayali, E.S. and Demirkesen, E. (2004). "Plasma-sprayed human bone-derived hydroxyapatite coatings: effective and reliable." *Mater. Lett.*, 58(21), 2599–2604.

González, P., Serra, J., Liste, S., Chiussi, S., Leon, B. and Pérez-Amor, M. (2003). "Raman spectroscopic study of bioactive silica based glasses." *J. Non-Cryst. Solids*, 320(1), 92–99.

Greenspan, D. C., Zhong, J.P. and LaTorre, G.P. (1994). “Effect of surface area to volume ratio on in vitro surface reactions of bioactive glass particulates.” *Bioceramics,* 7, 55–60.

Greenspan, D. C., Zhong, J.P., Chen, Z.F. and LaTorre, G.P. (1997). “The evaluation of degradability of melt and sol–gel derived Bioglass® in vitro.” *Bioceramics,* 10, 391–394.

Greenspan, D.C., Zhong, J.P. and Wheeler, D.L. (1998). “Bioactivity and Biodegradability: Melt vs. Sol-Gel Derived Bioglass [R] In Vitro and In Vivo.” *Bioceram. Conf.,* 345–348.

Hamza (2012). https://www.researchgate.net/publication/263849645

Hashmi, M.U., Shah, S.A., Umer, F. and Alkedy, A.S. (2013). “Effect of sintering temperature on microstructure and in vitro behavior of bioactive glass-ceramics.” *Ceram-Silik.,* 57, 313–318.

Hench, L.L. (2009). “Genetic design of bioactive glass.” *J. Eur. Ceram. Soc.*, 29(7), 1257–1265.

Jones, J. and Clare, A. (2012). *Bio-glasses: an introduction*. John Wiley & Sons.

Kobayashi, T., Itoh, S., Nakamura, S., Nakamura, M., Shinomiya, K. and Yamashita, K. (2007). “Enhanced bone bonding of hydroxyapatite-coated titanium implants by electrical polarization.” *J. Biomed. Mater. Res. A,* 82(1), 145–151.

Kokubo, T., Kushitani, H., Sakka, S., Kitsugi, T. and Yamamuro, T. (1990). “Solutions able to reproduce in vivo surface-structure changes in bioactive glass-ceramic A-W3.” *J. Biomed. Mater. Res. A,* 24(6), 721–734.

Kokubo, T., and Takadama, H. (2006). “How useful is SBF in predicting in vivo bone bioactivity?.” *Biomaterials,* 27(15), 2907–2915.

Laczka, M., Cholewa-Kowalska, K., Kulgawczyk, K., Klisch, M. and Mozgawa, W. (1999). "Structural examinations of gel-derived materials of the $CaO–P_2O_5–SiO_2$ system." *J. Mol. Struct.*, 511, 223–231.

Laczka, M., Cholewa-Kowalska, K., Laczka-Osyczka, A., Tworzydlo, M. and Turyna, B. (2000). "Gel-derived materials of a $CaO-P_2O_5-SiO_2$ system modified by boron, sodium, magnesium, aluminum, and fluorine compounds." *J. Biomed. Mater. Res.*, 52(4), 601–612.

Lao, J., Nedelec, J.M., Moretto, P. and Jallot, E. (2008). "Micro-PIXE–RBS methods highlighting the influence of phosphorus on the in vitro bioactivity of sol–gel derived glass particles in the $SiO_2–CaO–P_2O_5$ system." *Nucl. Instrum. Methods Phys. Res. Sect. B Beam Interact. Mater. At.*, 266(10), 2412–2417.

Lei, B., Chen, X., Wang, Y., Zhao, N., Du, C. and Fang, L. (2009). "Synthesis and bioactive properties of macroporous nanoscale $SiO_2–CaO–P_2O_5$ bioactive glass." *J. Non-Cryst. Solids*, 355(52), 2678–2681.

Letaïef, N., Lucas-Girot, A., Oudadesse, H., Dorbez-Sridi, R. and Boullay, P. (2014). "Investigation of the surfactant type effect on characteristics and bioactivity of new mesoporous bioactive glass in the ternary system $SiO_2–CaO–P_2O_5$: Structural, textural and reactivity studies." *Microporous Mesoporous Mater.*, 195, 102–111.

Li, H.C., Wang, D.G., Hu, J.H. and Chen, C.Z. (2013). "Effect of various additives on microstructure, mechanical properties, and in vitro bioactivity of sodium oxide-calcium oxide-silica-phosphorus pentoxide glass–ceramics." *J. Colloid Interface Sci.*, 405, 296–304.

Li, H.C., Wang, D.G., Hu, J.H. and Chen, C.Z. (2014). "Influence of fluoride additions on biological and mechanical properties of $Na_2O–CaO–SiO_2–P_2O_5$ glass–ceramics." *Mater. Sci. Eng. C*, 35, 171–178.

Li, H.C., Wang, D.G., Chen, C.Z., Weng, F. and Shi, H. (2016). "Influence of different amount of Na 2 O additive on the structure, mechanical properties and degradability of bioactive wollastonite." *Ceram. Int.*, 42(1), 1439–1445.

Liu, W., Wu, X., Zhan, H. and Yan, F. (2012). "Synthesis of bioactive poly (ethylene glycol)/SiO_2-CaO-P_2O_5 hybrids for bone regeneration." *Mater. Sci. Eng. C*, 32(4), 707–711.

Lu, W.H., Li, K.D., Lu, C.H., Teoh, L.G., Wu, W.H. and Shen, Y. C. (2013). "Synthesis and Characterization of Mesoporous SiO_2–CaO–P_2O_5 Bioactive Glass by Sol–Gel Process." *Mater. Trans.*, 54(5), 791–795.

Lucas-Girot, A., Mezahi, F.Z., Mami, M., Oudadesse, H., Harabi, A. and Le Floch, M. (2011). "Sol–gel synthesis of a new composition of bioactive glass in the quaternary system SiO_2–CaO–Na_2O–P_2O_5: comparison with melting method." *J. Non-Cryst. Solids*, 357(18), 3322–3327.

Lukito, D., Xue, J. M. and Wang, J. (2005). "In vitro bioactivity assessment of 70 (wt.)% SiO_2–30 (wt.)% CaO bioactive glasses in simulated body fluid." *Mater. Lett.*, 59(26), 3267–3271.

Lusvardi, G., Malavasi, G., Menabue, L., Aina, V. and Morterra, C. (2009). "Fluoride-containing bioactive glasses: surface reactivity in simulated body fluids solutions." *Acta Biomater.*, 5(9), 3548–3562.

Ma, J., Chen, C.Z., Wang, D.G. and Hu, J.H. (2011). "Synthesis, characterization and in vitro bioactivity of magnesium-doped sol–gel glass and glass-ceramics." *Ceram. Int.*, 37(5), 1637–1644.

Ma, J., Chen, C.Z., Wang, D.G., Meng, X.G. and Shi, J.Z. (2010). "Influence of the sintering temperature on the structural feature and bioactivity of sol–gel derived SiO_2–CaO–P_2O_5 bioglass." *Ceram. Int.*, 36(6), 1911–1916.

Marsich, L., Moimas, L., Sergo, V. and Schmid, C. (2009). “Raman spectroscopic study of bioactive silica-based glasses: The role of the alkali/alkali earth ratio on the Non-Bridging Oxygen/Bridging Oxygen (NBO/BO) ratio.” *J. Spectrosc.*, 23(3–4), 227–232.

Merwin, G.E. (1986). “Bioglass middle ear prosthesis: preliminary report.” *Ann. Otol. Rhinol. Laryngol.*, 95(1), 78–82.

Masoud, M., Fatholla, M. and Mohammadreza, T. (2010). “Investigation of physic-chemical reactivity of a mesoporous bioactive SiO_2-CaO-P_2O_5 glass in simulated body fluid.” *j non-cryst solids*, 2010, 356:1470-1478.

Milea, C.A., Bogatu, C. and Duta, A., (2011). “The influence of the parameters in silica sol-gel process.” *Eng. Sci.*, Vol. 4 (53) No. 1-2011.

Moghanian, A., Firoozi, S. and Tahriri, M. (2017a). “Characterization, in vitro bioactivity and biological studies of sol-gel synthesized SrO substituted 58S bioactive glass.” *Ceram. Int.*

Moghanian, A., Firoozi, S. and Tahriri, M. (2017b). “Synthesis and in vitro studies of sol-gel derived lithium substituted 58S bioactive glass.” *Ceram. Int.*, 43(15), 12835–12843.

Mozafari Masoud., Moztarzadeh Fathollah. and Tahriri Mohammadreza., (2010). “Investigation of the physico-chemical reactivity of a mesoporous bioactive SiO_2–CaO–P_2O_5 glass in simulated body fluid.” *J. Non-Cryst. Solids*, 356, 1470–1478.

MYseN, B.O., Virgo, D., Scarfe, C.M. and others. (1980). “Relations between the anionic structure and viscosity of silicate melts—a Raman spectroscopic study.” *Am Miner.*, 65(7–8), 690–710.

Nazabal, V., Poulain, M., Olivier, M.,Pirasteh, P., Camy, P., Doualan, J.L., Guy, S., Djouama, T., Boutarfaia, A. and Adam, J.L. (2012). “Fluoride and oxyfluoride glasses for optical applications.” *J. Fluorine Chem.*, 134, 18-23.

Notingher, I., Boccaccini, A.R., Jones, J., Maquet, V. and Hench, L.L. (2002). "Application of Raman microspectroscopy to the characterisation of bioactive materials." *Mater. Charact.*, 49(3), 255–260.

Ohtsuki, C., Kamitakahara, M. and Miyazaki, T. (2009). "Bioactive ceramic-based materials with designed reactivity for bone tissue regeneration." *J. R. Soc. Interface*, 6(Suppl 3), S349–S360.

O'Kane, C., Duffy, H., Meenan, B.J. and Boyd, A.R. (2008). "The influence of target stoichiometry on the surface properties of sputter deposited calcium phosphate thin films." *Surf. Coat. Technol.*, 203(1), 121–128.

Ong, J.L. and Chan, D.C. (2000). "Hydroxyapatite and their use as coatings in dental implants: a review." *Crit. Rev. Biomed. Eng.*, 28(5&6).

Onoki, T., and Hashida, T. (2006). "New method for hydroxyapatite coating of titanium by the hydrothermal hot isostatic pressing technique." *Surf. Coat. Technol.*, 200(24), 6801–6807.

Oonishi, H., Hench, L.L., Wilson, J., Sugihara, F., Tsuji, E., Matsuura, M., Kin, S., Yamamoto, T., Mizokawa, S. and others. (2000). "Quantitative comparison of bone growth behavior in granules of Bioglass, A-W glass-ceramic, and hydroxyapatite." *J. Biomed. Mater. Res.*, 51(1), 37–46.

Peitl, O., Dutra Zanotto, E. and Hench, L.L. (2001). "Highly bioactive P_2O_5–Na_2O–CaO–SiO_2 glass-ceramics." *J. Non-Cryst. Solids*, 292(1–3), 115–126.

Prabhu, Muthusamy., Kavitha, Kandia., Manivasakan, P alanisamy., Rajendran, Venkatachalam. and Kulandaivelub, Palanisami., (2013). "Synthesis, characterization and

biological response of magnesium-substituted nano bioactive glass particles for biomedical applications." *Ceram. Int.* 39, 1683-1694.

Radev, L. (2014). "Influence of thermal treatment on the structure and in vitro bioactivity of sol-gel prepared CaO-SiO_2-P_2O_5 glass-ceramics." *Process. Appl. Ceram.*, 8(3), 155–166.

Rafiqul Ahsan, M. and Golam Mortuza, M. (2005). "Infrared spectra of xCaO (1-x-z) SiO2zP2O5 glasses." *J. Non-Cryst. Solids*, 351(27–29), 2333–2340.

Rajendran, V., Nishara Begum, A., Azooz, M.A. and El Batal F.H., (2002). "Micro structural dependence on relevant physical–mechanical properties on SiO_2–Na_2O–CaO–P_2O_5 biological glasses." *Biomater*, 23, 4263–4275.

Rao, K. J. (2002). *Structural Chemistry of Glasses*, Elsevier**,** Amsterdam.

Rezwan, K., Chen, Q.Z., Blaker, J.J. and Boccaccini, A.R. (2006). "Biodegradable and bioactive porous polymer/inorganic composite scaffolds for bone tissue engineering." *Biomaterials*, 27(18), 3413–3431.

Saravanapavan, Priya. and Hench, Larry. L., (2003). "Mesoporous calcium silicate glasses. I. Synthesis." *J. Non-Cryst. Solids*, 318, 1–13.

Sava, B.A., Elisa, E., Vasili, I.C., Nastase, F. and Simon S., (2012). "Investigations on sol–gel process and structural characterization of SiO_2-P_2O_5 powders." *J. Non-Cryst.Solids*, 358, 2877–2885.

Shelby, J.E. (2005). *Introduction to Glass Science and Technology*. Royal Society of Chemistry.

Simon, V., and Mocuta, H. (2004). "glass formation and dissolution properties of Na_2O-CaO-P_2O_5 glasses in simulated body fluids."

Singh, R.K., Kothiyal, G.P. and Srinivasan, A. (2009). "In vitro evaluation of bioactivity of CaO–SiO_2–P_2O_5–Na_2O–Fe_2O_3 glasses." *Appl. Surf. Sci.*, 255(15), 6827–6831.

Singh, R.K. and Srinivasan, A. (2010). “Bioactivity of SiO_2–CaO–P_2O_5–Na_2O glasses containing zinc–iron oxide.” *Appl. Surf. Sci.*, 256(6), 1725–1730.

Siqueira, R.L. and Zanotto, E.D. (2013). “The influence of phosphorus precursors on the synthesis and bioactivity of SiO_2–CaO–P_2O_5 sol–gel glasses and glass–ceramics.” *J. Mater. Sci. Mater. Med.*, 24(2), 365–379.

Snyders, R., Bousser, E., Music, D., Jensen, J., Hocquet, S. and Schneider, J.M. (2008). “Influence of the Chemical Composition on the Phase Constitution and the Elastic Properties of RF-Sputtered Hydroxyapatite Coatings.” *Plasma Process. Polym.*, 5(2), 168–174.

Sooksaen, P., Pengsuwan, N., Karawatthanaworrakul, S., and Pianpraditkul, S. (2015). “Formation of porous apatite layer during in vitro study of hydroxyapatite-aw based glass composites.” *Adv. Condens. Matter Phys.*, 2015.

Sooraj Hussain, N., Lopes, M.A. and Santos, J.D. (2004). “A comparative study of CaO–P_2O_5–SiO_2 gels prepared by a sol–gel method.” *Mater. Chem. Phys.*, 88(1), 5–8.

Sopcak, T., Medvecky, L., Girman, V. and Durisin, J. (2015). “Mechanism of precipitation and phase composition of CaO–SiO_2–P_2O_5 systems synthesized by sol–gel method.” *J. Non-Cryst. Solids*, 415, 16–23.

Sun, Y., Zhang, Z., Liu, L. and Wang, X. (2015a). “FTIR, Raman and NMR investigation of CaO–SiO 2–P 2 O 5 and CaO–SiO_2–TiO_2–P_2O_5 glasses.” *J. Non-Cryst. Solids*, 420, 26–33.

Tilocca, A. and Cormack, A.N. (2007). “Structural effects of phosphorus inclusion in bioactive silicate glasses.” *J. Phys. Chem. B*, 111(51), 14256–14264.

Theophile (2012). Introduction to Infrared Spectroscopy
https://www.researchgate.net/publication/224831013

Vulpoi, Adriana., Baia, Lucian., Simon, Simion. and Simon, Viorica., (2012). "Silver effect on the structure of SiO_2-CaO-P_2O_5 ternary system." *Mater. Sci. Eng., C,* 32,178–183.

Wang, X., Li, X., Ito, A. and Sogo, Y. (2011). "Synthesis and characterization of hierarchically macroporous and mesoporous CaO–MO–SiO_2–P_2O_5 (M= Mg, Zn, Sr) bioactive glass scaffolds." *Acta Biomater.*, 7(10), 3638–3644.

Wong, J. (1976). "Vibrational spectra of vapor-deposited binary phosphosilicate glasses." *J. Non-Cryst. Solids*, 20(1), 83–100.

Wu, C. and Chang, J. (2012a). "Mesoporous bioactive glasses: structure characteristics, drug/growth factor delivery and bone regeneration application." *Interface Focus*, rsfs20110121.

Wu, C. and Chang, J. (2012b). "Mesoporous bioactive glasses: structure characteristics, drug/growth factor delivery and bone regeneration application." *Interface Focus*, 2(3), 292–306.

Yadav, A.K. and Singh, P. (2015). "A review of the structures of oxide glasses by Raman spectroscopy." *RSC Adv.*, 5(83), 67583–67609.

Yamane, M. and Asahara, Y. (2000). *Glasses for Photonics*, Cambridge Univ. Press, UK.

Yang, X., Zhang, L., Chen, X., Sun, X., Yang, G., Guo, X., Yang, H., Gao, C. and Gou, Z. (2012). "Incorporation of B_2O_3 in CaO-SiO_2-P_2O_5 bioactive glass system for improving strength of low-temperature co-fired porous glass ceramics." *J. Non-Cryst. Solids*, 358(9), 1171–1179.

Yousefi, A.M., Oudadesse, H., Akbarzadeh, R., Wers, E. and Lucas-Girot, A. (2014). "Physical and biological characteristics of nanohydroxyapatite and bioactive glasses used for bone tissue engineering." *Nanotechnol. Rev.*, 3(6), 527–552.

Yunos, D. M., Bretcanu, O. and Boccaccini, A.R. (2008). "Polymer-bioceramic composites for tissue engineering scaffolds." *J. Mater. Sci.*, 43(13), 4433.

Zarifah, N.A., Matori, K.A., Sidek, H.A.A., Wahab, Z.A., Salleh, M.M., Zainuddin, N., Khiri, M.Z.A., Farhana, N.S. and Omar, N.A.S. (2016). "Effect of hydroxyapatite reinforced with 45S5 glass on physical, structural and mechanical properties." *Procedia Chem.*, 19, 30–37.

Zhang, L., and Gou, Z. (2012). "Incorporation of B_2O_3 in CaO-SiO_2-P_2O_5 bioactive glass system for improving strength of low-temperature co-fired porous glass ceramics." *J Non-Cryst Solids*, 358, 1171–1179.

Zhao, S., Li, Y. and Li, D. (2010). "Synthesis and in vitro bioactivity of CaO–SiO_2–P_2O_5 mesoporous microspheres." *Microporous Mesoporous Mater.*, 135(1), 67–73.

Zheng, K. and Boccaccini, A.R. (2017). "Sol-gel processing of bioactive glass nanoparticles: A review." *Adv. Colloid Interface Sci.*

List of publications

- Kiran P., Ramakrishna V, Trebbin M, Udayashankar N.K, Shashikala H.D, (2017) "Effective role of CaO/P_2O_5 ratio on SiO_2-CaO-P_2O_5 glass system", *Journal of Advanced Research* 8, 279–288. DOI:10.1016/j.jare.2017.02.001.
- Kiran P., Ramakrishna V, Udayashankar N.K and Shashikala H.D, (2017) "The effective role of alkali earth/alkali ratio on formation HCA nano particles for soda lime phospho silicate glass system", *Open Nano* 2, 47–56. DOI:10.1016/j.onano.2017.06.002.
- Kiran P., Ramakrishna V, Shashikala H.D and Udayashankar N.K (2017) **"** Effect of alkali earth oxides on hydroxy carbonated apatite formation for SiO_2-BaO-CaO-$N_{a2}O$-P_2O_5 glass system", *Applied Nano Science*. DOI: 10.1007/s13204-017-0616-5.
- Kiran P., Udayashankar N.K and Shashikala H.D (2017) "Effective role of P_2O_5 on invitrobioactivity of soda lime phosphosilicate glasses", *Materials Today Proceedings.* DOI:10.1016/j.matpr.2017.06.402, PII:S2214-7853(17)31206-3.
- Kiran P., Udayashankar N.K and Shashikala H.D (2016) "The Effective Role of P_2O_5 on Structural and Morphological Properties of SiO_2-CaO-P_2O_5 Dried Gels". *International Advanced Research Journal in Science, Engineering and Technology*, ISSN (Online) 2393-8021 ISSN (Print) 2394-1588. DOI: 10.17148/IARJSET.2016.31234.

List of conferences attended

- P. Kiran., N.K. Udayashankar, H.D. Shashikala (2013). "Effect of partial substitution of Na_2O in sol-gel derived SiO_2-CaO-P_2O_5 glass system". International union of materials research society, Materials society of India, International conference in Asia (IUMRS-ICA-2013), December 16-20, Indian Institute of Science, Bangalore, Karnataka, India. (International conference).

- P. Kiran, N.K. Udayashankar, H.D. Shashikala (2013). "Synthesis and characterization of sodium calcium phopshosilicate glasses". Condensed mater physics and applications (CMPA-2013), December 27-28, Manipal University, Manipal, Karnataka, India. (National conference).

- P. Kiran, V.Ramakrishna, N.K. Udayashankar, H.D. Shashikala (2014). "The effective role of network modifiers in soda lime phopshosilicate glasses". International seminar on glasses and other functional materials (ISGFM-2014), December 11-13, Acharya Nagarjuna University, Guntur, Andhra Pradesh, India. (International conference).

- P. Kiran, N.K. Udayashankar and H.D. Shashikala (2016). "Effective role of P_2O_5 on in vitro bioactivity of soda lime phosphosilicate glasses". International conference on recent trends in engineering and material sciences (ICEMS-2016), March 17-19, Jaipur National University, Jaipur, Rajasthan, India. (International conference).

CURRICULAM VITAE

KIRAN PEDANABOYINA

Address for correspondence
Research Scholar
Department of Physics
National Institute of Technology Karnataka, Surathkal
Mangalore - 575 025
Phone: +91 8147251820
E-mail:.sr.kirankumarsr@gmail.com

Educational Qualifications

- 2011–2017: Doctoral Research towards Ph.D

Thesis title: "synthesis, characterisation and hydroxy carbonated apatite (HCA) formation studies on sol-gel derived SiO_2-CaO-P_2O_5, SiO_2-CaO-Na_2O-P_2O_5, SiO_2-CaO-BaO-Na_2O-P_2O_5 glass systems".

Department of Physics, National Institute of Technology Karnataka, Surathkal, Mangalore-575025, India.

Specialization: Condensed matter physics (Experimental)

- 2006–2008: Master of Science (M.Sc in Physics)

Department of Physics, Acharya Nagarjuna University PG center, Nuzvid, Krishna district, Andhrapradesh,India.

Specialization: Condensed Matter Physics

Research Experience

2011-2017: Worked as Research Scholar in National Institute of Technology Karnataka. (6 Years.).

Research Topic: "synthesis, characterisation and hydroxy carbonated apatite (HCA) formation studies on sol-gel derived SiO_2-CaO-P_2O_5, SiO_2-CaO-Na_2O-P_2O_5, SiO_2-CaO-BaO-Na_2O- P_2O_5 glass systems".

Teaching Experience

- Institution: **NITK**

Designation: **Worked as Teaching Assistant in National Institute of Technology Karnataka. Handled Courses for B.Tech and M.Sc labs from June-2011 to December-2016.**

- Institution: **SSN PG and Degree college, Ongole, Prakasam (Dt), Andhrapradesh (2010 to 2011)**

Designation**: Lecturer for M.Sc and Taught M.Sc lab courses**

Department: **Physics**

- Institution: **MSR Degree college, Kondapi, Prakasam (Dt), Andhrapradesh (2008 to 2009)**

Designation: **Lecturer for B.Sc and Taught B.Sc lab courses**

Department: **Physics**

Fellowships/Awards

- Cleared NITK Research fellowship test conducted by the Physics department in July 2011.
- Qualified Graduate Aptitude Test (GATE) in Engineering in 2010. All India Rank: **630.**
- ANU PG CET Rank in 2006: **32**

Declaration

I hereby declare that the above mentioned profile is correct to the best of my knowledge.

Place: NITK, Surathkal. Date: 02-11-2017

(P. Kiran)

References

Dr. N.K. Udayashankar, **Professor**, Department of Physics, NITK Surathkal,

Contact number: +919902064124, **Email:** nkuday_01@yahoo.com

Dr. H.D.Shashikala, **Professor**, Department of Physics, NITK Surathkal,

Contact number: +919945286261, **Email:** sasiholavana@gmail.com